Stanislav Ustinov

FAST AND ACCURATE SIMULATION OF FLUID POWER CIRCUITS IN THE PRESENCE OF SMALL VOLUMES USING ADVANCED METHODS AND MODELS FOR NUMERICAL STIFFNESS ELIMINATION

ACTA UNIVERSITATIS LAPPEENRANTAENSIS 1078

Stanislav Ustinov

FAST AND ACCURATE SIMULATION OF FLUID POWER CIRCUITS IN THE PRESENCE OF SMALL VOLUMES USING ADVANCED METHODS AND MODELS FOR NUMERICAL STIFFNESS ELIMINATION

Dissertation for the degree of Doctor of Science (Technology) to be presented with due permission for public examination and criticism in the Auditorium 1314 at Lappeenranta-Lahti University of Technology LUT, Lappeenranta, Finland on the 2nd of June, 2023, at noon.

Acta Universitatis
Lappeenrantaensis 1078

Supervisor Professor Heikki Handroos
LUT School of Energy Systems
Lappeenranta-Lahti University of Technology LUT
Finland

Reviewers Associate Professor Liselott Ericson
Fluid and Mechatronic Systems (FLUMES)
Lindköping University
Sweden

Dr. Ing. Matthias Liermann
Danfoss Power Solutions
Danfoss
Germany

Opponents Associate Professor Liselott Ericson
Fluid and Mechatronic Systems (FLUMES)
Lindköping University
Sweden

Dr. Ing. Matthias Liermann
Danfoss Power Solutions
Danfoss
Germany

ISBN 978-952-335-941-3
ISBN 978-952-335-942-0 (PDF)
ISSN 1456-4491 (Print)
ISSN 2814-5518 (online)

Lappeenranta-Lahti University of Technology LUT
LUT University Press 2023

Abstract

Stanislav Ustinov
Fast and accurate simulation of fluid power circuits in the presence of small volumes using advanced methods and models for numerical stiffness elimination
Lappeenranta 2023
72 pages
Acta Universitatis Lappeenrantaensis 1078
Diss. Lappeenranta-Lahti University of Technology LUT
ISBN 978-952-335-941-3, ISBN 978-952-335-942-0 (PDF), ISSN 1456-4491 (Print), ISSN 2814-5518 (online)

The modeling and simulation of fluid power systems are essential parts of the real-time simulation of virtual prototypes of mobile working machines. In several cases, in the dynamic simulation of such fluid power systems, a longer simulation time is required. This makes the traditional mathematical models inefficient for real-time simulations, particularly when simulating fluid power systems because of the small volumes in stiff differential equations of pressure. On the other hand, the accuracy and stability of the traditional models also suffer from a numerical stiffness problem, while these models are accelerated by a reduction of the integration time steps.

To solve the problem of small volumes in stiff fluid power circuits, different explicit and implicit solvers are used. The most common methods are pseudo-dynamic methods and singular perturbation theory-based solvers. This dissertation, in addition to the existing methods, demonstrates various advanced methods and models to improve the simulation speed of stiff fluid power circuits in the presence of small volumes, and to keep the accuracy at a high level compared to the slower traditional mathematical models of such circuits.

Based on the results of the experiments performed with several fluid power circuits, which contained small volumes in their structure, the model for the Advanced Pseudo-Dynamic Solver was formulated. There are two main differences between the Advanced Pseudo-Dynamic Solver in comparison with the classical pseudo-dynamic solver. First, the calculation of the outlet volume flow rate related to the small volume is included in the inner loop of the solver, which allowed the numerical stability of the solution to be increased. In addition, the adaptive convergence criterion is proposed in the model, which allowed to increase the simulation speed and accuracy of pressure and piston position response. Obtained simulation results confirmed that the proposed solver is much more efficient in the solution of the fluid power circuits than the conventional lumped fluid theory-based method, as well as the classical pseudo-dynamic solver. Finally, the Advanced Pseudo-Dynamic Solver-based model can be calculated faster than the conventional model of the

fluid power circuit with small volumes owing to the possibility of the application of a larger integration time step.

Another effective method for the simulation of fluid power circuits is the Method of Multiple Scales. This method is based on the singular perturbation method used earlier for the real-time simulation of stiff fluid power circuits in the presence of small volumes. The results of the research showed that the method of multiple scales is much more accurate than the traditional mathematical model of fluid power circuits. Even more, the method demonstrated better accuracy performance compared to the classical singular perturbation theory-based method due to the elimination of cumulative error. The tested simulation speed of the proposed method allows for the simulation of stiff fluid power systems in real time and makes it possible to use this method in different real-time or faster than real-time applications.

The third method proposed in this dissertation is a novel hybrid model for the simulation of stiff fluid power circuits. The main feature of the model is the utilization of a recurrent neural network instead of stiff differential equations of pressure with small volume. At the same time, the dynamics of the rest system are traditionally presented with algebraic and differential equations. The testing results of the introduced hybrid model showed that this novel method can reduce the simulation time, which makes the model suitable for real-time applications. Moreover, the accuracy of the model remains at a fairly high level compared to traditional mathematical models.

Keywords: real-time simulation, small volume, numerical stiffness, fluid power system, method of multiple scales, advanced pseudo-dynamic solver, recurrent neural network

Acknowledgements

The current study was held in Lappeenranta-Lahti University of Technology, Finland, from the beginning of 2019 to the end of 2022. The research was quite challenging and demanding for me, but nevertheless, it was very interesting and the process of doctoral dissertation preparation was enjoyable.

First of all, I would like to express my gratitude to my supervisor, the head of the Laboratory of Intelligent Machines, Heikki Handroos, for his advice, high-level supervision, and guidance. Thanks to my colleagues from the Laboratory of Intelligent Machines. Additional thanks to my co-authors Julia Malysheva, Mehran Kiani-Oshtorjani and Huapeng Wu - you have all helped me a lot in the preparation of this disseration with your experience and valuable advice.

Finally, I would like to thank my parents Oleg and Svetlana, to my friends, especially to Ilya Kurinov and all the people who somehow inspired me through this challenging process.

Stanislav Ustinov
May 2023
Lappeenranta, Finland

To my parents.

Contents

List of publications

This dissertation is based on the following papers. The rights have been granted by publishers to include the papers in the dissertation.

I. J. Malysheva, S. Ustinov and H. Handroos, "Computationally Efficient Practical Method for Solving the Dynamics of Fluid Power Circuits in the Presence of Singularities," in IEEE/ASME Transactions on Mechatronics, vol. 26, no. 5, pp. 2385-2395, Oct. 2021.

II. M. Kiani-Oshtorjani, S. Ustinov, H. Handroos, P. Jalali and A. Mikkola, "Real-Time Simulation of Fluid Power Systems Containing Small Oil Volumes, Using the Method of Multiple Scales," in IEEE Access, vol. 8, pp. 196940-196950, 2020.

III. S. Ustinov, H. Wu and H. Handroos, "A Hybrid Model for Fast and Efficient Simulation of Fluid Power Circuits With Small Volumes Utilizing a Recurrent Neural Network," in IEEE Access, vol. 10, pp. 48824-48835, 2022.

Author's contribution

Publication I.

The article was produced jointly with Julia Malysheva. The Author was responsible for the modeling and testing of the pseudo-dynamic solver separately, and partly responsible for literature research and further modifications of the pseudo-dynamic solver to obtain an advanced pseudo-dynamic solver and tests of the final advanced pseudo-dynamic solver. The writing and revision of the article was also partly provided by the author.

Publication II.

The article was produced as a joint research project with Mehran Kiani-Oshtorjani. The Author was responsible for fluid power circuit parameter determination, modeling and simulation, stiffness analysis of the system and partly responsible for literature research, tests of the Method of Multiple Scales system and writing of the research article.

Publication III.

The Author was responsible for literature research, modeling and simulation of classical fluid power circuit models, modeling and training of NARX Recurrent neural network used for the development of a hybrid model for both fluid power circuits used in the paper. The Author implemented the neural network to the classical fluid power circuit models. Simulation tests and simulation data preparation were also done by the Author. In addition, the Author was also fully responsible for writing, revisions, and proofreading of the article.

Nomenclature

Latin alphabet

A	Area
$a_1 ... a_3$	Empirical constants
B_e	Effective bulk modulus
$C_1 ... C_9$	Empirical constants
C_d	Discharge coefficient
C_v	Valve flow constant
E_{max}	Maximum bulk modulus of the oil
F	Force
F_c	Coulomb friction force
F_s	Static friction force
F_μ	Friction force
K, k_t	Semi-empirical flow coefficients
K_v	Valve gain
k_v	Viscous friction coefficient
m	Mass
p	Pressure
Q	Volumetric flow rate
S_c	Full stroke of the cylinder
t	Time
T_n	Time variable
U	Input voltage
V	Volume
V_{dead}	Dead volume
v_s	Sliding speed coefficient
x	Cylinder piston displacement

Greek alphabet

α	Quadratic area ratio
Δp	Pressure drop
Δt	Time step
ε	Infinitesimal parameter in Singular Perturbation Theory
ζ	Damping ratio
κ	Condition number
λ	Eigenvalue of Jacobian matrix
ρ	Density
σ_0	Flexibility coefficient
σ_1	Damping coefficient
ψ	Nonlinear mapping
ω_n	Natural angular frequency

Superscripts

$iter$	Current value of parameter
$prev$	Value of parameter at previous iteration

Subscripts

e	Effective
H	Number of layers
$lowlimit$	Low limit of parameter
min	Minimum value
max	Maximum value
$pseudo$	Parameter inside the inner loop of Pseudo-Dynamic Solver
s	Supply
t	Tank
$tolhigh$	Higher tolerance criterion
$tollow$	Lower tolerance criterion

Abbreviations

ANN	Artificial Neural Network
AdvPDS	Advanced Pseudo-Dynamic Solver
GRU	Gated Recurrent Unit neural network
LSTM	Long Short-Term Memory neural network
MMS	Method of Multiple Scales
MSE	Mean-Square Error
NARMAX	Nonlinear Autoregressive Moving Average network with Exogenous inputs
NARX	Nonlinear Autoregressive network with Exogenous inputs
NFIR	Nonlinear Finite Impulse Response neural network
ODE	Ordinary Differential Equations
RNN	Recurrent Neural Network
RRMSE	Relative Root-Mean-Square Error
SPT	Singular Perturbation Theory

1 Introduction

1.1 Background of the research

Nowadays, computer simulation of mobile working machines and industrial robots is a very important part of the global industry. Virtual models and prototypes are used to predict important parameters of machines and devices and to improve the business potential of related companies. Mechanics and hydraulics play an important role in modeling such machines. Fluid power systems, which are widely used in the real-life design of various mobile machines, such as logging harvesters, cranes, excavators, and industrial robots, are in strong need of modeling. The recent trend in modeling hydraulically driven digital twins (Zhidchenko et al., 2018) and virtual prototypes (Mikkola, 1999; Park et al., 2020; I. Malysheva et al., 2018; Zheng, Ge, and Liu, 2015) has shown that mathematical modeling of fluid power systems plays a vital role in the development of industrial simulators of such mobile working machines. For this purpose, real-time and faster than real-time techniques (Liermann, Feller, and Lindinger, 2021) are often used to get a fast response in the system. Real-time simulation in this case refers to the use of a computer or other device to simulate a system or process in real time. In this type of simulation, the simulation model is run in parallel with the real system, and the output of the simulation is used to control or interact with existing system. However, singularities may exist in the computer simulation of fluid power circuits that directly affect the computational speed of the whole virtual mobile working machine system and make a real-time simulation of the system very difficult or totally impossible.

Generally speaking, there are two main problems with singularities arising in fluid power circuit modeling and simulation. The first problem is related to the pressure drop approaching zero in fluid power circuits. This phenomenon is associated with difficulties in the use of the traditional turbulent flow orifice equation in the mathematical model of the circuit because of the infinite value of the flow rate derivative. To overcome this problem, several combined orifice models were proposed by Ellman and Piché, 1996; Ellman and Piché, 1999. Another computationally efficient solution was suggested in a research paper by Åman, Handroos, and Eskola, 2008 in which the polynomial relation between the flow rate and pressure drop was derived for cases when the pressure drop approaches zero. The model got its name from the two-regime flow model in which the third-order polynomial is used for describing the laminar and transition flow areas, whereas the traditional square root turbulent orifice equation of flow is used for the turbulence regime.

Another important issue in the computer simulation of the dynamics of various fluid power circuits is associated with the numerical stiffness of ordinary differential equations (ODE) (Curtiss and Hirschfelder, 1952), for example in continuity equations of volumetric flow. The numerical stiffness in fluid power circuits can be explained by the fact that

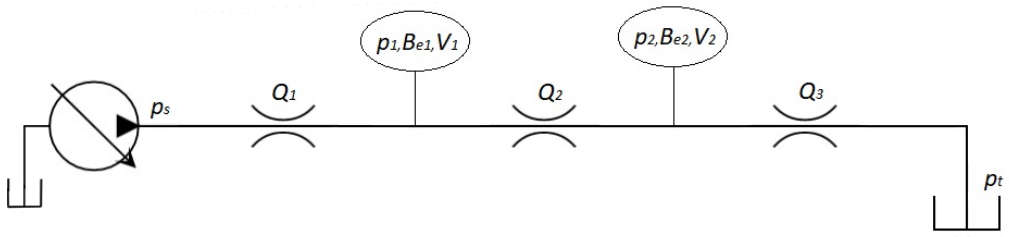

Figure 1.1: Simple three-orifice fluid power circuit (Ustinov, Wu, and Handroos, 2022).

such circuits include volumes of different orders of magnitude. This can affect the numerical integration of ODEs, and classical explicit integration solvers and subroutines are not able to generate a stable dynamic response at a high integration time step in dynamic simulation, slowing it down by implementing significantly small time steps. The numerical stiffness of fluid power circuits can often be associated with small pipe volumes or high values of effective Bulk modulus in a fluid power circuit. However, the problem of small volumes is the most important due to existence of such pipe volumes in a big number of industrial fluid power systems. The solution for the fluid power circuits with one or more small volumes is necessary to be derived by using special numerical solvers to avoid the problem of numerical instability in a dynamic simulation model of such stiff circuits (Piché and Ellman, 1994).

To demonstrate the effect of small volume on the simulation, we may assume that a simple, three-orifice fluid power circuit, as depicted in Figure 1.1, contains a small pipe volume V_2 between the second and third orifice. Generally, the circuit contains the constant pressure variable displacement pump, which is assumed to be an ideal flow source and tank for recovery of the fluid. We assume that circuits are modeled traditionally, with Lumped-element modeling and a 4th order Runge–Kutta subroutine as the integrator for solving differential equations existing in the system. In this case, the computer simulation of such a circuit will be slower than the same circuit with volume V_2, for instance, one hundred times bigger than the small volume under consideration. Consequently, a small volume in the circuit generates a stiff differential equation of pressure. This means, that the pressure p_2 response in a 50-second computer simulation of a circuit with a bigger volume V_2, which is equal to 1 liter, will be the same at both integrator time steps 1×10^{-4} s and 1×10^{-3} s, which is observable from Figure 1.2a. In its turn, the 50-second simulation of the stiff fluid power circuit gives totally different pressure responses at the time steps of 1×10^{-4} s and 1×10^{-3} s, as seen from Figure 1.2b. Hence, the simulation of a fluid power circuit with small volume requires more real time to simulate the same time period due to the difference in integrator time step in one order: the correct response of

the stiff circuit can be achieved only at the time step of 1×10^{-4} s. In the case of a mobile working machine, which fluid power circuit may contain several small volumes, the simulation in real time or faster than real time can be problematic.

The problem with small volumes, and, as a result, the numerical stiffness of differential equations in the fluid power circuits, arises in various scientific papers, and special implicit (Åman, 2011) solvers are developed. This problem was first mentioned in 1990 by Bowns and Wang, 1990, who proposed an implicit iterative technique to overcome the problem of numerical stiffness due to the small volumes in hydraulic pipes. However, the technique was still computational time demanding due to a large amount of iterations in the loop, which also affects simulation speed.

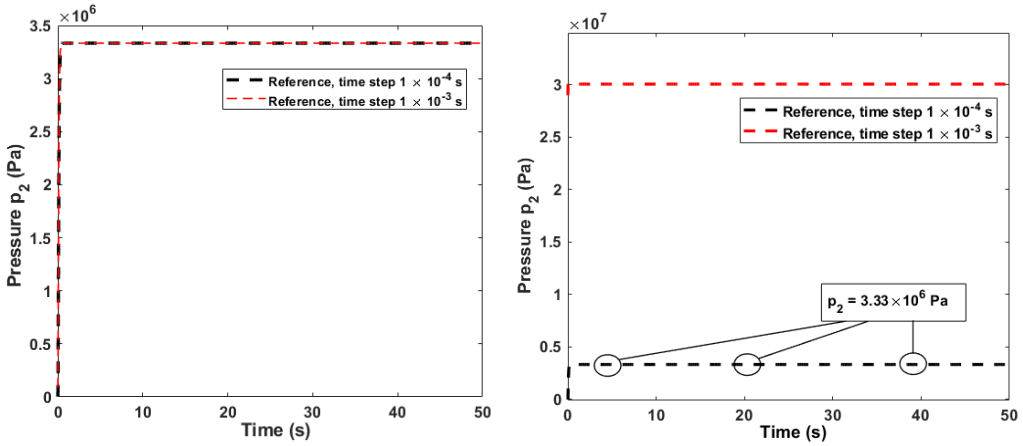

(a) (b)

Figure 1.2: Pressure p_2 response at simulation time steps 1×10^{-4} and 1×10^{-3} with big and small volume V_2: (a) Volume $V_2 = 1$ l (b) Volume $V_2 = 0.01$ l (small volume) (Ustinov, Wu, and Handroos, 2022).

Another effective iterative technique was first presented by Åman and Handroos, 2008; Åman and Handroos, 2009; Åman and Handroos, 2010. This implicit solver was named the Pseudo-Dynamic Solver. This solver consists of two loops, an outer (or main) loop, and an inner (or pseudo) loop. The main loop contains algebraic and differential equations of the whole fluid power system, excluding the stiff differential equation of pressure associated with the small volume in the circuit. The integration of such continuity equation of volumetric flow occurs in the pseudo loop of the solver with an artificially enlarged volume instead of the real small volume in the system's mathematical model. The main purpose of the pseudo loop is to receive the steady-state response of the pressure by iterating such pressure with artificial volume until the predefined convergence criterion for

pressure derivative or pressure difference between two neighboring iterations is reached.

One of the most reliable methods proven to be computationally efficient in simulating fluid power systems, in theory and practice, is the fluid power circuit model proposed by Kiani-Oshtorjani, Mikkola, and Jalali, 2019. This model is based on the singular perturbation theory. In the concept of this approach lies the idea of the substitution of stiff ODEs with small volumes for algebraic equations, modified for fluid power systems simulation in accordance with this theory. The method was also tested in simulating multibody systems with fluid power components (Rahikainen et al., 2018), and an accurate and fast response of the system was achieved. However, the method has its own drawbacks related to the cumulative error in certain cases of use. To solve the problem of cumulative error, a special corrector factor for the model should be used.

A very significant contribution to the topic of simulation of fluid power circuits was made by numerous research carried out by the research group of Petter Krus at Linkoping University (Krus et al., 1990; Krus, 2009; Axin et al., 2010; Braun and Krus, 2012; Braun and Krus, 2013; Baer, Ericson, and Krus, 2020), which was started in the 1990s and continues to the present day. The study led to the development of HOPSAN simulation software. This software is based on the transmission line method, the main idea of which is based on the statement that each physical element has a natural time delay. In the case of fluid power circuits, the time delay is the same order of magnitude compared to the time step utilized for numerically stable and accurate simulation of the fluid power circuit (Braun, Nordin, et al., 2020). As the result, HOPSAN simulation software implements this idea by use the discretization for hydraulic capacitive elements or, in simple words, dividing the circuit into separate components and simulating these components separately. Each separated component of the circuit is simulated with the implementation of a local implicit solver, which allows the elimination of the problem of numerical stiffness in circuits with small volumes as well. As a result, the transmission line method is a robust and convenient method that allows us to maintain the accuracy of simulation response and the high speed of simulation at the same time with physically interpreted transmission delay of pressure in fluid power elements by the limitation of speed of sound (Liermann, Feller, and Lindinger, 2021). To the present day, the method is one of the excellent solutions for simulating fairly complex hydraulic systems in real-time or faster than real-time applications. However, it is important to note that in this study we consider methods that have no huge effect to the large-scale dynamics, and modifications that are done to the models are minimal, since in case of transmission line method, all the components are calculated separately with purpose to speed up the whole simulation of the system. Moreover, more computational power can be used for this kind of co-simulation problem.

In several works (Bidini and Mariani, 1997; Krishna and Bares, 1999; Krishna and Bares,

1998), the components of fluid power systems, or the entire fluid power circuits, were introduced as Artificial Neural Networks(ANN) with input, output and multiple hidden layers. The utilization of this type of system modeling showed that the use of neural networks in fluid power circuit modeling guarantees a fast response in the system that allows a simulation of the system in real-time or faster than real-time applications. In addition, predictive neural network models of various dynamic systems with ODEs were studied in (Pan and Duraisamy, 2018) and (Chen et al., 2018). New methods were proposed in both papers in order to improve the performance of ANNs based on simple ODEs and complex nonlinear dynamic systems. Nevertheless, the most significant and beneficial simulation results were obtained by using recurrent neural networks (RNN) (J. Malysheva, Li, and Handroos, 2020; Vermaak and Botha, 1998; Patel and Dunne, 2003) in the modeling and simulation of different dynamic systems, including fluid power circuits.

However, the systems based on neural networks are simulated as a black box, and the dynamics of the system used in the network, are totally neglected. Substituting a stiff differential equation with small volumes with a computationally efficient and accurate neural network can be a viable solution for the problem of singularity arising in the simulation of such stiff fluid power systems. It means that it is only possible to replace areas with stiff differential equations with the ANN, and the dynamics of the entire system will be saved in the rest of the mathematical model of fluid power circuit. At the same time, the speed of simulation is supposed to be improved due to the absence of stiff differential equations in the areas with small volumes.

Since the problem of numerical stiffness is a problem of current interest in the field of modeling and simulation of hydraulically driven mobile working machines, the motivation of the research work done in this dissertation is associated with the possibility of enhancement, or creation of stiffness elimination methods, solvers, and models. A lot of existing methods and models have a great number of disadvantages that can be overcome by modifying or by reinforcing the operation of such methods. In addition, new techniques should be tested in order to find other fast and accurate solutions to the problem of numerical stiffness.

1.2 Research questions

The research problem of the study is formed from the issue of the numerical stiffness of fluid power circuits due to the small volumes inside. This is an actual problem that still requires the reconsideration of existing methods of numerical stiffness elimination and searching for new methods and models in order to improve the computer simulation of mobile working machines and fluid power circuits in particular. The main research questions of the study are as follows:

1. Test the existing methods of stiffness elimination in fluid power circuits, for example Pseudo-Dynamic Solver and Singular Perturbation theory-based model. Which disadvantages exist in these methods and models, and what can be done to improve the accuracy and speed-up practical fluid power circuits modeled with these methods?

2. How can a classical Pseudo-Dynamic Solver be improved to obtain a stable and fast response from the pressure in small volumes in any type of fluid power circuits and for each pressure level?

3. How can the problem of accuracy for Singularly Perturbed circuits be solved without using any correcting factors?

4. Is it possible to use Artificial neural networks as surrogate in practical fluid power circuits, substituting a stiff differential equation with small volumes with the above-mentioned neural network to eliminate the system stiffness?

1.3 Research methods

The main objective of the literature review performed in subsection 1.1 of the introduction was to analyze the state-of-the-art approaches, solvers, and fluid power models dealing with the problem of numerical stiffness in presence of small volumes. It was investigated that state-of-the-art methods still can have a number of disadvantages, for example, accumulated error, or poor simulation speed in particular cases and conditions. Provided methods were analyzed in order to obtain the most significant issues and research methods for the problem solution were observed.

The main tools for the verification of proposed algorithms, solvers, and models were simulation experiments where models were based on mathematical modeling and computer simulation using Lumped-element modeling as the main method for conventional fluid power circuits mathematical modeling and simulation software for fluid power circuit parameter response observations. All the novel algorithms and methods were compared with the conventional mathematical model of two different practical fluid power circuits that were modeled and simulated, firstly using conventional Lumped-element modeling and secondly, the algorithms and models developed in this research.
Through experiments and testing of the pseudo-dynamic solver, it was important to find out what parameters affect the simulation and integration speed and the accuracy of the pressure response, and what can be done to improve these significant values. Thus, an improved AdvPDS-based model was formed with an adaptive criterion of convergence depending on the empirically studied pressure calculated in the internal loop of the solver.

In the case of the MMS-based model, the multiple-scale analysis approach was applied to the singularly perturbed model of a practical fluid power circuit in order to eliminate the cumulative error occurring in singularly perturbed systems. Experiments were not only aimed at comparison of MMS-based and conventional Lumped-element modeling method-based fluid power circuit model but also have taken into account singularly perturbed model to show the difference in simulation speed and accuracy of the proposed model.

The use of artificial intelligence was considered a positive direction for the elimination of numerical stiffness problem related to small volumes since RNNs are robust and reliable in predicting time series problems (e.g. dynamic systems simulation through time). Then, the RNN was used to formulate the Hybrid model, which particularly utilizes the network as a surrogate to substitute stiff equation of pressure and other parts of the system work with the conventional Lumped-element modeling method.

1.4 Scientific contribution

The main scientific contribution of the dissertation is associated with the development of new methods and models that can be beneficial in the simulation of numerically stiff fluid power circuits. These methods and models are developed in a way to find a trade-off between simulation speed and accuracy of the system response. These research findings are as follows:

- Advanced Pseudo-Dynamic Solver (AdvPDS). This solver is based on a classical Pseudo-Dynamic Solver with reconsideration of its structure. Two new main principles are lying in the basis of AdvPDS, comparing it to the classical solver: the consistency and adaptivity. Consistency means that all flow rates and pressure in the small volume itself are calculated inside the loop of the solver. Adaptivity means the use of adaptive criterion of convergence, depending on the pressure levels of the system. Adaptive criterion allows discovery of the trade-off between simulation speed and accuracy of the system response, while using the single criterion in a classical Pseudo-dynamic Solver in several cases can slow-down the system, or vice-versa make it fast, but inaccurate.

- Method of Multiple Scales (MMS). This method works together with the Singular Perturbation Theory. MMS was tested in the simulation of practical fluid power circuits, and the results of the testing showed that numerically stiff fluid power circuits can be speed up by substitution of a stiff differential equation by an MMS based equation; at the same time, there is no cumulative error, which may exist in Singularly Perturbed fluid power systems.

- Hybrid fluid power circuit model. The word "Hybrid" is related to the utilization of pre-trained RNN inside the traditional fluid power circuit model, where it substitutes the stiff equation of pressure in a small volume. The method allows for the reduction of numerical stiffness of the whole system and significantly speeds up the simulation with a high accuracy of pressure response.

1.5 Dissertation outline

The main purpose of the dissertation is to demonstrate the results of multiple research related to the development of advanced models for the numerical stiffness elimination of fluid power circuits in the presence of small volumes. The structure of the dissertation is divided into the following parts:

1. Section 1 - Introduction. The current section describes the background of the research and sheds light on the research problem, the main research questions, and scientific contribution of the dissertation.

2. Section 2 - Research methods. This section of the dissertation describes all research methods used in research related to the topic of the dissertation. Research methods include the Lumped-element modeling, which is used in the traditional mathematical modeling of fluid power circuits, the existing method of numerical stiffness elimination, such as Pseudo-Dynamic Solver of pressure in small volumes, and Singular perturbation theory. The theoretical background of Recurrent neural networks for hybrid fluid power circuit modeling is also included in this section.

3. Section 3 - Fluid power circuits under investigation. This section contains the main issues in traditional mathematical modeling of fluid power circuits used in research tests related to this dissertation. The section includes detailed models of such circuits with equations and system parameters.

4. Section 4 - Advanced methods for numerical stiffness elimination: Tests and results. This section is related to the introduction of the main findings of the current research study. The Advanced Pseudo-Dynamic solver, Method of Multiple Scales, and Hybrid method of modeling fluid power circuits are introduced and tested in this section. Results of the tests are also presented.

5. Section 5 - Conclusion. This section is a short summary of the dissertation, which contains the research discussion and the direction for the future studies and research.

2 Theoretical background

This section is a collection of the theoretical background of the present dissertation. The theory of the section includes the conventional methods, such as lumped-element modeling, used in traditional mathematical modeling of fluid power circuits. The Pseudo-dynamic solver and Singular Perturbation Theory used in the development of the Advanced Pseudo-Dynamic Solver and the Method of Multiple Scales model are described as the main existing methods of numerical stiffness elimination. A theoretical detailed description of recurrent neural network architecture models, considered in the development of the hybrid model, was also included in to the present section.

2.1 Lumped-element fluid power modeling

Lumped-element modeling is a prevalent method used in the traditional modeling of fluid power circuits of various complexity. All hydraulic components and volumes in fluid power circuits can be represented in accordance with this method, which assumes that a fluid power system can be divided into sections with separate volumes, where the pressure can be distributed. Such sections are separated by orifices or throttles, which are representatives of volumetric flows in a fluid power circuit. Flow control valves, directional valves, or any valve-type component of fluid power circuits are also expressed as throttles. A differential equation is formed for each pressure in such a fluid power system, where the derivative of pressure can be expressed with the general formula (Merritt, 1967):

$$\dot{p}_i = \frac{B_e}{V_i}(Q_i - Q_{i+1} - \frac{dV_i}{dt}) \tag{2.1}$$

where p_i is the pressure in ith section, B_e is the effective bulk modulus, V_i is the volume in the same section, Q_i and Q_{i+1} are the inlet and outlet volumetric flows, and $\frac{dV_i}{dt}$ is the time rate changes of volume V_i.

The common equation for the expression of turbulent flow for classic run-off orifice can be calculated as follows (Borutzky, Barnard, and Thoma, 2002):

$$Q_i = C_d A_i \sqrt{\frac{2(p_{i-1} - p_i)}{\rho}} \tag{2.2}$$

where C_d denotes the discharge coefficient, A_i is the cross-sectional area of orifice i, ρ is the density of the hydraulic fluid, and p_i and p_{i-1} are the outlet and inlet pressures, respectively. In this research study, this equation appears in the modeling of simple three-orifice fluid power circuits. The modified version of the equation is used in the modeling of the directional and flow control valves in related fluid power circuits, described later in Section 3.

2.2 Numerical stiffness determination

Assume that we have simple fluid power circuit of three orifices in series, described in Section 1 and depicted in figure 1.1. The circuit contains a small pipe volume V_2 between the second and third orifice. Pressures and flows in such system are calculated with equations (2.1) and (2.2), respectively. We can analyze the numerical stiffness, as well as the influence of volume size on the stiffness of the presented fluid power circuit, by deriving the Jacobian matrix and estimating the dominant eigenvalues of the matrix. The initial step is to derive the state-space representation of the circuit. It is assumed, that we have constant effective bulk modulus B_e, and the orifices are identical, which leads to the same discharge coefficient C_d and area for all three orifices. In the case of state variables vector as $\mathbf{x} = [x_1\ x_2]^T = [p_1\ p_2\ ]^T$ and input $u = p_s$ (input pressure), we may derive the state equations as follows:

$$\dot{x_1} = \frac{B_e C_d A}{V_1}\left(\sqrt{\frac{2(u-x_1)}{\rho}} - \sqrt{\frac{2(x_1-x_2)}{\rho}}\right) \tag{2.3}$$

$$\dot{x_2} = \frac{B_e C_d A}{V_2}\left(\sqrt{\frac{2(x_1-x_2)}{\rho}} - \sqrt{\frac{2(x_2-p_t)}{\rho}}\right) \tag{2.4}$$

Then, Jacobian matrix is formed by extracting partial derivatives of state equations, as follows:

$$\mathbf{J} = \frac{\partial \mathbf{F}}{\partial \mathbf{x}}\bigg|_{\mathbf{x}=\bar{\mathbf{x}},\mathbf{u}=\bar{\mathbf{u}}} \tag{2.5}$$

where $\mathbf{F}$ is the left-hand side of the first and second equation of (state space) , $\mathbf{x}$ is the model state vector, $\mathbf{u}$ is the model input vector, and $(\bar{\mathbf{x}}, \bar{\mathbf{u}})$ is the operating point. The Jacobian matrix for the considered three orifice fluid power circuit can be written as follows:

$$\begin{bmatrix} -\frac{B_e C_d A}{\sqrt{2}\rho V_1}\left(\frac{1}{\sqrt{(x_1-x_2)/\rho}} + \frac{1}{\sqrt{(u-x_1)/\rho}}\right) & \frac{B_e C_d A}{\sqrt{2}\rho V_1\sqrt{(x_1-x_2)/\rho}} \\ \frac{B_e C_d A}{\sqrt{2}\rho V_2\sqrt{(x_1-x_2)/\rho}} & -\frac{B_e C_d A}{\sqrt{2}\rho V_2}\left(\frac{1}{\sqrt{(x_2-p_t)/\rho}} + \frac{1}{\sqrt{(x_1-x_2)/\rho}}\right) \end{bmatrix} \tag{2.6}$$

To assess the degree of numerical stiffness of the model, we utilize a condition number of the Jacobian matrix, which can be expressed as per the principles of numerical analysis theory:

$$\kappa(\mathbf{J}) = \frac{|\lambda_{max}(\mathbf{J})|}{|\lambda_{min}(\mathbf{J})|} \tag{2.7}$$

where $\lambda_{min}(\mathbf{J})$ and $\lambda_{max}(\mathbf{J})$ are the maximum and minimum eigenvalues of the Jacobian matrix, respectively, which for $\mathbf{J} \in \mathbf{M}_{n\times n}$ should satisfy $|\mathbf{J} - \lambda\mathbf{I}| = \mathbf{0}$, where $\mathbf{I}$ is the identity matrix. The condition number provides insight into the disparity of the system's eigenvalues, wherein low values of κ indicate favorable conditioning of the problem, while high values of κ suggest that the problem is ill-conditioned and that the system can be numerically stiff. Determining the condition number requires specifying the system configuration, or operating point selection. Under physical restrictions of the system we can select operating point, where our state variables and inputs are determined.

In case of particular three-orifice circuit, we shall examine two scenarios in selected operating point. In the first scenario, $V_2 = 10^{-3}\ m^3$, which implies that the volume between second and third orifice is relatively substantial. In this case, the condition number κ will be small, showing that system is not stiff. On the other hand, in the second scenario, the volume is reduced to $V_2 = 10^{-5}$ m^3, and the corresponding condition number surges significantly to larger numbers. An assessment of the system Jacobian matrix reveals that this phenomenon results from the small volume V_2, which emerges in the denominator of the Jacobian matrix elements, leading to substantial differences in the magnitude of the eigenvalues and causing the mathematical model to become numerically stiff. Thus, we get a rather high numerical stiffness for systems in which there is at least one small volume

2.3 Existing methods of numerical stiffness elimination

2.3.1 Pseudo-dynamic method

The Pseudo-Dynamic Solver, which belongs to a family of implicit iterative solvers, was initially proposed by Åman and Handroos, 2008. The solver was also studied and improved in subsequent research, particularly in (Åman and Handroos, 2009; Åman and Handroos, 2010). The main concept of the pseudo-dynamic solver lies in searching for a steady-state solution for pressures related to small volumes in stiff fluid power circuits. At the same time, the pressures built up in larger volumes are solved with the conventional integration algorithms, e.g., 4th order Runge–Kutta integrator. To provide such functioning of the system, two integration loops are used in the system: the main loop, which contains algebraic and differential equations related to larger volumes, and the inner loop, associated with the model of pressure with the small volume. The inner loop, using an artificially enlarged fluid volume, searches for the steady-state value of pressure passing by the transition process of pressure formation. The steady-state value of pressure is sought out during the single time step of the main loop (J. Malysheva, Ustinov, and Handroos, 2021).

In the inner loop of the Pseudo-Dynamic Solver, the continuity equation of pressure is utilized as a main pressure-modeling equation, as follows:

$$\dot{p} = \frac{B_e}{V_{pseudo}}(Q_{in} - Q_{out}) \tag{2.8}$$

where V_{pseudo} is the artificial pseudo-volume, B_e is the effective bulk modulus of the oil, and Q_{in} and Q_{out} are the inlet and outlet volumetric flows, respectively. According to Åman and Handroos, 2009, the pseudo-volume is recommended to be set at least 10 times higher than the actual small volume used in the mathematical model. The inlet and outlet volumetric flows in the inner loop of the solver can be defined as a function of pressure drop accordingly:

$$Q = f(\Delta p) \tag{2.9}$$

The integration of differential equation 2.8 inside the inner loop of the solver occurs by using an explicit fixed-step, fourth-order Runge–Kutta integration subroutine, with independent sufficiently small time step t_i. The operation of the inner loop continues until the convergence criterion is satisfied. The criterion is a parameter, which is pre-defined by the user and represents the first derivative of the pressure. It is important to note that the activation of the inner loop suspends the main loop until the steady-state pressure value in the inner loop is found.

2.3.2 Singular perturbation theory

Singular perturbation theory (SPT), as a valid method for numerical stiffness elimination, was first mentioned by Åman, 2011. Later, the fluid power circuit model, based on the modification of SPT, was firstly introduced by Kiani-Oshtorjani, Mikkola, and Jalali, 2019.

In SPT problems, a small parameter existing in the governing equation plays a key role. The regular perturbation treats the problems in which the solution can be obtained by assigning the small parameter to zero, whereas in the singular perturbation problems, the mentioned parameter cannot be ignored without a considerable loss of accuracy in the results. For instance, in such cases, when the bulk modulus divided into hydraulic volume is small, the continuity equations of volumetric flow fall into the latter category. A well-known approach for perturbation problems of the latter type is the SPT. As mentioned in the work of Kiani-Oshtorjani, Mikkola, and Jalali, 2019, with this theory, the ordinary differential equations, that contain the infinitesimal parameter ε, are converted into a quasi-steady state model based on Tikhonov's theorem (Tikhonov, 1952) in SPT. Consider the following system of singular equations:

$$\dot{\phi} = f(\phi, \psi, t, \varepsilon) \qquad \phi(t_0) = \zeta(\varepsilon) \tag{2.10a}$$
$$\dot{\psi} = g(\phi, \psi, t, \varepsilon) \qquad \psi(t_0) = \xi(\varepsilon) \tag{2.10b}$$

where $\phi \in R^m$ and $\psi \in R^n$ and ε is an infinitesimal parameter. Then, the quasi-steady state model of the system in 2.10a is (Noethen and Walcher, 2011):

$$\dot{\phi} = f(\phi, h(t,\phi), t, \varepsilon) \qquad \phi(t_0) = \zeta(\varepsilon) \tag{2.11a}$$
$$\bar{\psi}(t) = h(t, \bar{\phi}) \tag{2.11b}$$

where the over-bar denotes the perturbed variables, and h is an algebraic equation that is determined during the order reduction. The i-th volume can be considered as a small fluid volume in comparison with the neighboring volumes in the circuit. Consequently, applying the SPT to this volume, we can get (Kiani-Oshtorjani, Mikkola, and Jalali, 2019):

$$p_i = \frac{p_{i+1} + \alpha p_{i-1}}{1 + \alpha} \tag{2.12}$$

where, $\alpha = \left(\frac{A_{i-1}}{A_{i+1}}\right)^2$. The substitution of this relation to the volumetric flow continuity equation with the small volume reducing the stiffness of the whole circuit due to the replacement of stiff differential equation by the algebraic. However, the model is not perfect, and it requires a corrector factor in order to avoid the accumulative error that may be produced by the model.

2.4 Recurrent neural networks for fast simulation of fluid power circuits

Speaking about the fast and accurate simulation of fluid power circuits, the use of Artificial Neural Networks (ANN) should be considered. The most suitable type of neural network used for the simulation of dynamic systems, and fluid power circuits as well, is the Recurrent Neural Networks (RNN). Several studies prove that dynamic systems based on RNNs are quite fast and can be simulated in real time or faster than real time, which can be beneficial for different related simulation applications. However, recurrent neural networks can be different types or architectures, and selection of RNN architecture is a very important issue in the modeling of dynamic systems.

The most common RNN architectures used in modeling dynamic systems are the nonlinear finite impulse response (NFIR), the nonlinear autoregressive network with exogenous inputs (NARX), and the nonlinear autoregressive moving average network with exogenous inputs (NARMAX). There are also more complex and advanced architectures used

in dynamic systems modeling, which are Long Short-Term Memory (LSTM) and Gated Recurrent Unit (GRU) neural networks (Ustinov, Wu, and Handroos, 2022).

The NFIR architecture, described in (Schram, Verhaegen, and Krijgsman, 1996), is the simplest RNN architecture of all the architectures mentioned above. The operating process of this network occurs through feeding all values of past inputs to achieve the current output value. The defining equation for the network is formulated as follows:

$$y(t) = \Psi_H(x(t-1),...,x(t-d)) \tag{2.13}$$

where $y(t)$ is the RNN output vector at time t, Ψ_H is mapping performed by a multilayer feedforward network, d is the past values of series $x(t)$, and $x(t)$ is the RNN input vector at time t. The main advantage of the NFIR architecture is its stability, while all past inputs are fed to the network.

The NARX neural networks principle is related to the utilization of the outputs of the network for feeding the input with past states of the outputs and inputs, while saving the state of the system at every step of the network operation. The ordinary NARX RNN can be defined by the following equation (Siegelmann, Horne, and Giles, 1997):

$$\begin{aligned} y(t) = \Psi_H(&x(t-1),...,x(t-d),\\ &y(t-1),...,y(t-d)) \end{aligned} \tag{2.14}$$

where $y(t)$ is the RNN output vector at time t. The main feature of the NARX RNN is an accurate approximation of output values, which make it more accurate than NFIR. However, in certain cases, it can be inherently less stable due to operation in a closed loop using the past values of the output.

Another architecture that can be presented as an advanced NARX structure is NARMAX RNN. The main difference with NARMAX RNN architecture is the ability to use the error of previous values in the loop through the feedback. Thus, the defining equation for NARMAX networks is the following (Lacny, 2012):

$$\begin{aligned} y(t) = \Psi_H(&y(t-1),...,y(t-d),\\ &x(t-1),...,x(t-d),\\ &e(t-1),...,e(t-d)) \end{aligned} \tag{2.15}$$

where $e(t-1)$ is an RNN error vector at time $t-1$. In the NARMAX architecture, all elements defined by x and e are sometimes called controlled and uncontrolled inputs (J. Malysheva, Li, and Handroos, 2020). This means that NARMAX is the most prevalent architecture in cases with real-world data, including the system error generated by noise. The structure also uses the error supplied through the system feedback as an input dataset,

which makes the method more complex than the above-mentioned NFIR and NARX.

In addition to the mentioned RNN architectures, more complex architectures are used in dynamic systems modeling. These architectures are more suitable for training and may easily store long-term dependencies. Such architectures, which are LSTM and GRU neural networks, were studied and compared (Tuttle et al., 2021). Both architectures show significantly good performance in the case of complex dynamics persisting in the system. In the case of LSTM networks, the accuracy of predictions is at a high level, but selecting numerous hyperparameters can affect the performance of the network. GRU networks are similar to LSTM due to their functionality; however, in several cases, it can be applied in less time to train the network.

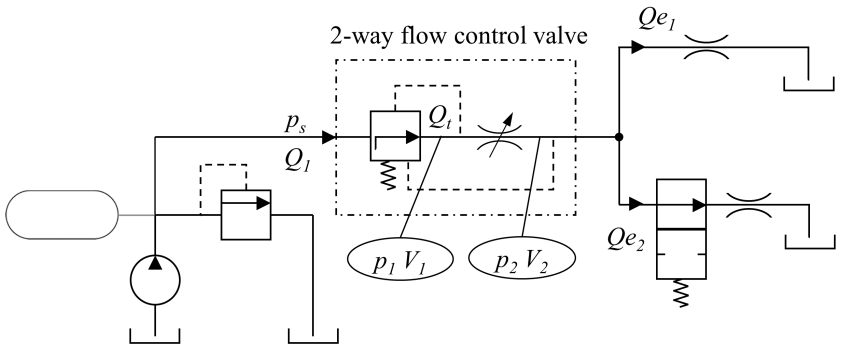

Figure 3.1: Two-way flow control valve schematic (J. Malysheva, Ustinov, and Handroos, 2021).

3 Stiff fluid power circuits under investigation

In this subsection, the two fluid power circuits that were utilized in simulation experiments of advanced stiffness elimination methods were introduced. First, the circuits were modeled as a conventional mathematical model based on Lumped-element modeling method with 4th order Runge–Kutta integration subroutine. These mathematical models of the circuits will be marked as "Reference" models in further tests and simulations. Both circuits contain a small pipe volume. The modified versions of the circuits were used in demonstration of AdvPDS, MMS and Hybrid methods, and models of stiffness elimination.

3.1 Circuit 1: Two-way flow control valve

The first circuit investigated in the study is a two-way flow control valve. The fluid power circuit related to the corresponding system is schematically depicted in Fig. 3.1. The circuit scheme contains of a pressure power source, two-way flow control valve, orifice, and a 2/2 directional control valve. A two-way flow control valve, in its turn, consists of two main components: pressure compensator and control throttle. The volume between the components of two-way flow control valve is assumed to be a small volume in continuity equation of volumetric flow, the presence of which increases the stiffness of the whole circuit. The power source is assumed to be an ideal flow source with constant pressure. It is composed of a hydraulic accumulator, pump, pressure relief valve, and tank. To reach the tank, the hydraulic fluid flow passes through a two-way control valve and two orifices after the valve. One of the orifices is an ordinary sharp-edged orifice, whereas the other is a 2/2 directional control valve, the opening of which is controlled by signal U_d. Pressure in the circuit under consideration can be integrated from the following continuity

equations of volumetric flow:

$$\dot{p}_1 = \frac{B_e}{V_1}(Q_1 - Q_t) \tag{3.1}$$

$$\dot{p}_2 = \frac{B_e}{V_2}(Q_t - Q_{e1} - Q_{e2}) \tag{3.2}$$

where B_e is the effective bulk modulus of oil, V_1 and V_2 are volumes of pipelines, where V_1 is a small volume between the pressure compensator and control throttle, Q_1 and Q_t are volumetric flows through the pressure compensator and control throttles, respectively, and Q_{e1} and Q_{e2} are orifice and directional control valve volumetric flows, respectively. Volume flows Q_1 and Q_t can be obtained as follows:

$$Q_1 = K\sqrt{|p_s - p_1|}sign(p_s - p_1) \tag{3.3}$$

$$Q_t = k_t\sqrt{|p_1 - p_2|}sign(p_1 - p_2) \tag{3.4}$$

where p_s is the supply pressure, K and k_t are the semi-empirical flow coefficients for the pressure compensator throttle and for the control throttle, respectively, which are integrated from the following differential equations:

$$\dot{K} = \frac{C_5 - p_1 + p_2 - (C_1 + C_2(p_s - p_1))K}{C_3} \tag{3.5}$$

$$\ddot{k_t} = (U_e - C_9)C_6C_7^2 - 2\dot{k_t}C_8C_7 - k_tC_7^2 \tag{3.6}$$

where C_1, C_2, C_3, C_5, C_6, C_7, C_8, C_9 are empirical constants (Handroos and Vilenius, 1991) and U_e is the signal applied to control the throttle, in other words, throttle opening. Volume flows Q_{e1} and Q_{e2} are obtained according to the following flow equations:

$$Q_{e1} = k_1\sqrt{p_2 - p_t} \tag{3.7}$$

$$Q_{e2} = k_2\sqrt{p_2 - p_t} \tag{3.8}$$

where k_1 and k_2 are semi-empirical flow coefficients for the orifice and directional control valve, respectively, and p_t is the pressure in the tank. The initial values and constants of the system described in the following equations are shown in Table 3.1.

Table 3.1: Circuit 1 parameters

B_e	$1.5{\cdot}10^{9}$ Pa	C_1	$4.65{\cdot}10^{7}$
V_1	$1.0{\cdot}10^{-5}$ m^3	C_2	$-1.79{\cdot}10^{4}$
V_2	$1.0{\cdot}10^{-3}$ m^3	C_3	$4.0{\cdot}10^{11}$
k_1	$5.62{\cdot}10^{-7}$	C_5	$1.02{\cdot}10^{6}$
k_2	$5.73{\cdot}10^{-7}$	C_6	$5.26{\cdot}10^{-7}$
p_t	0 Pa	C_7	200
K	$0.05{\cdot}10^{-9}$	C_8	0.45
k_t	$1.0{\cdot}10^{-7}$	C_9	1.2

3.2 Circuit 2: Hydraulic cylinder controlled by a directional control valve

The second circuit under consideration is the practical fluid power system with a more complex architecture and which is applicable for real-time simulation. The circuit contain two-chamber, double-acting hydraulic cylinder with a mass attached to the end of the horizontal cylinder's rod. The mass is not totally fixed, having one degree of freedom to slide with the cylinder piston's movements. The control of the cylinder occurs by the 4/3-proportional directional control valve. The pressure in the system is supported by the constant pressure pump, which is assumed to be an ideal flow source. A pressure compensator is also used in the circuit between the pump and the directional control valve. All the components in the system are connected with the hydraulic pipes of different volumes.

The circuit contains one extremely small pipe volume, located between the pressure compensator and the directional control valve. Fig. 3.2 depicts the whole circuit; the small volume is denoted as V_v. All the initial and constant parameters of the described system are listed in Table 3.2. The mathematical model of the circuit is represented with various differential and algebraic equations. Activation of the circuit occurs by the applied voltage signal U, obtained from the following equation:

$$\ddot{U}_s = K_v \omega_n^2 U - 2\zeta \omega_n \dot{U}_s - \omega_n^2 U_s \tag{3.9}$$

where K_v is the valve gain, U_s is the signal proportional to the valve spool displacement, ζ is the valve damping ratio, and ω_n is the natural angular frequency. The volumetric flow Q_v through the throttle of the pressure compensator is calculated according to a semi-empirical approach, expressed by following algebraic and differential equations, as in (Handroos and Vilenius, 1991):

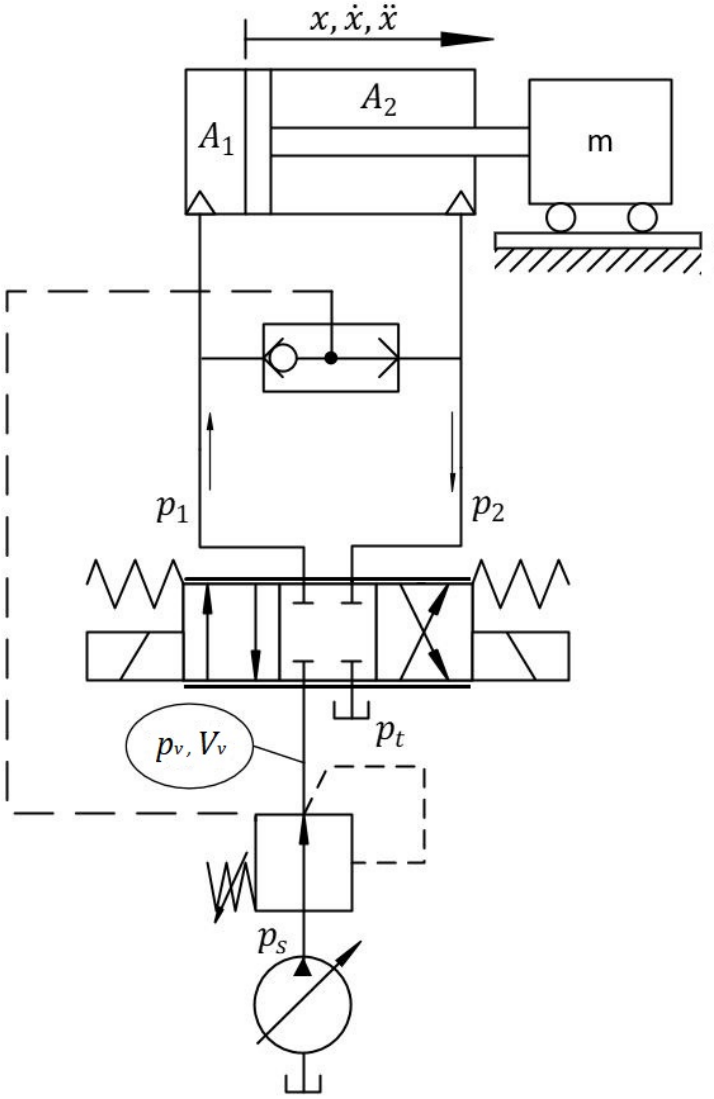

Figure 3.2: Circuit 2 schematic (Ustinov, Wu, and Handroos, 2022).

$$\begin{aligned} Q_v &= K\sqrt{p_s - p_v}, \\ \dot{K} &= \frac{1}{C_3}(C_5 - p_v + p_{shuttle} - (C_1 + C_2(p_s - p_v))K) \end{aligned} \tag{3.10}$$

where K is the semi-empirical flow coefficient, C_1, C_2, C_3, and C_5 denote empirical constants (Handroos and Vilenius, 1991), p_s and p_v are the constant pump pressure and the

pressure in small volume between the pressure compensator and directional flow control valve, respectively. The output pressure of the shuttle valve between way A and B (Fig. 3.2) $p_{shuttle}$ is dependent on the maximum value of pressures p_1 and p_2 and can be expressed as: $p_{shuttle} = max(p_1, p_2)$.

The volume flow rates Q_1 and Q_2 of the 4/3-proportional directional control valve are calculated with the use of the turbulent orifice model with a triangular groove cross-section, as follows:

$$\begin{aligned} Q_1 &= \begin{cases} C_v(U_s - U_d)\sqrt{|p_v - p_1|}sign(p_v - p_1), U_s \geq U_d \\ C_v(U_s - U_d)\sqrt{|p_1 - p_t|}sign(p_1 - p_t), U_s \leq -U_d \\ 0, \text{otherwise} \end{cases} \\ Q_2 &= \begin{cases} -C_v(U_s - U_d)\sqrt{|p_2 - p_t|}sign(p_2 - p_t), U_s \geq U_d \\ -C_v(U_s - U_d)\sqrt{|p_v - p_2|}sign(p_v - p_2), U_s \leq -U_d \\ 0, \text{otherwise} \end{cases} \end{aligned} \tag{3.11}$$

where C_v is the flow constant that accounts for cross-sectional areas and the geometry of the valve orifices, U_d is the insensitivity area for the applied signal, and p_1, p_2, p_v, and p_t are the pressures in two cylinder chambers, the pressure in small volume V_v, and the pressure in the tank, respectively.

Pressures in the system are integrated from the continuity equations of volumetric flow in accordance with the lumped-element modeling, as follows:

$$\begin{aligned} \dot{p}_1 &= \frac{B_{e1}}{V_1}\left(Q_1 - A_1\dot{x}\right) \\ \dot{p}_2 &= \frac{B_{e2}}{V_2}\left(-Q_2 + A_2\dot{x}\right) \\ \dot{p}_v &= \frac{B_{e3}}{V_v}\left(Q_v - Q_3\right) \end{aligned} \tag{3.12}$$

where V_v is the small volume between the pressure compensator and directional control valve, Q_v is the volumetric flow rate through the throttle of pressure compensator, $\dot{x}$ is the sliding speed of the piston, A_1 and A_2 are cross-sectional areas for two chambers of the cylinder, V_1 and V_2 are volumes of the pipes and cylinder chambers in way A and way B, respectively. B_{e1}, B_{e2}, and B_{e3} are effective bulk moduli for each pressure in the circuit, which can be represented as follows:

$$B_{ei} = a_1 E_{max} \log\left(a_2 \frac{p_i}{p_{max}} + a_3\right) \tag{3.13}$$

where E_{max} is the maximum bulk modulus of the oil, p_{max} is the maximum pressure in the system, p_i denotes pressure corresponding to the specific bulk modulus, and a_1, a_2, and

a_3 are the empirical constants (Jelali and Kroll, 2003). Volumes V_1 and V_2, in its turn, are calculated as follows:

$$\begin{aligned} V_1 &= A_1 x + V_{dead} \\ V_2 &= A_2 (S_c - x) + V_{dead} \end{aligned} \tag{3.14}$$

where S_c is the full stroke of the cylinder, x is the position of the cylinder piston, and V_{dead} is the dead volume, which represents the pipelines volume. The outlet flow Q_3 from (3.12) is defined based on the valve position, which can be determined as follows:

$$Q_3 = \begin{cases} Q_1, U_s \geq U_d \\ -Q_2, U_s \leq -U_d \\ 0, \text{otherwise} \end{cases} \tag{3.15}$$

The equation of motion for the system with a total force acting on it can be represented by the following relation:

$$F_{tot} = p_1 A_1 - p_2 A_2 - F_\mu = m\ddot{x} \tag{3.16}$$

where F_μ denotes friction between the walls of the cylinder and piston, m is the mass of the load attached to the end of the piston's rod, and $\ddot{x}$ is the acceleration of the piston. The friction model used for the simulation is based on the LuGre friction model, described in the following works (Canudas de Wit et al., 1993; Canudas de Wit et al., 1995; Olsson, 1996). LuGre model can be introduced with the following set of equations:

$$\begin{aligned} \dot{z} &= \dot{x} - \frac{|\dot{x}|}{g(\dot{x})} z \\ g(\dot{x}) &= \frac{1}{\sigma_0} \left(F_c + (F_s - F_c) e^{(-|\frac{\dot{x}}{v_s}|)^2} \right) \\ F_\mu &= \sigma_0 z + \sigma_1 \dot{z} + k_v \dot{x} \end{aligned} \tag{3.17}$$

where F_μ is the total friction force; z is the non-measurable internal state, F_c is the Coulomb friction force, $\dot{x}$ is the sliding velocity of the piston, v_s is the sliding speed coefficient, F_s is the static friction force, k_v is the viscous friction coefficient, and σ_0 and σ_1 are the flexibility and damping coefficients, respectively.

Table 3.2: Circuit 2 parameters

p_s	140×10^5 Pa	C_1	4.65×10^7	A_1	8.04×10^{-4} m^2	C_v	2.315×10^{-9}
p_1	9×10^5 Pa	C_2	-1.79×10^4	A_2	4.24×10^{-4} m^2	U_d	2 V
p_2	9×10^5 Pa	C_3	4.0×10^{11}	m	200 kg	K_v	0.99
p_v	9×10^5 Pa	C_5	10^6	V_{dead}	1.0×10^{-3} m^3	ω_n	331 rad/s
p_t	9×10^5 Pa	K	0.05×10^{-9}	V_v	1.0×10^{-5} m^3	ζ	0.62
S_c	1 m	σ_0	320 N/m	k_v	1.28×10^3 Ns/m	F_c	2.15×10^6 N
x_0	$0.75 - 1$ m	σ_1	6.368 Ns/m	v_s	347 m/s	F_s	1.1376×10^{10} N

4 Summary of research findings

This section of the present work demonstrates the methods and models that were developed and studied during the preparation of this dissertation. Advanced methods include The Advanced Pseudo-Dynamic solver (AdvPDS), the Method of Multiple Scales (MMS), and the Hybrid method of modeling and simulation of fluid power circuits, which uses the Recurrent Neural Network (RNN) to substitute the areas with small volumes with the artificial neural network. The results of computer simulations of all the advanced methods are provided and discussed in detail. All the simulation results for the study were produced in MATLAB 2020 Mathworks software in an environment with the following characteristics: Intel Core i5-8400 CPU, 2.80 GHz with 8 GB of RAM, running OS Windows 10 64-bit.

4.1 Advanced Pseudo-Dynamic solver

4.1.1 Description of the solver

Advanced Pseudo-Dynamic Solver or AdvPDS is solver that is initially developed and presented in Publication I. This solver belongs to the family of iterative implicit solvers. AdvPDS is designed to find the pressure of small fluid volumes at relatively high simulation speeds, compared to the traditional mathematical models and solvers. The solver was developed on the basis of the classical Pseudo-Dynamic Solver, described earlier in Section 2 and differs from it only in two features (J. Malysheva, Ustinov, and Handroos, 2021):

1. Consistency - Volumetric flow calculations are moved into the inner loop of the solver

2. Adaptivity - Adaptive criteria of convergence is applied

AdvPDS in its current form was developed during the tests of classical Pseudo-Dynamic Solver in different fluid power circuits, particularly, in both Circuit 1 and 2. The solver was used with the aim of speeding up the simulation process of the circuit. During the simulation of Circuit 1, with the Pseudo-Dynamic solver, it was investigated that sometimes it takes a lot of time to use this solver due to its iterative nature. An unstable response was also obtained. Empirically, through the tests of the solver, it was investigated as to whether the solver may use more iterations when the volumetric flows are calculated in the Outer loop of the Pseudo-Dynamic solver. In addition, to overcome this problem, it was decided to make the calculation of the whole pressure more consistent by moving flow equations into the Inner loop of the solver.

Another feature of AdvPDS, compared to classical Pseudo-Dynamic Solver, is the use of adaptive criteria of convergence. The adaptivity of the criteria can be explained by the

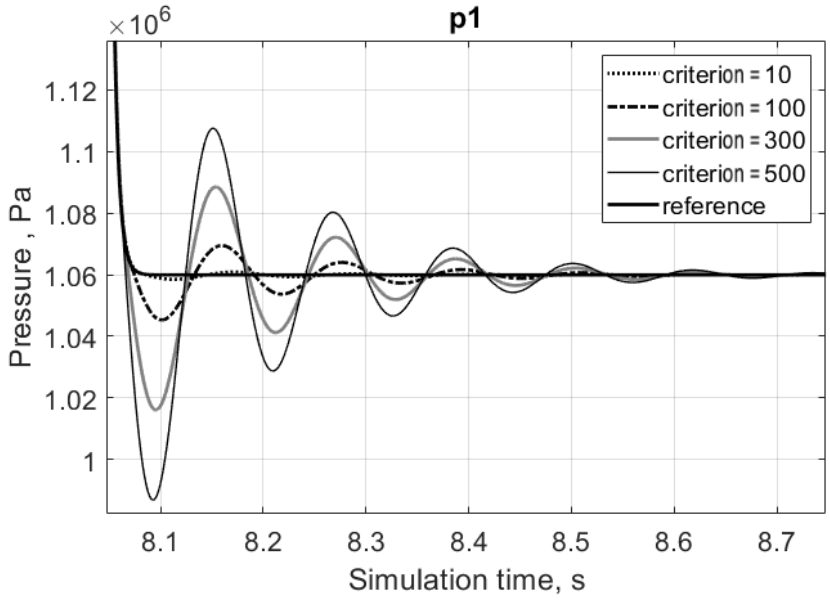

Figure 4.1: Pressure at different criteria of convergence in low-pressure areas (J. Malysheva, Ustinov, and Handroos, 2021).

usage of different numbers for the criterion at different levels of pressure in the fluid power circuit. Experimentally, it was established that using classical Pseudo-Dynamic Solver with the first modification creates fluctuations of pressure at low-pressure levels (less than 22 bar for both Circuit 1 and Circuit 2). The effects of the criteria of convergence on pressure fluctuations was investigated and studied through the experiments and are illustrated in Figure 4.1. The experiments showed that the use of the smaller number of criterion in the inner loop of the solver causes fewer fluctuations in pressure, making the model more accurate, as the reference traditional mathematical model. Otherwise, the bigger criterion increases the amplitude of pressure fluctuations, increasing the model average error (J. Malysheva, Ustinov, and Handroos, 2021).

However, use of the small criterion can slow down the simulation due to the need for more iterations inside the inner loop to reach the convergence. To overcome this problem, it was decided to make the criteria adaptive, which allows small criteria usage only at low-pressure levels, which should be less than 22 bar. At higher levels of pressure, the bigger criterion should be used. The adaptivity of the criterion allows the system to be more accurate and fast enough to be considered for real-time and even faster than real-time applications. This principle of a trade-off in accuracy-speed relation makes the AdvPDS one of the most efficient solvers for solving pressures in small fluid volumes.

The algorithm of the inner loop of AdvPDS differs from the classical Pseudo-Dynamic

Solver and is presented in Algorithm 1. Circuit 2 was taken as the example for demonstration of the algorithm. The circuit contain small pipe volume V_v between the pressure compensator and directional control valve. It means that the pressures p_1 and p_2 are calculated with usual integration subroutine in the outer loop, while pressure in small volume p_v is calculated in the inner loop of AdvPDS. The inner loop starts with the calculations of volumetric flows Q_3 and Q_v. After that, the derivative of pressure $\dot{p}_v$ is calculated according to the continuity equation of volumetric flow. Pressure p_v is integrated with inner loop integrator time step Δt_i, which differs from the outer loop time step, using classical explicit integrator subroutines (e.g., Runge-Kutta 4th order). Then, the pressure difference Δp_v of the current and previous iteration is calculated as follows(J. Malysheva, Ustinov, and Handroos, 2021):

$$\Delta p_v = p_v^{iter} - p_v^{prev} \tag{4.1}$$

If pressure is higher than the predetermined low pressure limit $p_{low\,limit}$, the big criterion of convergence $p_{v\,tol\,high}$ should be used. Vice versa, the small criterion is used in the case of a low pressure level. However, in both cases, if the criterion is satisfied, the last values of pressure p_v and flow Q_v are returned to the outer loop and the inner loop break. If not, the loop starts the next iteration with saving the value of pressure as p_v^{prev}. In this case, the calculation of the pressure and flow will continue until the criterion of convergence, which has to be smaller than the iteration pressure difference Δp_v, is satisfied.

Algorithm 1 Inner loop of AdvPDS(MATLAB)

Inputs: Δt_i, $t_{i\,max}$, V_{pseudo}, B_{e3}, p_1, p_2, p_v^{prev}, (Previous outer loop value of p_v)
1. $t_{i0} = 0$;
Inner Loop:
2. **for** $t_i = t_{i0} : \Delta t_i : t_{i\,max}$: (From start to end simualtion time with time step of Δt_i)
3. Calculate Q_3, Q_v
4. Calculate $\dot{p}_v$ (p_v^{iter} at current iteration)
5. Integrate $\dot{p}_v$ (p_v^{iter} at current iteration, integrator, e.g., Runge-Kutta 4th order)
6. Calculate: $\Delta p_v = p_v^{iter}$ - p_v^{prev} (Pressure difference Δp_v)
7. **if** ($p_v^{iter} < p_{low\,limit}$)**:**
8. **if** ($\Delta p_v < p_{v\,tol\,low}$)**:**
9. **return** p_v, Q_v (Return values to the outer loop)
10. **break** (Break the inner loop)
11. **else:**
12. $p_v^{prev} = p_v^{iter}$ (Save value of p_v^{prev} for the next iteration)
13. **continue** (Continue loop)
14. **end**
15. **else:**
16. **if** ($\Delta p_v < p_{v\,tol\,high}$)**:**
17. **return** p_v, Q_v (Return values to the outer loop)
18. **break** (Break the inner loop)
19. **else:**
20. $p_v^{prev} = p_v^{iter}$ (Save value of p_v^{prev} for the next iteration)
21. **continue** (Continue loop)
22. **end**
23. **end**
24. **end**
Outputs: p_v, Q_v

4.1.2 Simulation results

To demonstrate the results of the simulation experiments, also partially described in Publication I, both Circuit 1 and Circuit 2, described in Section 3, were selected for the experiments. To show the advantages and efficiency of AdvPDS, the classical or reference Lumped-element modeling-based models of Circuit 1 and Circuit 2 were simulated and compared with the AdvPDS-based model. The reference and AdvPDS model are compared in terms of simulation speed and accuracy, which is represented by the Relative Root-Mean-Square Error (RRMSE), defined as follows:

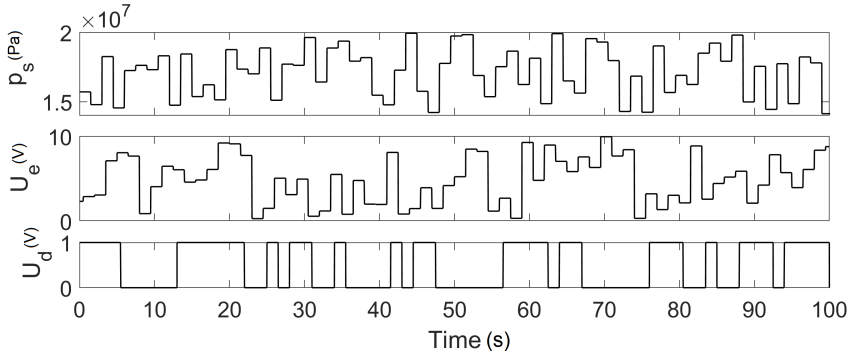

Figure 4.2: Input values of p_s, U_d, and U_e for simulation of Circuit 1 through the time (J. Malysheva, Ustinov, and Handroos, 2021).

$$RRMSE(\%) = \frac{\sqrt{\frac{1}{N}\sum_{i=1}^{N}(x_i - x_i^m)^2}}{\sum_{i=1}^{N}(\mid x_i \mid)} \times 100 \tag{4.2}$$

where N is the number of points, x_i is the value of the reference model at the operating point, and x_i^m is the value of any comparable model at the same point.

Circuit 1 was simulated within 100.5 s, using both the reference and AdvPDS-based models. Inputs for the circuits were p_s, U_d, and U_e, which were randomly distributed through the simulation time in ranges between 140-200 bar, 0 and 1 Volt, and -10 and 10 Volts, respectively. The inputs of the circuit are depicted in Figure 4.2. The simulation of the reference model held at a time step of 1.0×10^{-6} s that showed a numerically stable response of the system and was the largest time step possible to use. The simulation of 100.5 s, using this model, took around 5 h of real time, which is very slow, and it is definitely impossible to simulate the model in real-time or faster than real-time applications.

The stiffness of Circuit 1 was reduced by implementation of AdvPDS in the model of the circuit. Numerical stiffness, that appears in the stiff differential equation of pressure p_1 in a small volume of 1.0×10^{-5} m^3, was eliminated by embedding equations of pressure p_1 and volumetric flow Q_t to the inner loop of the AdvPDS-based model. Other differential equations in the model were integrated as usual with the Runge-Kutta 4th order integration subroutine. According to several experimental tests, the adaptive criteria for AdvPDS was selected as 300/10 Pa, where 300 Pa was used for high levels of pressure and 10 Pa for low levels of pressure. Due to the elimination of the numerical stiffness in the AdvPDS-based model, integrator time steps of 1.0×10^{-4} s and 1.0×10^{-5} s were set for the outer loop and inner loop, respectively, which made the model work much faster than the reference

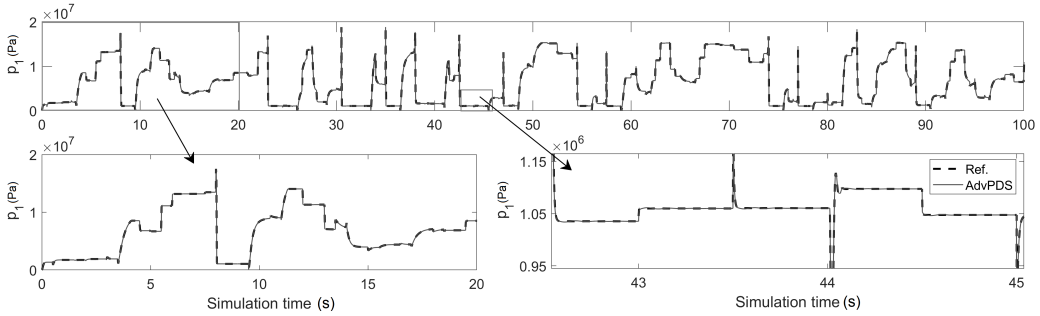

Figure 4.3: Pressure p_1 responses comparison of Reference model and AdvPDS-based model with enlarged areas (J. Malysheva, Ustinov, and Handroos, 2021).

model with a smaller time step of 1.0×10^{-6} s. In total, it took only 147.98 s of real time for the AdvPDS-based model to complete the simulation of 100.5 seconds, which is around 122 times faster than it took for the reference model.

The responses of the pressure p_1, built up in the small volume in the AdvPDS model and pressure p_1 in the reference model, were plotted and compared in Fig. 4.3. The figure also displays enlarged areas of the plot, where one can observe the high accuracy of the AdvPDS-based model, due to the coincidence of the plot lines. A high accuracy of the response can be associated with use of adaptive criteria of convergence in the inner loop of AdvPDS, which allows simulation of the circuit without loss of accuracy in the low pressure areas. The overall error of the pressure p_1 of the circuit represented by RRMSE is only 0.6186 %, which proves that the AdvPDS-based model achieves a trade-off between a high simulation speed and very high accuracy of the model.

Circuit 2 was simulated within 20 s with an integrator time step of 1.0×10^{-5} s for the reference model. The integrator time step was selected due to the numerical stability of the system and was the maximum possible time step for Circuit 2. The AdvPDS-based model was run at an integrator time step of 1.0×10^{-4} s for the outer loop of the solver. The inner loop integrator time step was selected as 1.0×10^{-4} s, which gave a numerically stable result for the system. The input signal of the model varied between -5 and 8 V, and its propagation through the time is visible in Figure 4.4. The input is repeatable and each change of voltage occurs every 1 s of time.

The inner loop of AdvPDS was used to substitute the equations used for calculations of pressure p_v built up in the small volume V_v due to its numerical stiffness. To select the adaptive criteria of convergence for the inner loop in the model, several tests of single-criterion AdvPDS were performed. The results of the tests are displayed in Table 4.1. From the results, it is seen that the difference in the system speed with the use of criteria value from 200 Pa to 1000 Pa is not significant; however, the accuracy of the system with criteria of 200 Pa is better than the accuracy of systems with a higher criterion of

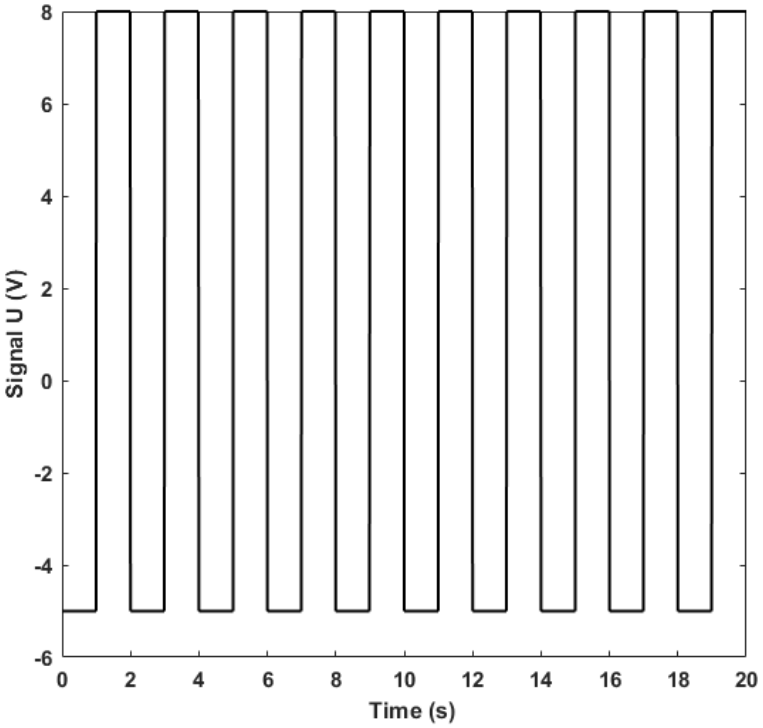

Figure 4.4: Input signal for Circuit 2 through time.

convergence (e.g., 300-1000 Pa). And vice versa, the accuracy of the system with a criterion of 50 Pa is not significantly worse than the accuracy of the system with a criterion of 10 Pa. Nevertheless, the speed of the system with the criterion of 50 Pa is much better (systems with criteria of 50 Pa and 10 Pa are simulated for real 95.94 s and 167.63 s, respectively). According to the test, it was decided to select adaptive criteria of 200/50 Pa, where the first criterion is used for high pressures in the system (higher than 22 bar) and 50 Pa criterion is used for low pressures (lower that 22 bar). This means that the system will be fast enough, and, at the same time, its accuracy will be at a high level in low-pressure areas.

The response of the pressure p_v built up in the small volume, as well as the cylinder position piston x_s against the responses obtained with the reference model, are plotted in Fig. 4.5. The obtained responses of the AdvPDS-based model in pressure and cylinder piston position were accurate in a high level and differed from the reference responses with RRMSEs of 4.6835% and 0.2117% for the pressure p_v and cylinder piston position x_s, respectively. As in the simulation of Circuit 1, the high level of accuracy of the AdvPDS-based model was achieved by the use of adaptive criteria of convergence in the

Table 4.1: Relationship between criteria value, simulation time, and calculation accuracy for the AdvPDS with a single criterion

Criterion, Pa	Simulation time, s	$RRMSE_{xs}$, %
10	167.63	0.2099
20	157.09	0.2120
50	95.94	0.2136
100	27.57	0.2155
200	24.60	0.2185
300	23.90	0.2213
400	23.50	0.2239
500	23.94	0.2263
600	23.13	0.2289
700	24.27	0.2313
800	23.40	0.2334
900	23.81	0.2358
1000	22.80	0.2379

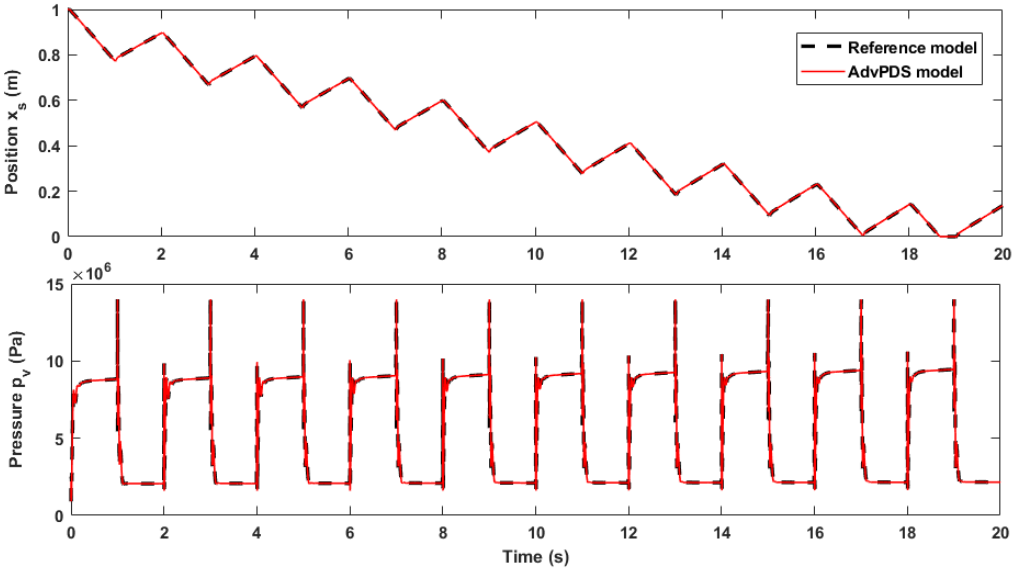

Figure 4.5: Piston position x_s and pressure p_v responses comparison of Reference model and AdvPDS-based model for Circuit 2

inner loop, which provided more precise results in numerical calculations of pressure in the low-pressure areas. In addition to the high accuracy of the AdvPDS-based model, the simulation speed of the circuit improved almost 10 times, compared to the reference model. For instance, the usage of the AdvPDS model with criteria of 200/50 Pa took only

Table 4.2: Simulation results of Circuit 1 and Circuit 2 using the reference model and the AdvPDS-based model (J. Malysheva, Ustinov, and Handroos, 2021)

Circuit	Solver	Real Time, seconds	Time Step (s) (outer/inner)	Simulation Time	RRMSE w.r.t. Ref.
1	Reference	100.5	$10^{-6}/-$	~ 5 h	$-$
	AdvPDS	100.5	$10^{-4}/10^{-5}$	147.98 s	$RRMSE_{p1} = 0.6186\%$
2	Reference	20	$10^{-5}/-$	202.99 s	$-$
	AdvPDS	20	$10^{-4}/10^{-4}$	24.3 s	$RRMSE_{pv} = 4.6835\%$
					$RRMSE_{xs} = 0.2117\%$

24.3 s of real time to simulate 20 s; however, for the reference model, it took 202.99 s. The results of the simulation of both Circuit 1 and Circuit 2, using the reference and the AdvPDS model, are also presented in Table 4.2.

4.2 Method of multiple scales

Another efficient method of numerical stiffness elimination, which works coupled with the Singular Perturbation Theory, is the Method of Multiple Scales (MMS). The method and its derivation are described in detail in Publication II.

The SPT-based method is able to give the steady-state solution of the systems only in the largest time scale, while the system should display the behavior of various dynamic scales. For each scale that can be appealed as an independent variable, a set of equations can be reproduced instead of one. For example, t and εt can be two independent variables, each of them representing a scale of time. However, the SPT-based fluid power model returns the steady-state response, the accumulative error generated due to the smaller scales creates the deviation of the response comparing to the actual situation, especially in cases where the dynamic behavior of systems cannot be neglected. To overcome the accumulative error of the SPT-based model, the special corrector factor should be used (Kiani-Oshtorjani, Mikkola, and Jalali, 2019). Another alternative of using the corrector factor is to develop a more precise model which will operate without any modifications. For instance, the Method of Multiple Scales (MMS) can be utilized to derive a fluid power model operating on the small hydraulic volumes. According to the method, the new independent time variables can be introduced as (Kiani-Oshtorjani, Ustinov, et al., 2020):

$$T_n = \varepsilon^n t \qquad n = 0, 1, 2, \ldots \tag{4.3}$$

Thus, all derivatives in the equation can be rewritten in the following way:

$$\frac{d}{dt} = \frac{dT_0}{dt}\frac{\partial}{\partial T_0} + \frac{dT_1}{dt}\frac{\partial}{\partial T_1} + \ldots \tag{4.4}$$

In addition, one can assume that the solution of the equation can be written as:

$$p_i(t,\varepsilon) = p_0(T_0,T_1,...) + \varepsilon p_1(T_0,T_1,...) + O(\varepsilon^2) \tag{4.5}$$

It is important note that the number of time scales is a function of the accuracy that should be achieved. In case of expanding the solution until the 2nd order $O(\varepsilon)$, the time scales of T_0 and T_1 are required. Replacement of Eq.(4.5) to (4.4) and then inserting the output to Eq. 2.1 yields to:

$$\left(\frac{\partial}{\partial T_0} + \varepsilon\frac{\partial}{\partial T_1} + \varepsilon^2\frac{\partial}{\partial T_2}\right)\left(p_0 + \varepsilon p_1 + \varepsilon^2 p_2\right) = \frac{B_e}{V_i}\left(Q_{i-\frac{1}{2}} - Q_{i+\frac{1}{2}}\right) \tag{4.6}$$

On the contrary, volumetric flows $Q_{i-\frac{1}{2}}$ and $Q_{i+\frac{1}{2}}$ are the functions of pressure built up in the small pipe volume. If these volumetric flows are computed based on the SPT pressure, they will have an error. Therefore, they have to be calculated by applying the exact value of p_i. Considering Eq. (2.2), the $Q_{i+\frac{1}{2}}$ can be obtained as follows:

$$Q_{i+\frac{1}{2}} = C_c A\sqrt{p_i - p_{i+1}} = C_c A\sqrt{p_0 - p_{i+1} + \varepsilon p_1 + \varepsilon^2 p_2} \tag{4.7}$$

Consequently, by getting $p_0 - p_{i+1}$ out of the square root and by using the Taylor series for $\sqrt{1+x} \approxeq 1 + \frac{x}{2} - \frac{x^2}{8}$ in which $x < 1$, it is concluded:

$$\begin{aligned} Q_{i+\frac{1}{2}} = C_c A\sqrt{p_0 - p_{i+1}}\left(1 + \frac{p_1\varepsilon + p_2\varepsilon^2}{2(p_0 - p_{i+1})} - \frac{p_1^2\varepsilon^2}{8(p_0 - p_{i+1})^2}\right) = \\ \bar{Q}_{i+\frac{1}{2}}\left(1 + \frac{p_1\varepsilon + p_2\varepsilon^2}{2(p_0 - p_{i+1})} - \frac{p_1^2\varepsilon^2}{8(p_0 - p_{i+1})^2}\right) \end{aligned} \tag{4.8}$$

in which $\bar{Q}_{i+\frac{1}{2}} = C_c A\sqrt{p_0 - p_{i+1}}$ is the volumetric flow computed based on the SPT-based pressure and further mentioning as perturbed volumetric flow. The similar statement is actual for $Q_{i-\frac{1}{2}}$ resulting in the following dependence:

$$Q_{i-\frac{1}{2}} = \bar{Q}_{i-\frac{1}{2}}\left(1 - \frac{p_1\varepsilon + p_2\varepsilon^2}{2(p_{i-1} - p_0)} - \frac{p_1^2\varepsilon^2}{8(p_{i-1} - p_0)^2}\right) \tag{4.9}$$

Substitution of the volumetric flows in Eqs. (4.8) and (4.9) in Eq. (4.6) and separating the equations of order $O(\varepsilon^0)$, $O(\varepsilon^1)$, and $O(\varepsilon^2)$ sum up to the following equations:

$$O(\varepsilon^0): \frac{\partial p_0}{\partial T_0} = \frac{B_e}{V_i}(\bar{Q}_{i-\frac{1}{2}} - \bar{Q}_{i+\frac{1}{2}}) \tag{4.10}$$

$$O(\varepsilon^1): \frac{\partial p_1}{\partial T_0} + \frac{B_e}{V_i} p_1 \left(\frac{\bar{Q}_{i-\frac{1}{2}}}{2(p_{i-1} - p_0)} + \frac{\bar{Q}_{i+\frac{1}{2}}}{2(p_0 - p_{i+1})} \right) = -\frac{\partial p_0}{\partial T_1} \tag{4.11}$$

$$\begin{aligned} O(\varepsilon^2): \frac{\partial p_2}{\partial T_0} + \frac{B_e}{V_i} p_2 \left(\frac{\bar{Q}_{i-\frac{1}{2}}}{2(p_{i-1} - p_0)} + \frac{\bar{Q}_{i+\frac{1}{2}}}{2(p_0 - p_{i+1})} \right) = \\ \frac{B_e}{V_i} \left(\frac{\bar{Q}_{i+\frac{1}{2}} p_1^2}{8(p_0 - p_{i+1})^2} - \frac{\bar{Q}_{i-\frac{1}{2}} p_1^2}{8(p_{i-1} - p_0)^2} \right) - \frac{\partial p_1}{\partial T_1} - \frac{\partial p_0}{\partial T_2} \end{aligned} \tag{4.12}$$

Equation (4.10) is equivalent in the SPT-based model due to the existence of small pipe volume V_i, producing pressure in SPT equation as obtained in Eq. (2.12) as $p_0 = \frac{p_{i+1} + \alpha p_{i-1}}{1+\alpha}$. As a result, $\frac{\partial p_0}{\partial T_1} = 0$, also recalling the $\bar{Q}_{i-\frac{1}{2}}$ and $\bar{Q}_{i+\frac{1}{2}}$ relations, Eq. (4.11) will be resolved as:

$$p_1 = \Lambda(T_1) exp\left(-\int_0^{T_0} \frac{B_e}{V_i} \left[\frac{\bar{Q}_{i-\frac{1}{2}}}{2(p_{i-1} - p_0)} + \frac{\bar{Q}_{i+\frac{1}{2}}}{2(p_0 - p_{i+1})} \right] dT_0 \right) \tag{4.13}$$

Considering $\frac{dp_1}{p_1} = \frac{d(\varepsilon p_1)}{\varepsilon p_1}$, and expecting the constant pressure drop through the small pipe volume $\sqrt{p_{i-1} - p_{i+1}}$, Eq. (4.13) is determined as follows:

$$\begin{aligned} \frac{\partial p_2}{\partial T_0} + \frac{B_e}{V_i} p_2 \left(\frac{\bar{Q}_{i-\frac{1}{2}}}{2(p_{i-1} - p_0)} + \frac{\bar{Q}_{i+\frac{1}{2}}}{2(p_0 - p_{i+1})} \right) = \frac{B_e}{V_i} \left(\frac{\bar{Q}_{i-\frac{1}{2}}}{8(p_{i-1} - p_0)} + \right. \\ \left. \frac{\bar{Q}_{i+\frac{1}{2}}}{8(p_0 - p_{i+1})} \right) \Lambda^2 exp\left(-2 \int_0^{T_0} \frac{B_e}{V_i} \left[\frac{\bar{Q}_{i-\frac{1}{2}}}{2(p_{i-1} - p_0)} + \frac{\bar{Q}_{i+\frac{1}{2}}}{2(p_0 - p_{i+1})} \right] dT_0 \right) - \\ \frac{\partial \Lambda}{\partial T_1} exp\left(-\int_0^{T_0} \frac{B_e}{V_i} \left[\frac{\bar{Q}_{i-\frac{1}{2}}}{2(p_{i-1} - p_0)} + \frac{\bar{Q}_{i+\frac{1}{2}}}{2(p_0 - p_{i+1})} \right] dT_0 \right) \end{aligned} \tag{4.14}$$

The terms on the right sight of Eq. (4.14) are secular, which denotes the growing of these terms to infinity with time, and it means that they have to be assigned to zero. Thus, we can get:

$$\frac{\partial \Lambda}{\partial T_1} - \Lambda^2 \frac{B_e}{V_i}\left(\frac{\bar{Q}_{i-\frac{1}{2}}}{8(p_{i-1}-p_0)} + \frac{\bar{Q}_{i+\frac{1}{2}}}{8(p_0-p_{i+1})}\right) exp\left(-\int_0^{T_0} \frac{B_e}{V_i}\left[\frac{\bar{Q}_{i-\frac{1}{2}}}{2(p_{i-1}-p_0)} + \frac{\bar{Q}_{i+\frac{1}{2}}}{2(p_0-p_{i+1})}\right] dT_0\right) = 0 \tag{4.15}$$

As a result:

$$\Lambda = -\frac{1}{fT_1} \tag{4.16}$$

in which $f = \frac{B_e}{V_i}\left(\frac{\bar{Q}_{i-\frac{1}{2}}}{8(p_{i-1}-p_0)} + \frac{\bar{Q}_{i+\frac{1}{2}}}{8(p_0-p_{i+1})}\right) exp\left(-\int_0^{T_0} \frac{B_e}{V_i}\left[\frac{\bar{Q}_{i-\frac{1}{2}}}{2(p_{i-1}-p_0)} + \frac{\bar{Q}_{i+\frac{1}{2}}}{2(p_0-p_{i+1})}\right] dT_0\right)$. Substituting Eq. (4.16) into (4.13) yields to the following:

$$p_1 = -\frac{1}{T_1}\frac{8V_i}{B_e}\left(\frac{\bar{Q}_{i-\frac{1}{2}}}{(p_{i-1}-p_0)} + \frac{\bar{Q}_{i+\frac{1}{2}}}{(p_0-p_{i+1})}\right)^{-1} \tag{4.17}$$

By considering $T_1 = \varepsilon t$ and combining p_0 and εp_1 according to Eq. (4.5), the pressure built up in small volume p_i is taken as:

$$p_i = \frac{p_{i+1} + \alpha p_{i-1}}{1+\alpha} - \frac{1}{t}\frac{8V_i}{B_e}\left(\frac{\bar{Q}_{i-\frac{1}{2}}}{(p_{i-1}-p_0)} + \frac{\bar{Q}_{i+\frac{1}{2}}}{(p_0-p_{i+1})}\right)^{-1} \tag{4.18}$$

This means the dependence of SPT-based model deviation from the precise solution, mainly on the pressure drop $p_{i-1} - p_{i+1}$, bulk modulus B_e, and volume V_i, which can be disclosed by the Eq. 4.18. In the case where the pressure drop passing through the small volume tends to zero $p_{i-1} - p_{i+1} \to 0$ denotes that there is no pressure change from p_{i-1} to p_{i+1}, then $\varepsilon p_1 \to 0$ then the SPT-based model can run without error, performing as a precise solution (Kiani-Oshtorjani, Ustinov, et al., 2020).

The similar statement is correct for bulk modulus and the pipe volume size, which means that the SPT-based model is more precise in calculations if the size of the small volume

tends to zero as $\varepsilon p_1 \to 0$ if $V_i \to 0$. Finally, the substitution of the stiff differential equation of pressure in a fluid power circuit with Equation 4.18 should give a more accurate response of this pressure in simulation.

4.2.1 Simulation results

To demonstrate the features and benefits using MMS in fluid power circuit computer simulation, several simulations of numerically stiff Circuit 2, with three different input signals, were performed. Results of all three simulations are also presented in Publication II. The input signals used in all simulations were as follows: $sin(0.25t)$, $sin(0.75t)$, and $u(t)$. All three sets of input signals were applied to the reference, or original model, SPT-based model and MMS-based model. All the models were simulated for 200 s at every set of inputs.

The first simulation of all three models was made at the input signal of $sin(0.25t)$. The largest possible integrator time step of the reference model with this input signal was 10^{-4}, due to the stiffness of the differential equation of pressure p_v in small volume V_v. The same integrator time step was used for the SPT-based model. In the case of the MMS-based model, it was possible to enlarge the integrator time step to 4×10^{-4} without making the model numerically unstable and saving a very high level of accuracy, which is expressed through the RRMSE, defined in Eq. 4.2 and equals 1%. In the case of the SPT-based model, the response is not accurate enough (RRMSE = 10.9%), which can also be observed in Figure (4.6a), where the cylinder piston position x for three models is plotted. The perturbed model requires a corrector factor for the flow rate coming out of the small volume to work in a reliable way, otherwise the accumulative error will make the model numerically unstable. The MMS-based model does not need a corrector factor. The RRMSE through time is plotted in Figure (4.6b). This plot proves the existence of the accumulative error in the case of the SPT-based model, while the MMS-based model has a smooth and low error response.

The responses of pressures p_1 and p_2 inside cylinder chambers 1 and 2 are also plotted in Figures. (4.6c) and (4.6d), respectively. The plots show that the MMS-based model pressure response is close to the response of the reference model, whereas the pressures obtained by the SPT-based model is underestimated compared to the reference model. In addition, it is important to note the possibility of increasing the integrator time step of the MMS-based model in order to run it faster. This means that a simulation with a similar input signal ($sin(0.25t)$) can be performed at an integrator time step of 5×10^{-5} s for an MMS-based model yielding the increase of RRMSE to 1.64%, which can also be found in the second row of Table (4.3). This can be a good trade-off between the simulation speed and accuracy of the simulation, and as a result, it is possible to adjust the time step to find the best match for both simulation speed and accuracy.

The second simulation of reference, the SPT-based and MMS-based models, was held us-

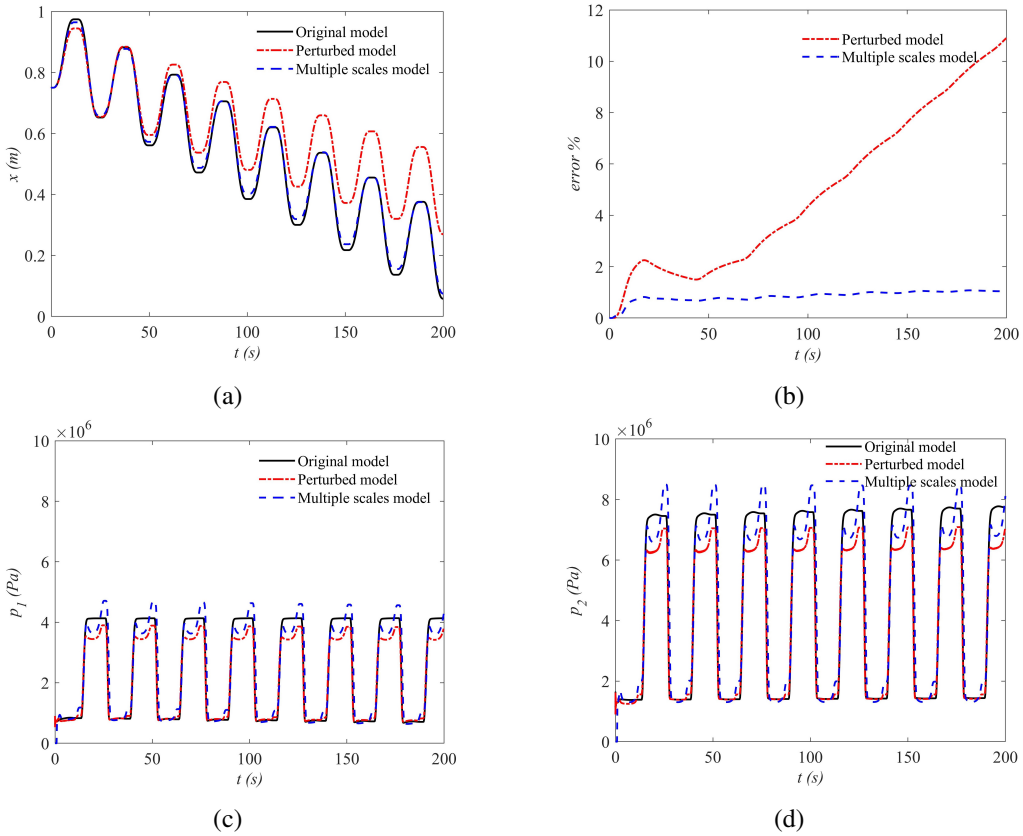

Figure 4.6: The results of the simulation with the input signal of $sin(0.25t)$ (a) piston position comparison between original(reference) model, SPT-based, and MMS-based model and (b) their RRMSE (c) pressure in cylinder chamber 1 p_1 and (d) pressure in cylinder chamber 2 p_2 (Kiani-Oshtorjani, Ustinov, et al., 2020).

ing an input signal of $sin(0.75t)$. The values for integrator time steps remained the same as in the first simulation, and were 5×10^{-4} s, 5×10^{-4} s and 4×10^{-4} s for reference, SPT-based, and MMS-based models, respectively. The response of cylinder piston position x can be observed in Figure (4.7a). As in the first simulation with an input signal of $sin(0.75t)$, one can observe the accurate response of the MMS-based model in comparison with the reference model, while the SPT-based model, after 30 sec, started to deviate with growing accumulative error. The error can be visualized in Fig. 4.7b in the form of RRMSE for MMS-based and SPT-based models. By the 200-th second of the simulation, the RRMSE of the SPT-based model accumulates to 10.6%, while the response of the RRMSE of the MMS-based model is smooth through the time and equals to only 0.6%.

The third simulation of the models was performed using a pulse input of $u(t)$, where

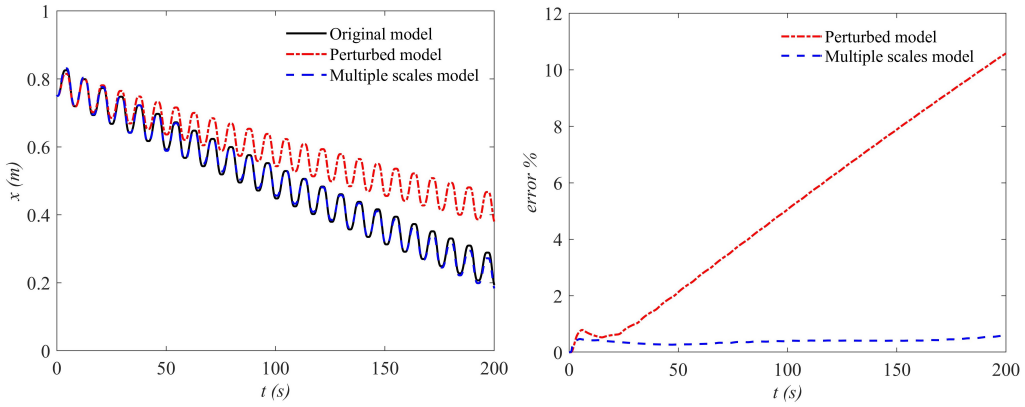

(a) (b)

Figure 4.7: The results of the simulation with the input signal of $sin(0.75t)$ (a) piston position comparison between original(reference) model, SPT-based model, and MMS-based model and (b) their RRMSE (Kiani-Oshtorjani, Ustinov, et al., 2020).

the signal is varied from -10 to 10 V, and it is plotted in Fig. (4.8a). The use of the pulse input allowed for the running of the stiff reference model at a very small time step of 5×10^{-5} s due to the numerical instability of the model with larger integrator time steps. At the same time, it was possible to run the SPT-based model with a maximal time step of 1×10^{-4} s. The MMS-based model in its turn was able to run at the largest possible integrator time step of 1×10^{-3} s. The response of the pressure in cylinder chamber p_1 can be observed from Figure (4.8b) for reference, SPT-based and MMS-based models. The plot shows that the MMS-based model pressure response almost repeats the reference model pressure response, while the SPT-based model does not perform as accurately as the MMS-based model. Moreover, from the position and RRMSE plots, depicted in Fig. (4.8c) and Fig. (4.8d) respectively, one can observe that the MMS-based model is simulated accurately with an extremely small RRMSE of 0.09% with respect to the reference model. In comparison with the SPT-based model, where the RRMSE is accumulated to 13.2% by the end of the simulation, the MMS-based model has almost negligible deviation. The possibility to run the MMS-based model at very large integrator time step makes it an acceptable choice for real-time or faster than real-time simulation. In addition, the accuracy of the model is very high. Finally, the results of all simulations of the three above-mentioned models, in the form of the difference in integrator time step and RRMSE, can be observed in Table 4.3.

4.3 Hybrid method of simulation utilizing recurrent neural network

The stiffness of a fluid power circuit in the presence of small volumes can be eliminated with a so-called hybrid model of such a circuit, presented in Publication III. The main difference of the hybrid model compared to the traditional mathematical model is the

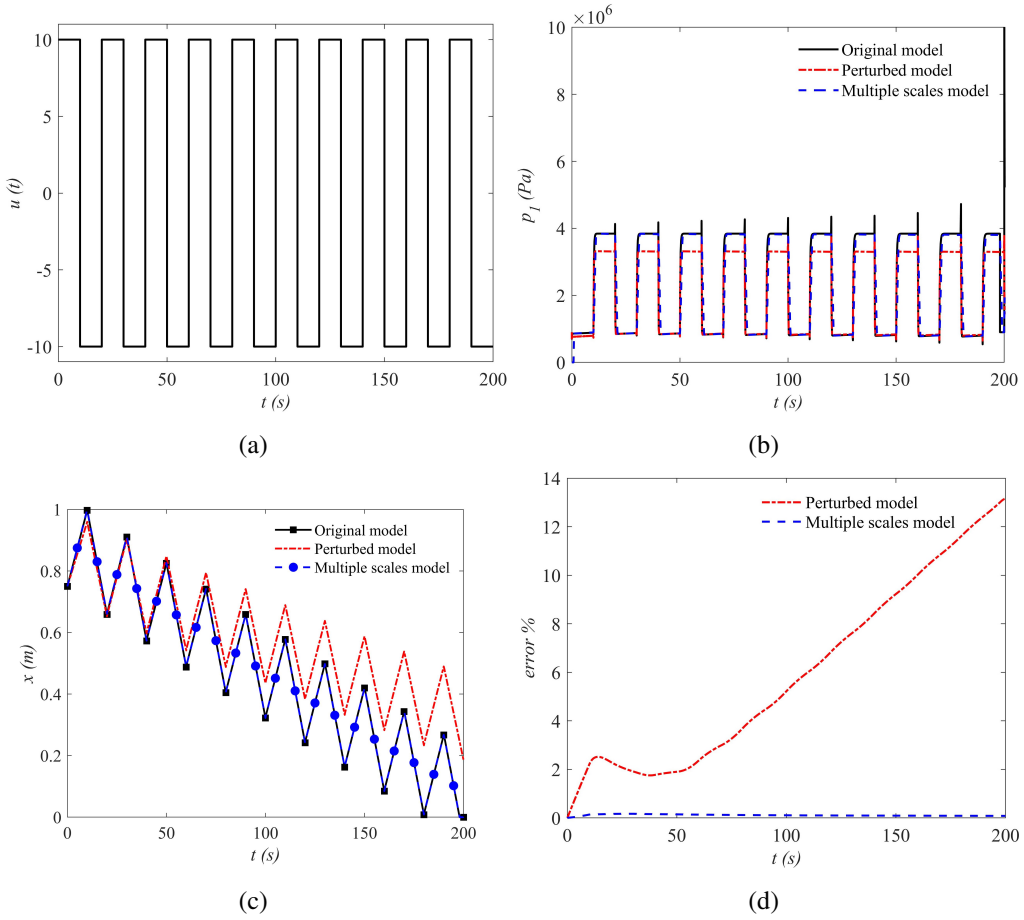

Figure 4.8: (a) Pulse input $u(t)$ from -10 to 10 Volts and (b) pressure in cylinder chamber 1 p_1 (c) the piston position obtained by small time step referred to as original (reference) model, SPT-based model, and the MMS-based model (d) the RRMSE of SPT-based and MMS-based models with respect to the original (reference) model (Kiani-Oshtorjani, Ustinov, et al., 2020).

Table 4.3: Results of comparison of reference, SPT-based and MMS-based model (Kiani-Oshtorjani, Ustinov, et al., 2020)

Input signal	Time step (s)			RRMSE %	
$\frac{U}{U_d}$	Reference model	SPT-based model	MMS-based model	SPT-based model	MMS-based model
$sin(0.25t)$	10^{-4}	10^{-4}	4×10^{-4}	10.9	1.0
$sin(0.25t)$	10^{-4}	10^{-4}	5×10^{-4}	10.9	1.64
$sin(0.75t)$	10^{-4}	10^{-4}	4×10^{-4}	10.6	0.6
$u(t)$	5×10^{-5}	10^{-4}	10^{-3}	13.2	0.09

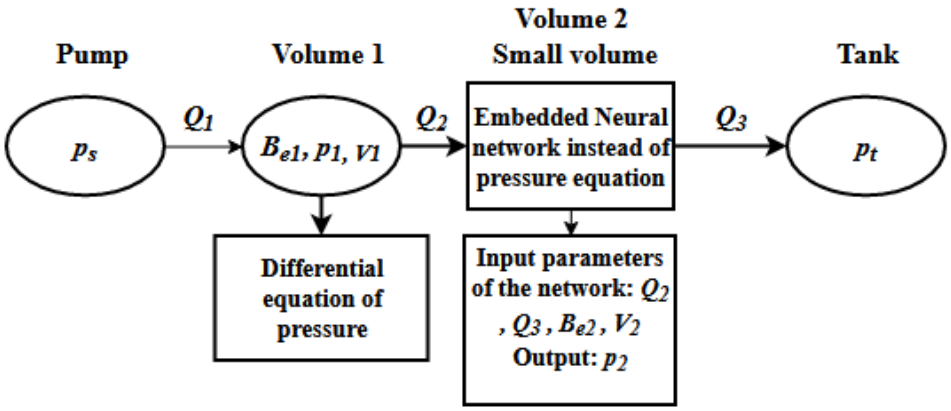

Figure 4.9: Schematic representation of hybrid model in simple fluid power system

presence of an Artificial neural network (ANN), substituting the stiff differential equation of pressure. The schematic representation of the hybrid model is represented in Figure 4.9. The most efficient ANN dealing with dynamic systems are RNN, and the architectures are described in more detail in 2.4. The RNN should be trained based on the original fluid power circuit simulation parameters. This section gives an example of the development of hybrid models in more detail.

4.3.1 Hybrid model development example

The features of selection of RNN architecture for fluid power system simulation were also described in J. Malysheva, Li, and Handroos, 2020. According to the author, the data obtained from the simulation model of the circuit similar to Circuit 3 does not contain real system noise, and the use of a large number of RNN parameters can affect the simulation time and speed. At the same time, the maximal accuracy of the system with the embedded

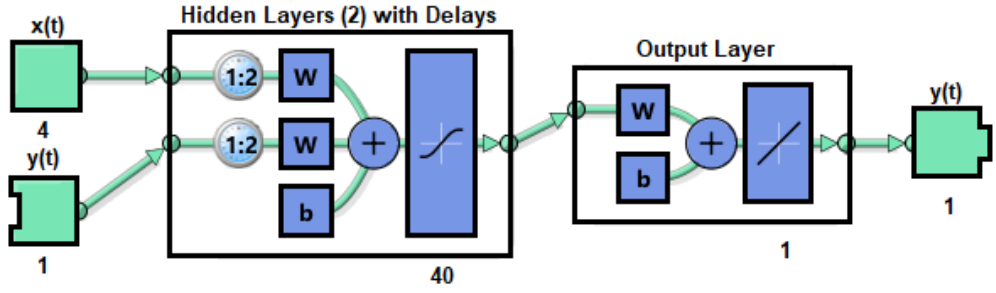

Figure 4.10: Structure of the NARX RNN used in hybrid model (Ustinov, Wu, and Handroos, 2022).

RNN is required. In such a case, the NARX RNN is the most suitable architecture of neural network for fluid power system simulation, even in the case of the simulation of one stiff differential equation, since it is more accurate than NFIR due to the use of output data as feedback. Ultimately, the NARX architecture provides a trade-off between speed and accuracy in simulating the final system, which is the main objective of any simulation. However, other options of RNN architectures can be studied more in future research, and the selection of the best performance RNN architecture for Hybrid models is still an open question.

Fig. 4.10 illustrates the basic structure of the NARX RNN that can be used in the modeling of the fluid power circuit. Note that the structure of such a network can be different, and number of neurons and layers should be selected depending on the complexity of the circuit. In this example, the RNN consists of one input layer with four input values, and one feedback value that can be used only during the training of the network, two hidden layers with 40 neurons, and one output layer with one output activated with a linear function. Because the system has to be modeled as a mathematical model of one differential equation of pressure, the number of layers and neurons are manually selected by trial and error during the training process to ensure the accuracy of the network. The sigmoid function $\sigma(x)$ is selected as the activation function for hidden layers of the network; the function is defined as follows:

$$\sigma(x) = \frac{1}{1+e^{-x}} \tag{4.19}$$

where x is the argument of the function $\sigma(x)$ and e is the Euler's number.

The whole development of the hybrid model is divided into two stages. The first stage of development included the collection of the training data and training of the NARX RNN. The second stage of the development is related to the implementation of the neural

network to the stiff fluid power circuits from Section 3. In this development example, the modeling and simulation of the systems were performed in MATLAB R2020a software in a form of MATLAB code, and the formulation of the RNN was performed through the embedded MATLAB Deep Learning Toolbox.

4.3.2 Data collecting and training of the RNN

The data collected for the training is based on the simulation results of the practical fluid power Circuit 2, described in Section 3. The reference system, based on a traditional mathematical model, was simulated for 3,000 seconds, with an integrator time step of 1.0×10^{-5} s and an input voltage that was supplied randomly in a range between -10 and 10 Volts. The integrator time step was selected empirically to ensure the correct response of the system in the presence of small volume. The data set of 300 million samples was created from several parameters of the system, where each sample displayed the data of the parameters obtained at every time step of the simulation. The number of samples was reduced to 3 million by saving each 100th sample to reduce the computational load of the computer and provide relatively fast training of the neural network. The input data chosen for the training were data arrays of volumetric flows, effective bulk modulus of oil, and the fixed small volume obtained from the simulation of the original system mentioned above. Pressure in the small volume was also saved and utilized as the output data for the training of the neural network. This data was chosen for training, validation, and testing of the neural network. Since all the input data, except the small volume, is variable, the neural network based on such data will work with any system with similar variable parameters. In the case of changes of the small volume, new training of the network might be required (Ustinov, Wu, and Handroos, 2022).

At the beginning of the training, the training data has to be distributed for training, validation, and testing sets, for instance in the proportion of 70/15/15 percent. The input and output data has to be normalized in a range between -1 and 1 to achieve effective training results. The NARX RNN is trained multiple times in order to find the appropriate number of neurons in hidden layers for the most accurate and effective simulation. The Levenberg-Marquardt algorithm is utilized in the training process as a main backpropagation-based training algorithm due to its relatively fast training of the network and accurate results (Wilamowski and Irwin, 2011). The Early-Stopping technique is also utilized in cases when the generalization stopped improving. The network should be trained several times, for a maximum of 1,000 epochs with a different number of neurons in each hidden layer. The results of the training are displayed in Table 4.4. The results show that the number of neurons affects the training time of the neural network, and at the same time, the most accurate validation performance was obtained at training 8 and 9 with 40 and 45 neurons in a hidden layer, respectively. Based on the obtained data, the number of neurons in the RNN was selected to achieve the most accurate result, and the most accurate network in terms of Mean-Square error (MSE) was selected for the Hybrid model simulation.

Table 4.4: Hybrid model development example: results of the training of the NARX RNN with normalized data (Ustinov, Wu, and Handroos, 2022)

Training	Number of neurons in hidden layers	Validation stop (Epoch)	Mean-Square Error (MSE)	Training time
1	5	472	0.000313	17 min
2	10	474	0.000290	28 min
3	15	1000	0.000241	1 h 19 min
4	20	1000	0.000266	1 h 50 min
5	25	1000	0.000237	2 h 18 min
6	30	1000	0.000248	1 h 58 min
7	35	1000	0.000241	2 h 33 min
8	40	1000	0.000216	3 h 33 min
9	45	1000	0.000229	3 h 39 min
10	50	1000	0.000243	4 h 30 min

In this example, the most accurate network (see Fig. 4.11a and 4.11b) contains 40 neurons in hidden layers. The validation performance of the network was expressed in the form of MSE, equal to 0.000216 (normalized data). The training time of the selected network was 3 hours and 33 minutes.

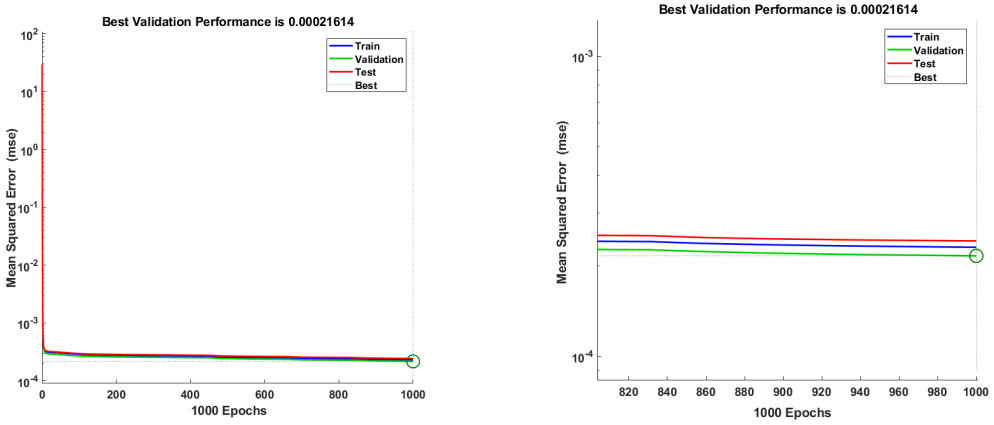

(a) (b)

Figure 4.11: Hybrid model development example: validation, train and test performance of the selected NARX RNN (a) full performance between 1 and 1000 epochs (b) a close look at the performance plot between 800 and 1000 epochs (Ustinov, Wu, and Handroos, 2022).

4.3.3 Implementation of the RNN in the hybrid model

After the training, the most accurate and fastest network should be implemented in the code of the traditional or reference mathematical model of the studied fluid power circuit. The network should be added to the code, for example in the form of a MATLAB function, as a substitute for the numerically stiff equation with small volume. As a first step, the traditional mathematical model is simulated to obtain the input dataset for the hybrid system simulation. The dataset of inputs consists of effective bulk modulus, volumetric inlet and outlet flows, and small volume.

Note that the simulation of each hybrid system should be performed after obtaining the inputs for the network, and this means that the simulation of the traditional mathematical model should be completed and input values should be saved. After that, the hybrid system can be simulated an unlimited number of times.

The simulation of the hybrid system includes the stage of preprocessing the RNN before the main model simulation with the use of the data obtained from the previous simulation. The whole system is automatically simulated using the pressure data obtained from the RNN preprocessing stage at the corresponding simulation time step (Ustinov, Wu, and Handroos, 2022).

4.3.4 Simulation results

To demonstrate the advantages of the hybrid model, trained NARX RNN is implemented to the practical Circuit 2. The goal of the simulation of Circuit 2 is to test the hybrid model at different input data, to ensure the reliability of the model and to demonstrate the ability of RNN in the hybrid model to operate correctly despite the input parameters. The comparison of the hybrid model with the traditional reference model, based on traditional Lumped-element modeling-based model, should also be done. To examine the hybrid model, two different sets of input signals (Fig. 4.12a and 4.12b) are applied to Circuit 2. First, the circuit is simulated for 50 seconds with a randomly distributed input signal in a range between -10 and +10 volts (Fig. 4.12a). The maximal simulation time step of the reference model that can be applied to the system is 1.0×10^{-5} s. The hybrid model runs at a time step of 1.0×10^{-4} s, due to the elimination of numerical stiffness of the system by substitution of stiff differential equation into NARX RNN.

As the result, the actual simulation time for the real 50 seconds is 501.47 seconds for the reference model. Compared to the simulation time of the hybrid model (53.27 s), the reference is almost ten times slower. Nevertheless, the simulation time difference between the two models is associated with the time step difference at the same level of accuracy, which can be observed among the simulation results in Table 4.5 (see Fig. 4.13).

The responses of pressure p_v related to small volume as well as the cylinder piston po-

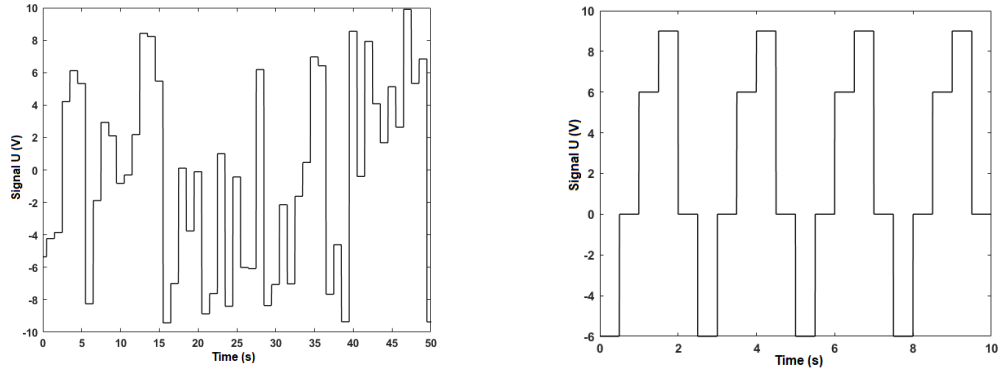

(a) (b)

Figure 4.12: Signal U for Circuit 2 simulations: (a) random input signal and (b) repeatable input signal (Ustinov, Wu, and Handroos, 2022).

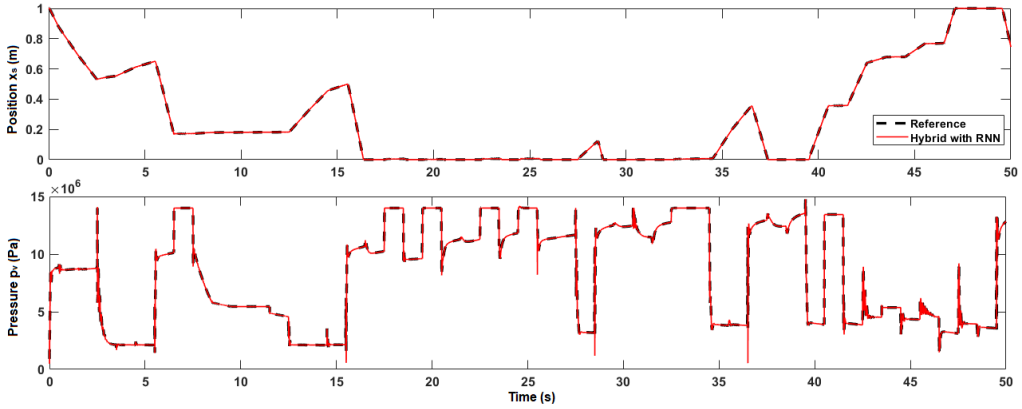

Figure 4.13: Circuit 2 responses of cylinder piston position x_s and pressure p_v at random input voltage comparing the reference model and hybrid model with utilized RNN (Ustinov, Wu, and Handroos, 2022).

sition x_s for the reference and hybrid models with a random input signal are illustrated by plots in Fig. 4.13. The accuracy of the hybrid model in comparison to the reference is well-observed in the plot. The RRMSE for the reference model defined in (4.2) and represented in the simulation results (Table 4.5) was calculated for the hybrid system and equals 0.089% for the cylinder piston position x_s and 1.479% for pressure in small volume p_v.

Another simulation of Circuit 2 is performed within 10 seconds, utilizing the repeatable input signal in a range between -6 and +9 Volts, with a time period of 2.5 seconds. Both reference and hybrid models of Circuit 2 are simulated. The simulation time steps remain

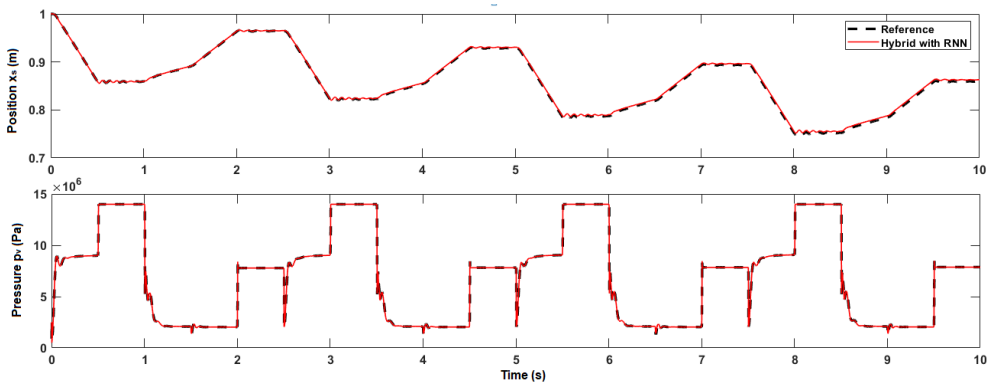

Figure 4.14: Circuit 2 responses of cylinder piston position x_s and pressure p_v at repeating input voltage comparing the reference system and hybrid system with utilized RNN (Ustinov, Wu, and Handroos, 2022).

the same for the reference and hybrid models, which are 1.0×10^{-5} s and 1.0×10^{-4} s, respectively. The responses of cylinder piston position x_s and pressure in small volume p_v are plotted in Fig. 4.14. It is clear from the plot that the hybrid model piston position and pressure in small volume responses are accurate enough compared to the reference model responses, with a resultant RRMSE of 0.260% and 2.441% for cylinder piston position x_s and pressure p_v, respectively.

The simulation times of the circuit, with a repeatable input signal for the reference and hybrid models, are presented in Table 4.5. The actual time of hybrid model simulation is only 9.89 seconds, while the simulation of the reference model requires almost ten times as much time (102.96 seconds).

At the end of the simulation, it can be concluded that, at both the random and repeatable sets of input signals, the performance of the hybrid model is stable and accurate despite the RNN being utilized instead of the stiff differential pressure equation, trained on the random data obtained from the 3,000-second simulation. Moreover, the simulation time of the hybrid system is significantly shorter than with the traditional mathematical model. It means that the conversion of the model, for instance to C++ code, may allow simulating it in real-time, or even faster than real-time applications.

However, it is also important to note that a hybrid model based on the same neural network and used to simulate other fluid power circuits may behave differently. For example, in a simple three-orifice circuit simulation scenario, the simulation speed of the hybrid model is usually higher than that of the reference model, with a simulation time step of 1.0×10^{-3} s and 1.0×10^{-4} s for the hybrid and reference models, respectively, but the rise time slightly increases, as shown in Figure 4.15. This effect is similar to what happens when increasing the size of a small volume to achieve stable numerical integration. This

Table 4.5: Circuit 2 simulation results (Ustinov, Wu, and Handroos, 2022)

Input	System	Real time, s	Time step, s	Simulation time, s	RRMSE, %
Random	Reference	50	1.0×10^{-5}	501.47	-
	Hybrid		1.0×10^{-4}	53.27	$RRMSE_{x_s} = 0.089\%$
					$RRMSE_{p_v} = 1.479\%$
Repeatable	Reference	10	1.0×10^{-5}	102.96	-
	Hybrid		1.0×10^{-4}	9.89	$RRMSE_{x_s} = 0.260\%$
					$RRMSE_{p_v} = 2.441\%$

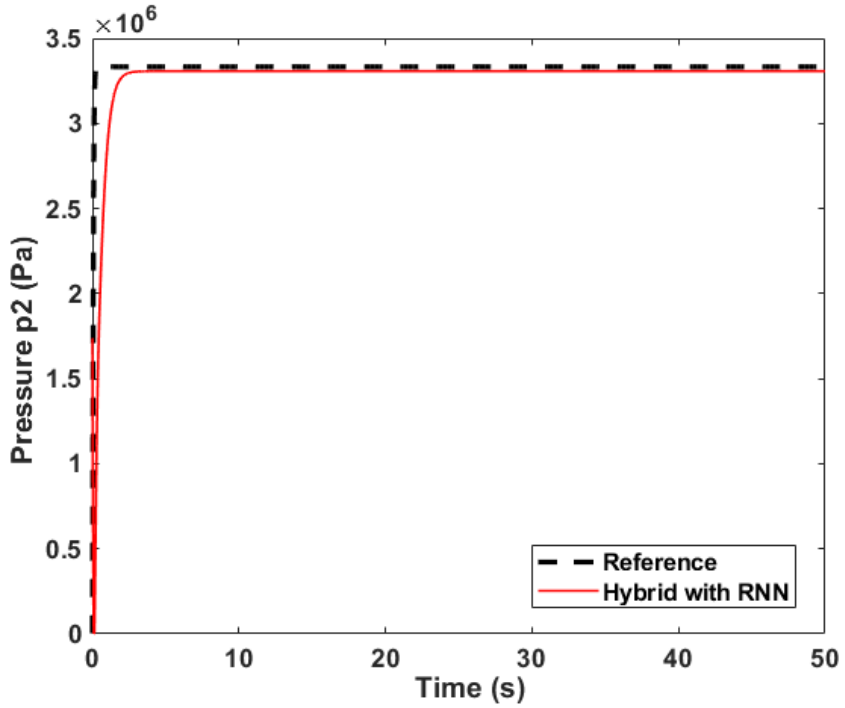

Figure 4.15: Simple three orifice fluid power circuit pressure responses of reference and hybrid models (Ustinov, Wu, and Handroos, 2022).

effect may occur due to the use of a single neural network for different fluid power circuits and can be solved by retraining the neural network on another model.

5 Conclusion

The purpose of this dissertation is to present three new methods of simulation fluid power circuits in the presence of singularities, particularly, the numerical stiffness of differential equations of pressure with small pipe volumes in such equations. First of all, examples of stiff fluid power circuits are presented and the most common methods and techniques of overcoming numerical stiffness are studied. Then, to develop new methods of numerical stiffness elimination, several old techniques already existing in the field of fluid power circuit computer simulation were studied in detail and tested. Due to the imperfection of these methods, new advanced methods and models were developed. Such methods are Advanced Pseudo-Dynamic Solver(AdvPDS), Method of Multiple Scales(MMS) and the hybrid method of simulation, utilizing neural networks instead of the stiff differential equation of pressure built up in small volumes. New methods were applied to the classical Lumped-element modeling-based models of such circuits in order to improve the simulation in terms of simulation speed and system output response accuracy. New models, based on the above-mentioned advanced methods of numerical stiffness elimination were tested in multiple simulations of such circuits. The summary of the tests are described below.

In Publication I, the Advanced Pseudo-Dynamic Solver with adaptive criterion has been proposed for the fast and accurate solution of stiff fluid power circuits. The solver is based on the classical Pseudo-Dynamic Solver and differs from it in two main aspects. The first difference, is the transfer of volumetric flow calculations in the mathematical model, from the main integration loop of the solver to the inner loop with the stiff differential equation of pressure in small volumes. Second, the AdvPDS solver has the adaptive criteria of convergence in the inner loop, which brings the rise of output response accuracy in low pressure areas and improvement of the system simulation speed. These changes are made according to the multiple tests of the classical Pseudo-Dynamic Solver in stiff fluid power circuits described in this dissertation. In addition, due to the unstable response of the classical Pseudo-Dynamic Solver in several complex circuits, the most preferable method of simulation of such circuits can be the AdvPDS-based model of the circuit. The AdvPDS was also tested in practical stiff fluid power circuits (Circuit 1 and Circuit 2) and showed great possibility for the simulation to achieve a trade-off between the simulation speed and output pressure or cylinder piston position accuracy. This precision in calculations is ensured by the adaptive criteria of convergence, as mentioned above. Despite the fact that both accuracy and speed of AdvPDS-based model have a fairly good trade-off, this method also has limitations, for example, such a scenario is possible that for some systems it will be necessary to pre-determine the pressure limits and, accordingly, the convergence criteria for effective use of the method in practice. This problem can be solved by improving the method using optimization algorithms for efficient search for convergence criteria. However, the study results shown that the solver can be used in different real-time or faster than real-time applications, for instance, as a part of multibody dynamic simulation of hydraulically driven mobile working machines or robots, in

digital twin or virtual prototype of such a machine.

In Publication II, the Method of Multiple Scales(MMS) for time-efficient and accurate simulation of stiff fluid power circuits, in which stiffness is associated with small volumes, was proposed. To demonstrate the features and advantages of the method, the comparison between the reference Lumped-element modeling-based, SPT-based, and MMS-based models are considered for three different input signals. A practical stiff fluid power circuit (Circuit 2) was studied as an example in the simulation. The same fluid power circuit is used to investigate the effects of the SPT-based and MMS-based models, applied to the differential equation of pressure built up in the small hydraulic volume, on the computational efficiency expressed through the integrator time step of the model and the accuracy of the system response. The experimental simulation of the three above-mentioned models implemented in the stiff fluid power circuit demonstrates that the SPT-based model requires the corrector factor to achieve an accurate output pressure and position responses, otherwise the accumulative error occurs through the simulation time of the model. In its turn, the MMS-based model reveals the potential of the simulation of the stiff fluid power circuits and shows an accurate response of the cylinder piston position at different input signals, even at large integrator time steps. However, despite acceptable accuracy and excellent simulation speed, the possibilities of the method can be limited, for example, by using several orifices connected to the volume. One further study might be to test the method in this setup.

Publication III proposes a novel so-called hybrid method to solve the fundamental problem of numerically stiff differential equations in the dynamic simulation of fluid power circuits. The idea of the method lies in the use of the NARX recurrent neural network in the simulation model, which acts as a substitution for the stiff continuity equation of volumetric flow with a small volume. The dynamics of the remaining parts of the system are preserved and modeled with conventional differential and algebraic equations. The neural network is trained using data from the practical stiff fluid power circuit (Circuit 2) simulation for receiving an accurate response from the system. To demonstrate the features and advantages of the hybrid method of fluid power circuit simulation, the classical Lumped-element modeling-based model and the hybrid model are compared. The practical Circuit 2 is experimentally tested at random and repeating inputs to show the features of hybrid model. In this demonstration, the response of the hybrid model is several times faster than the conventional reference model due to the elimination of the numerical stiffness problem by substitution of the stiff differential equation by the NARX recurrent neural network. At the same time, the accuracy of the hybrid model is relatively high, which allows a trade-off between the accuracy of the response and speed of the simulation. This model also has limitations associated with the time spent on training, as well as on tuning the neural network, which will act as a surrogate model built into the main fluid power circuit model. In addition, this model is dependent on the conditions and parameters of the system on which the training takes place, for example, in some cases it will be difficult to use a model trained on the data collected from one system with another system

with totally different parameters (for example, a different volume). Performance of the model depends on the training process of the neural network and the quality of dataset utilized for training. In other words, it will be difficult to use the same neural network in systems with radically different parameters, and the model will fully reveal itself in such applications as digital twins of a particular machine.

Finally, all the methods and models presented in this dissertation can be used in different real-time, faster than real-time, or multibody dynamic applications, such as digital twins or virtual prototypes of mobile working machines, cranes, and robots. The main advantage of the models is the possibility to reduce or eliminate the numerical stiffness of fluid power circuits in the presence of small volumes in pressure differential equations, which can slow down the simulation. As a result, the trade-off between the simulation speed, time-efficiency, and the accuracy of system outputs can be achieved. Future studies or development of new methods or models can be associated, for instance, with the use of the AdvPDS-based model of fluid power circuits as a part of the simulation model of a mobile working machine for real-time applications. Testing and comparison of various time series RNN architectures (e.g., LSTM, GRU architectures) to find the most time-efficient and accurate network for hybrid models for real-time simulation of fluid power circuits can also be an important topic in further research.

References

Åman, R. (2011). Methods and Models for Accelerating Dynamic Simulation of Fluid Power Circuits. PhD dissertation. Lappeenranta-Lahti University of Technology.

Åman, R. and Handroos, H. (2008). Pseudo-dynamic solution of pressures in small volumes in fluid power circuit simulation. In: *Proceedings of the 5th FPNI PhD Symposium Cracow*, pp. 406–416.

Åman, R. and Handroos, H. (2009). Comparison of Numerical Effectiveness of Three Methods for Modelling 2-Way Flow Control Valves. In: *Proceedings of the 7th International Conference on Fluid Power Transmission and Control (ICFP 2009)*. Vol. 1. Hangzhou, China: Beijing World Publishing Corporation, pp. 711–715.

Åman, R. and Handroos, H. (2010). Optimization of parameters of pseudo-dynamic solver for real-time simulation of fluid power circuits. In: *Workshop Proceedings, 7th International Fluid Power Conference Aachen*. Vol. 1, pp. 495–507.

Åman, R., Handroos, H., and Eskola, T. (2008). Computationally efficient two-regime flow orifice model for real-time simulation. *Simulation modelling practice and theory* 16(8), pp. 945–961. ISSN: 1569-190X.

Axin, M., Braun, R., Dell'Amico, A., Eriksson, B., Nordin, P., Pettersson, K., Staack, I., and Krus, P. (2010). Next Generation Simulation Software using Transmission Line Elements. In: vol. Fluid Power and Motion Control : Centre for Power Transmission and Motion Control, pp. 265–276. ISBN: 978-1-86197-181-4.

Baer, K., Ericson, L., and Krus, P. (2020). Robustness and performance evaluations for simulation-based control and component parameter optimization for a series hydraulic hybrid vehicle. *Engineering Optimization* 52(3), pp. 446–464.

Bidini, G. and Mariani, F. (1997). Simulation of hydraulic power plant transients using neural networks. *Proceedings of the Institution of Mechanical Engineers, Part A: Journal of Power and Energy* 211(5), pp. 393–398. ISSN: 0957-6509.

Borutzky, W., Barnard, B., and Thoma, J. (2002). An orifice flow model for laminar and turbulent conditions. *Simulation Modelling Practice and Theory* 10(3-4), pp. 141–152. ISSN: 1569190X.

Bowns, D. E. and Wang, L. M. (1990). The digital computation of pressures in hydraulic pipes with small volume using an iterative technique. *Proceedings of the Institution of Mechanical Engineers, Part C: Mechanical Engineering Science* 204(1), pp. 29–36. ISSN: 0263-7154.

Braun, R. and Krus, P. (2012). Multi-Threaded Real-Time Simulations of Fluid Power Systems Using Transmission Line Elements. In: vol. In proceedings of the 8th International Fluid Power Conference, pp. 131–138.

Braun, R. and Krus, P. (2013). Tool-Independent Distributed Simulations Using Transmission Line Elements And The Functional Mock-up Interface. In: vol. In proceedings of the 54th SIMS Conference, pp. 131–138.

Braun, R., Nordin, P., Ericson, L., Larsson, L. V., Krus, P., and Pettersson, M. (2020). Hopsan: An Open-Source Tool for Rapid Modelling and Simulation of Fluid and Mechatronic Systems. In: vol. BATH/ASME 2020 Symposium on Fluid Power and Motion Control. Fluid Power Systems Technology. V001T01A047. DOI: 10.1115/FPMC2020-2796. URL: https://doi.org/10.1115/FPMC2020-2796.

Canudas de Wit, C., Olsson, H., Åström, K. J., and Lischinsky, P. (1993). Dynamic friction models and control design. In: *Proceedings of the 1993 American Control Conference, San Francisco, California*, pp. 1920–1926.

Canudas de Wit, C., Olsson, H., Åström, K. J., and Lischinsky, P. (Mar. 1995). A new model for control of systems with friction. *IEEE Transactions on Automatic Control* 40(3), pp. 419–425. DOI: 10.1109/9.376053.

Chen, R. T. Q., Rubanova, Y., Bettencourt, J., and Duvenaud, D. (2018). Neural ordinary differential equations. *arXiv:1806.07366*.

Curtiss, C. F. and Hirschfelder, J. O. (1952). Integration of Stiff Equations. *Proceedings of the National Academy of Sciences* 38(3), pp. 235–243. ISSN: 0027-8424. DOI: 10.1073/pnas.38.3.235. eprint: https://www.pnas.org/content/38/3/235.full.pdf.

Ellman, A. and Piché, R. (1996). A modified orifice flow formula for numerical simulation of fluid power systems. In: *Proceedings of the 1996 ASME International Mechanical Engineering Congress and Exposition, Atlanta, Fluid power Systems and Technology*. Vol. 3, pp. 59–63.

Ellman, A. and Piché, R. (1999). A two regime orifice flow formula for numerical simulation. *Journal of Dynamic Systems, Measurements, and Control* 121(4), pp. 721–724.

Handroos, H. and Vilenius, M. (1991). Flexible Semi-Empirical Models for Hydraulic Flow Control Valves. *J Mech Design* 113(3), pp. 232–238. DOI: 10.1115/1.2912774.

Jelali, M. and Kroll, A. (2003). *Hydraulic Servo-systems: Modelling, Identification and Control*. Advances in Industrial Control. Springer-Verlag London. DOI: 10.1007/978-1-4471-0099-7.

Kiani-Oshtorjani, M., Mikkola, A., and Jalali, P. (2019). Numerical Treatment of Singularity in Hydraulic Circuits Using Singular Perturbation Theory. *IEEE/ASME Transactions on Mechatronics* 24(1), pp. 144–153. ISSN: 1083-4435. DOI: 10.1109/TMECH.2018.2876157.

Kiani-Oshtorjani, M., Ustinov, S., Handroos, H., Jalali, P., and Mikkola, A. (2020). Real-Time Simulation of Fluid Power Systems Containing Small Oil Volumes, Using the Method of Multiple Scales. *IEEE Access* 8, pp. 196940–196950. DOI: 10.1109/ACCESS.2020.3034698.

Krishna, M. and Bares, J. (1998). Hydraulic system modeling through memory-based learning. In: *Proceedings. 1998 IEEE/RSJ International Conference on Intelligent Robots and Systems. Innovations in Theory, Practice and Applications (Cat. No.98CH36190)*. Vol. 3, 1733–1738 vol.3. DOI: 10.1109/IROS.1998.724848.

Krishna, M. and Bares, J. (1999). Constructing Fast Hydraulic Robot Models for Optimal Motion Planning. *J. Aerosp. Eng.* 12, pp. 34–42.

Krus, P., Jansson, A., Palmberg, J.-O., and Weddfelt, K. (1990). Distributed simulation of hydromechanical systems. In: vol. In The Third Bath International Fluid Power Workshop.

Krus, P. (2009). Robust modelling using bi-lateral delay lines for real time and faster than real time system simulation. In: vol. n ASME 2009 International Design Engineering Technical Conferences and Computers and Information in Engineering Conference, American Society of Mechanical Engineers, pp. 131–138.

Lacny, L. (2012). Modelling of the dynamics of a gyroscope using artificial neural networks. *Journal of Theoretical and Applied Mechanics* 50(1), pp. 85–97.

Liermann, M., Feller, C., and Lindinger, F. (2021). Real-time simulation of fluid power systems. In: vol. ASME/BATH 2021 Symposium on Fluid Power and Motion Control.

Malysheva, I., Handroos, H., Zhidchenko, V., and Kovartsev, A. (2018). Faster than real-time simulation of a hydraulically actuated log crane. In: *2018 Global Fluid Power Society PhD Symposium (GFPS)*, pp. 1–6. DOI: 10.1109/GFPS.2018.8472405.

Malysheva, J., Li, M., and Handroos, H. (2020). Hydraulic System Modeling with Recurrent Neural Network for the Faster Than Real-Time Simulation. *IREMOS* 13(1). ISSN: 2533-1701.

Malysheva, J., Ustinov, S., and Handroos, H. (2021). Computationally Efficient Practical Method for Solving the Dynamics of Fluid Power Circuits in the Presence of Singularities. *IEEE/ASME Transactions on Mechatronics* 26(5), pp. 2385–2395. DOI: 10.1109/TMECH.2020.3038929.

Merritt, H. E. (1967). *Hydraulic Control Systems*. Wiley. ISBN: 978-0-471-59617-2.

Mikkola, A. (1999). Using the Simulation Model for Identification of the Fatigue Parameters of Hydraulically Driven Log Crane. *J Mech Design* 123(1), pp. 125–131. DOI: 10.1115/1.1343110.

Noethen, L. and Walcher, S. (2011). Tikhonov's theorem and quasi-steady state. *Discrete and Continuous Dynamical Systems - Series B* 16(3), pp. 945–961.

Olsson, H. (1996). Control Systems with Friction. PhD thesis. Lund, Sweden: Department of Automatic Control, Lund Institute of Technology.

Pan, S. and Duraisamy, K. (2018). Long-Time Predictive Modeling of Nonlinear Dynamical Systems Using Neural Networks. *Complexity* 2018, pp. 1–26.

Park, C.-G., Yoo, S., Ahn, H., Kim, J., and Shin, D. (2020). A coupled hydraulic and mechanical system simulation for hydraulic excavators. *Proceedings of the Institution of Mechanical Engineers, Part I: Journal of Systems and Control Engineering* 234(4), pp. 527–549. DOI: 10.1177/0959651819861612.

Patel, A. and Dunne, J. (2003). NARX Neural Network Modelling of Hydraulic Suspension Dampers for Steady-state and Variable Temperature Operation. *Vehicle System Dynamics* 40(5), pp. 285–328. DOI: 10.1076/vesd.40.5.285.17911.

Piché, R. and Ellman, A. (1994). Numerical integration of fluid power circuit models using two-stage semi-implicit runge-kutta methods. *Proceedings of the Institution of Mechanical Engineers, Part C: Journal of Mechanical Engineering Science* 208(3), pp. 167–175. ISSN: 0954-4062.

Rahikainen, J., Kiani, M., Sopanen, J., Jalali, P., and Mikkola, A. (2018). Computationally efficient approach for simulation of multibody and hydraulic dynamics. *Mechanism and Machine Theory* 130, pp. 435–446. ISSN: 0094114X. DOI: 10.1016/j.mechmachtheory.2018.08.023.

Schram, G., Verhaegen, M., and Krijgsman, A. (1996). System Identification with Orthogonal Basis Functions and Neural Networks. *IFAC Proceedings Volumes* 29(1). 13th World Congress of IFAC, 1996, San Francisco USA, 30 June - 5 July, pp. 4150–4155. ISSN: 1474-6670. DOI: https://doi.org/10.1016/S1474-6670(17)58331-7. URL: https://www.sciencedirect.com/science/article/pii/S1474667017583317.

Siegelmann, H., Horne, B., and Giles, C. (1997). Computational capabilities of recurrent NARX neural networks. *IEEE Transactions on Systems, Man, and Cybernetics, Part B (Cybernetics)* 27(2), pp. 208–215. DOI: 10.1109/3477.558801.

Tikhonov, A. N. (1952). Systems of differential equations containing small parameters in the derivatives. *Matematicheskii sbornik* 73(3), pp. 575–586. ISSN: 0368-8666.

Tuttle, J. F., Blackburn, L. D., Andersson, K., and Powell, K. M. (2021). A systematic comparison of machine learning methods for modeling of dynamic processes applied to combustion emission rate modeling. *Applied Energy* 292, p. 116886. ISSN: 0306-2619.

Ustinov, S., Wu, H., and Handroos, H. (2022). A Hybrid Model for Fast and Efficient Simulation of Fluid Power Circuits With Small Volumes Utilizing a Recurrent Neural Network. *IEEE Access* 10, pp. 48824–48835. DOI: 10.1109/ACCESS.2022.3172662.

Vermaak, J. and Botha, E. (1998). Recurrent neural networks for short-term load forecasting. *IEEE Transactions on Power Systems* 13(1), pp. 126–132. DOI: 10.1109/59.651623.

Wilamowski, B. and Irwin, J. (2011). *Intelligent Systems: The Industrial Electronics Handbook (2nd ed.)* CRC Press.

Zheng, Y., Ge, T., and Liu, J. (2015). Kinematics modeling and control simulation for a logging harvester in virtual environments. *Advances in Mechanical Engineering* 7(10), p. 1687814015611329. DOI: 10.1177/1687814015611329.

Zhidchenko, V., Malysheva, I., Handroos, H., and Kovartsev, A. (Sept. 2018). Faster than real-time simulation of mobile crane dynamics using digital twin concept. *Journal of Physics: Conference Series* 1096, p. 012071. DOI: 10.1088/1742-6596/1096/1/012071.

Publication I

Malysheva, J., Ustinov, S., and Handroos, H.
Computationally Efficient Practical Method for Solving the Dynamics of Fluid Power Circuits in the Presence of Singularities

Reprinted with permission from
IEEE/ASME Transactions on Mechatronics
Vol. 26, no. 5, pp. 2385-2395, 2021

Computationally Efficient Practical Method for Solving the Dynamics of Fluid Power Circuits in the Presence of Singularities

Julia Malysheva, Stanislav Ustinov, and Heikki Handroos, *Member, IEEE*

***Abstract*—In this article, a practical method is proposed for the efficient solution of fluid power systems with singularities originating (in particular) from the presence in the system of small volumes. The method is based on the use of an enhanced version of the pseudodynamic solver (the advanced pseudodynamic solver), which seeks the steady-state solution of pressure building up in the small volume. This solver can be attributed to the class of explicit solvers. There are two main advantages of the proposed solver. The first is the higher accuracy and numerical stability of the solution compared with the classical pseudo-dynamic solver, owing to the enhanced solver structure and the use of an adaptive convergence criterion. The second is the faster calculation time compared with conventional integration methods such as the fourth-order Runge–Kutta method, owing to the obtained possibility of larger integration time step usage. Thus, the advanced pseudodynamic solver can become a preferred method in the simulation of complex fluid power circuits. Simulation results of the C code implementation confirm that the advanced pseudodynamic solver is better than conventional solvers for the solution of the real-time systems that include fluid power components with small volumes.**

***Index Terms*—Advanced pseudodynamic solver (AdvPDS), real-time systems, Runge–Kutta integration, small hydraulic volumes modeling, stiff fluid power system modeling and simulation.**

I. Introduction

THE LEVEL of automation of mobile working machines, such as excavators, logging harvesters, or hydraulically driven cranes, as well as their complexity, have increased significantly over the past few decades. In the machine industry, this has led to emergence of novel approach in the new product development process, such as virtual prototyping [1]–[3]. Essentially, a virtual prototype of a mobile machine is the mathematical representation of all machine elements as well as their interactions. To estimate the performance of a mobile machine under development, a simulation of the virtual prototype is used. However, a major problem of virtual prototypes is often the speed of their simulation, which in particularly is related to the complexity and characteristics of the employed mathematical models. A number of studies have been dedicated to the problems of real-time [2], [4]–[6], and faster than real-time simulation [7] of the virtual prototypes of mobile machines.

The mechanical and fluid power components are the essential parts of any virtual prototype of mobile machines [1], [2], [8], [9], as well as various other types of mechatronic systems, such as aircrafts, heavy industrial process machines, ships, off-shore cranes, etc. The mathematical model of fluid power components can be presented with sets of algebraic and differential equations. By nature, such differential equations are highly nonlinear [10], and often contain singularities that make the model mathematically stiff. In particular, the stiffness in the modeling of fluid power systems is often associated with high values of the bulk modulus or with the presence of small volumes in the components of the circuit. Numerical stiffness of the model directly affects the simulation time, which is the vital aspect in real-time simulation in mechatronic applications. For instance, such problem is highlighted in [11], where authors try to solve a problem of real-time simulation of the excavator which is related to numerical stiffness in fluid power model. In order to achieve the real-time simulation speed, the model was divided into multiple submodels for parallel execution and a local stiff integration solver was applied to the hydraulic submodels. The same problem has been recently highlighted in a number of works dedicated to human-in-the-loop and hardware-in-the-loop systems that have fluid power components. For example in [12], authors had to simplify the fluid power model of the mechatronic component and to use third-order explicit solver with small time step in order to ensure the hardware-in-the-loop real-time simulation for developed controller strategy testing. Thus, the described above mechatronic applications showed the need for the development of the method that can provide a generic practical solution to accelerate simulation of mechatronic systems including small hydraulic volumes with a minor cost in the accuracy.

In [13], Bowns and Wang were the first to formulate the mathematical stiffness problem that arises during the solution of fluid power systems in the presence of small volumes, particularly in

Manuscript received October 30, 2019; revised April 20, 2020 and October 16, 2020; accepted November 4, 2020. Date of publication November 18, 2020; date of current version October 14, 2021. Recommended by Technical Editor H. Qiao and Senior Editor X. Chen. The work was supported by the Sustainable product processes through simulation (SIM) platform in LUT University. *(Corresponding author: Julia Malysheva.)*

The authors are with the Laboratory of Intelligent Machines, Lappeenranta-Lahti University of Technology, 53850 Lappeenranta, Finland (e-mail: iuliia.malysheva@lut.fi; stanislav.ustinov@lut.fi; heikki.handroos@lut.fi).

Color versions of one or more figures in this article are available at https://doi.org/10.1109/TMECH.2020.3038929.

Digital Object Identifier 10.1109/TMECH.2020.3038929

hydraulic pipes. Physically, the mathematical stiffness occurs when the pressure is rapidly changing, owing to the low compliance of the fluid in the pipe. According to their observations, this causes the solutions of the system differential equations to decay at widely varying rates. In addition, it should be noted that the mathematical stiffness of the problem is often a local phenomenon, meaning it only occurs occasionally. Thus, if the orifice is located in the hydraulic circuit, a stiffness approaching infinity arises if the relation $\partial\Delta p/\partial Q$ is small, which is true when the volume flow Q tends to zero. Moreover, according to [14]–[16], if the purely turbulent description of the orifice is used, the mathematical stiffness occurs also when the pressure drop Δp approaches zero.

To simulate the virtual prototype, meaning to obtain a solution for the mathematical model, numerical integration is used. The family of explicit Runge–Kutta methods that use an integration time step of fixed size are well established in the solution of systems of ordinary differential equations. However, it was shown in [17] that numerical integrators based on explicit Runge–Kutta methods are not A-stable (the numerical stability of the method is not guaranteed for any integration step size), which is apparently why they are not very efficient on stiff problems unless a very small integration time step is used. At the same time, integrators based on implicit methods have established themselves as A-stable or even L-stable, which allows the accurate solution of such problems. However, implicit methods are much more computationally expensive. In general, they involve solving a nonlinear system of algebraic equations at each time step. This in turn requires a modified Newton iteration scheme, which includes the calculation of iteration matrix of the form $(\mathbf{I} - \Delta t\beta_0\mathbf{J})$, where $\mathbf{I}$ is the identity matrix, $\mathbf{J}$ is the Jacobian, and $\Delta t\beta_0$ is a scalar, and also further its factorization. The iteration scheme is repeated until a convergence criterion is reached [18]. Due to such iteration scheme the amount of computations can vary from step to step which can result in simulation time overflows. Thus, implicit methods cannot be used directly in real-time applications. In contrast to implicit methods the previously mentioned explicit methods can ensure a constant simulation time in time-critical real-time applications.

On the other hand, the integration in fluid power systems can be performed with the help of special solvers [19]. To overcome the stiffness of differential equations in fluid power systems with small volumes, a pseudodynamic solver was proposed by Åman and Handroos [20]–[22]. This solver can be related to the class of explicit solvers. The goal of the solver algorithm was to increase the accuracy and to reduce the computational time for the simulation of stiff fluid power circuits. The proposed solver was based on the assumption that if the considered volume was small enough, the build-up pressure can be substituted by a steady-state pressure. The goal was achieved by implementing an iterative technique with substituting the small volume with a volume that is large enough to obtain a numerically stable response in pressure. The solver showed its applicability at relatively large integration time steps, whereas conventional stiff models used very small time steps to simulate the circuit without numerical instability, affecting the computational time of the simulation. However, in their work, only a short-term simulation (about 2 s) with predefined inputs was considered, which did not give a full picture of the solver characteristics.

Another interesting method of solving pressures in small volumes in fluid power systems was recently introduced by Kiani–Oshtorjani *et al.* [23] and further applied for the mechatronic system accelerated simulation in [6] and [24]. The proposed method was based on singular perturbation theory. The modified version of this theory was used for the algorithm. The main principle of the algorithm was the replacement of stiff differential equation of pressure by the algebraic equation in accordance with singular perturbation theory. The replacement of the differential equation allows a numerically stable response of the pressure to be achieved at different integrator time steps. Consequently, the time step of the integration can be increased without significant losses in calculation accuracy, which allows the method to be implemented in real-time simulations. Moreover, in the works [6] and [24], Rahikainen *et al.* emphasized that the fluid power system due to its stiffness needs much smaller integration time step than the multibody system during the coupled simulation which sufficiently increases the simulation speed of the whole mechatronic system. However, the method based on singular perturbation theory may have limited applicability, such as it only can be applied under certain conditions of the system when the boundary layer is exponentially stable [23].

The objective of the present research is to develop a method that quickly finds an accurate and numerically stable solution for stiff fluid power circuits with increased modeling accuracy, to accelerate their simulation. For this purpose, the classical pseudodynamic solver [20]–[22] was selected as a basis for the research. In this work, the characteristics of the pseudodynamic solver are studied in more detail by applying long-term simulation together with random inputs to the test fluid power circuits. Based on the obtained results the new advanced pseudodynamic solver (AdvPDS) of the enhanced structure is proposed. The developed solver provides a fast and accurate solution of more complex fluid power circuits in the presence of singularities caused by small volumes.

The rest of this article is organized as follows. Section II-B describes the systems under investigation. Section III contains a brief description of the classical pseudodynamic solver. The development and features of the AdvPDS are described in Section IV. Results and discussion are presented in Section V, where the results obtained by the developed method are compared with the results obtained using conventional way models of stiff fluid power circuits and classical pseudodynamic solver. Finally, Section VI concludes this article.

II. Fluid Power Circuit Modeling

Fluid power circuit modeling can be approached from the point of view of lumped fluid theory [9], [25]. According to this theory, any fluid power circuit can be considered as a number of separate volumes with evenly distributed pressures. The volumes are separated by throttles and orifices that create pressure drops in the fluid when passing through them. In turn, the pressure drop together with orifice geometrical parameters are used for the volume flow calculation. Finally, pressure built up in each

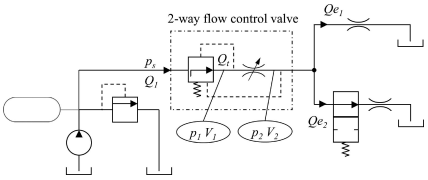

Fig. 1. Schematic representation of Circuit 1.

TABLE I
CIRCUIT 1 PARAMETERS

B_e	$1.5{\cdot}10^{9}$ Pa	C_1	$4.65{\cdot}10^{7}$
V_1	$1.0{\cdot}10^{-5}$ m^3	C_2	$-1.79{\cdot}10^{4}$
V_2	$1.0{\cdot}10^{-3}$ m^3	C_3	$4.0{\cdot}10^{11}$
k_1	$5.62{\cdot}10^{-7}$	C_5	$1.02{\cdot}10^{6}$
k_2	$5.73{\cdot}10^{-7}$	C_6	$5.26{\cdot}10^{-7}$
p_t	0 Pa	C_7	200
K	$0.05{\cdot}10^{-9}$	C_8	0.45
k_t	$1.0{\cdot}10^{-7}$	C_9	1.2

volume can be calculated using a continuity equation that relates the effective bulk modulus with respect to the considered volume and the difference between inlet Q_{in} and outlet Q_{out} volume flows [10], [26].

A. Circuit 1: Two-Way Flow Control Valve

The first system under investigation is a two-way flow control valve. The fluid power circuit related to the system is schematically depicted in Fig. 1. The circuit consists of a pressure power source, two-way flow control valve, orifice, and 2/2 directional control valve. A two-way flow control valve consists of two components: pressure compensator and control throttle. The volume between the pressure compensator and control throttle is assumed to be a small volume, the presence of which increases the stiffness of the system. The power source is assumed an ideal pressure source with constant pressure. It is composed of a hydraulic accumulator, pump, pressure relief valve, and tank. To reach the tank, hydraulic fluid flow passes through a two-way control valve and two orifices after the valve. One of the orifices is an ordinary sharp-edged orifice, whereas the other is a 2/2 directional control valve, the opening of which can be controlled by signal U_d. Pressure in the system can be integrated from the following continuity equations:

$$\dot{p}_1 = \frac{B_e}{V_1}(Q_1 - Q_t) \tag{1}$$

$$\dot{p}_2 = \frac{B_e}{V_2}(Q_t - Q_{e1} - Q_{e2}) \tag{2}$$

where B_e is the oil effective bulk modulus, V_1 and V_2 are pipeline volumes, where V_1 is a small volume, Q_1 and Q_t are volumetric flows through the pressure compensator and control throttles, and Q_{e1} and Q_{e2} are orifice and directional control valve volume flows, respectively. Volume flows Q_1 and Q_t can be obtained as follows:

$$Q_1 = K\sqrt{|p_s - p_1|}\text{sign}(\text{p}_\text{s} - \text{p}_1) \tag{3}$$

$$Q_t = k_t\sqrt{|p_1 - p_2|}\text{sign}(\text{p}_1 - \text{p}_2) \tag{4}$$

where p_s is the supply pressure, K and k_t denote the semiempirical flow coefficients for the pressure compensator throttle and for the control throttle, respectively. Both coefficients can be integrated from the following differential equations:

$$\dot{K} = \frac{C_5 - p_1 + p_2 - (C_1 + C_2(p_s - p_1))K}{C_3} \tag{5}$$

$$\ddot{k_t} = (U_e - C_9)C_6C_7^2 - 2\dot{k_t}C_8C_7 - k_tC_7^2 \tag{6}$$

where U_e is the signal applied to control throttle (opening), C_1, C_2, C_3, C_5, C_6, C_7, C_8, C_9 are empirical constants [27]. Volume flows Q_{e1} and Q_{e2} are obtained according to the following flow equations:

$$Q_{e1} = k_1\sqrt{p_2 - p_t} \tag{7}$$

$$Q_{e2} = k_2\sqrt{p_2 - p_t} \tag{8}$$

where k_1 and k_2 are semiempirical flow coefficients for the orifice and directional control valve, and p_t is the tank pressure. The initial values and constants of the system described in following equations are shown in Table I. To analyze the mathematical stiffness of the developed model of Circuit 1, its state-space representation should be derived. If we assign the state and input vectors as $\mathbf{x} = [x_1\, x_2\, x_3\, x_4\, x_5]^T = [p_1\, p_2\, K\, k_t\, \dot{k_t}]^T$ and $\mathbf{u} = [u_1\, u_2\, u_3]^T = [p_s\, U_e\, \varepsilon]^T$, respectively, then the state equations can be written as follows:

$$\begin{aligned}
\dot{x_1} &= \frac{Be}{V_1}(x_3\sqrt{u_1 - x_1} - x_4\sqrt{x_1 - x_2}) \\
\dot{x_2} &= \frac{Be}{V_2}(x_4\sqrt{x_1 - x_2} - k_1\sqrt{x_2} - u_3(k_2\sqrt{x_2})) \\
\dot{x_3} &= \frac{1}{C_3}(x_2 - x_1 + C_2x_1x_3 - C_2x_3u_1 - C_1x_3 + C_5) \\
\dot{x_4} &= x_5 \\
\dot{x_5} &= C_6C_7^2u_2 - 2C_7C_8x_5 - C_6C_7^2C_9 - C_7^2x_4.
\end{aligned} \tag{9}$$

The obtained state-space representation (9) is a multi-input–multi-output nonlinear model, where ε is the parameter that describes the binary input of the 2/2 directional control valve. If ε is equal to 0 the valve is closed and the term $k_2\sqrt{x_2}$ will be also equal to zero.

One way to detect the stiffness in the problem is to estimate the dominant eigenvalues of its Jacobian directly. In linear system theory, the eigenvalues of the system Jacobian describe the behavior modes inherent in the model. In nonlinear systems, eigenvalues and eigenvectors are time-varying. Nevertheless, it is possible to apply this approach to nonlinear problems through model linearization. Linearization means that constantly differentiating nonlinearities are linearly approximated about their operating points. As the linearized solutions can be considered as a good approximation of nonlinear system solutions about the operating point, the observations obtained locally can be generalized to the rest of the system. Further, to simplify the model we also assume that flows through the compensator and control throttles have constant coefficients K and k_t, which

is often valid and frequently employed in fluid power systems design. The Jacobian of the system can be calculated as

$$\mathbf{J} = \left.\frac{\partial \mathbf{F}}{\partial \mathbf{x}}\right|_{\mathbf{x}=\bar{\mathbf{x}},\mathbf{u}=\bar{\mathbf{u}}} \tag{10}$$

where $\mathbf{F}$ is the left-hand side of the first and second equation of (9) , $\mathbf{x}$ is the model state vector, $\mathbf{u}$ is the model input vector, and $(\bar{\mathbf{x}}, \bar{\mathbf{u}})$ is the operating point. The Jacobian for the considered system can be written as follows:

$$\begin{bmatrix} -\frac{Be}{2V_1}\left(\frac{K}{\sqrt{u_1-x_1}}+\frac{k_t}{\sqrt{x_1-x_2}}\right) & \frac{Be}{2V_1}\frac{k_t}{\sqrt{x_1-x_2}} \\ \frac{Be}{2V_2}\frac{k_t}{\sqrt{x_1-x_2}} & \frac{Be}{2V_2}\left(\frac{k_1+k_2}{\sqrt{x_2}}+\frac{k_t}{\sqrt{x_1-x_2}}\right) \end{bmatrix}. \tag{11}$$

To characterize the level of numerical stiffness of the model, we employ a condition number of the Jacobian, which, according to numerical analysis theory, can be written as

$$\kappa(\mathbf{J}) = \frac{|\lambda_{\max}(\mathbf{J})|}{|\lambda_{\min}(\mathbf{J})|} \tag{12}$$

where $\lambda_{\max}(\mathbf{J})$ and $\lambda_{\min}(\mathbf{J})$ are the maximum and minimum eigenvalues of the Jacobian, respectively, which for $\mathbf{J} \in \mathbf{M}_{n\times n}$ should satisfy $|\mathbf{J} - \lambda\mathbf{I}| = \mathbf{0}$, where $\mathbf{I}$ is the identity matrix. The condition number shows how much the eigenvalues of the system differ, i.e., small values of κ show that the problem is well-conditioned, whereas large values of κ indicate the ill-conditioned problem and the system can be considered as stiff. The condition number can be determined for the certain configuration of the system. This means that the Jacobian should be calculated in the operating point $(\bar{\mathbf{x}}, \bar{\mathbf{u}})$. To define such a point, the physical characteristics of the state variables should be considered. Thus, the following physical restrictions should be imposed on the state variables and inputs: $x_1, x_2 > 0, x_3 \in [0, 10^{-6}], x_4 > 10^{-7}, u_1 > 0, u_2 \in [0, 10], u_3 \in \{0, 1\}$. Under the restrictions, the operating point can be chosen as $\mathbf{x} = [198 \cdot 10^5,\ 1.5 \cdot 10^5,\ 10^{-6},\ 10^{-7},\ 0]^T$ and $\mathbf{u} = [200 \cdot 10^5,\ 6]^T$. Note, that x_1 and x_2 are calculated from first and second equation of (9) by substituting x_3 and x_4 with the constant values and assuming that all the rates are equal to zero.

At this point, let us consider the two cases. In the first case $V_1 = 10^{-3}\ m^3$, i.e., the volume between compensator and control throttle is quite large. The condition number of (11) in the chosen operating point for this case is $\kappa = 1.28$. In the second case the volume is reduced to $V_1 = 10^{-5}$ m^3 and the corresponding condition number becomes as large as $\kappa = 77.81$. Analyzing the system Jacobian (11), this effect can be seen through the fact that the small volume V_1 appears in the denominator of the Jacobian elements, and thus, makes the eigenvalues differ significantly in magnitude and the mathematical model (9) become numerically stiff.

B. Circuit 2: Pressure Compensating Proportional Valve

The next fluid power system considered here has a more complex structure and is more practical. The system is the part of the fluid power circuit of the hydraulic crane PATU 655 (Fig. 2), the modeling of which was considered in [4] and [7]. The considered part includes a differential cylinder with an attached sliding load, a 4/3-proportional directional valve with a pressure compensator, and a constant pressure pump. In the system, the small volume appears between the directional valve and pressure compensator. In Fig. 3, the small volume and the pressure developing within it are denoted by V_3 and p_3, respectively. The system is controlled through the voltage signal U supplied to the valve solenoids

$$\ddot{U}_s = K_v\omega_n^2 U - 2\zeta\omega_n\dot{U}_s - \omega_n^2 U_s \tag{13}$$

where K_v is the valve gain, U_s is the signal proportional to the valve spool displacement, ζ is the valve damping ratio, and ω_n is the natural angular frequency. The volume flow rates model of the 4/3-proportional directional valve using turbulent orifice

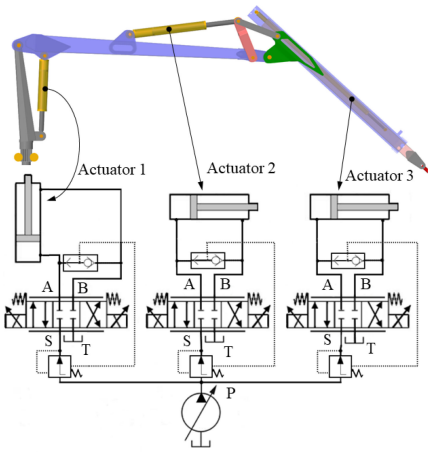

Fig. 2. Hydraulic crane PATU 655 actuated by the fluid power system.

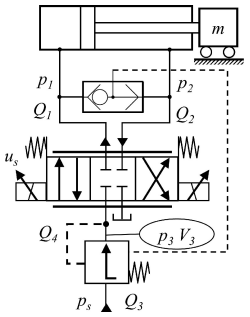

Fig. 3. Schematic representation of Circuit 2.

model with triangular groove cross section can be presented as

$$Q_1 = \begin{cases} C_\nu(U_s - U_{db})^2 \text{sign}(\text{p}_\text{s} - \text{p}_1)\sqrt{|\text{p}_\text{s} - \text{p}_1|}, & U_s \geq U_d \\ C_\nu(U_s - U_{db})^2 \text{sign}(\text{p}_1 - \text{p}_\text{t})\sqrt{|\text{p}_1 - \text{p}_\text{t}|}, & U_s \leq -U_d \\ 0, & \text{otherwise} \end{cases}$$

$$Q_2 = \begin{cases} -C_\nu(U_s - U_{db})^2 \text{sign}(\text{p}_2 - \text{p}_\text{t})\sqrt{|\text{p}_2 - \text{p}_\text{t}|}, & U_s \geq U_d \\ -C_\nu(U_s - U_{db})^2 \text{sign}(\text{p}_\text{s} - \text{p}_2)\sqrt{|\text{p}_\text{s} - \text{p}_2|}, & U_s \leq -U_d \\ 0, & \text{otherwise} \end{cases}. \quad (14)$$

In (14), C_ν is the flow constant that accounts for cross-sectional areas of the valve orifices, U_{db} is the dead band voltage of the valve, and p_1, p_2, p_s, and p_t are the pressures in two cylinder chambers, the supply pressure, and the pressure in the tank, respectively. In this work, the directional valve is assumed ideal, such that there are no internal leakages. The volume flow Q_3 related to the pressure compensator is modeled using the semiempirical approach developed in [27]

$$Q_3 = K\sqrt{p_s - p_3},$$

$$\dot{K} = \frac{1}{C3}(C5 - p_3 + p_{\text{shuttle}} - (C1 + C2(p_s - p_3))K) \quad (15)$$

where $p_{\text{shuttle}} = \max(p_1, p_2)$ is the output of the shuttle valve (see Fig. 3). The volume flow Q_4 between valve and pressure compensator can be considered as equal to Q_1 if $U_s \geq U_{db}$, and equal to $-Q_2$ if $U_s \leq -U_{db}$.

According to Newton's second law, the equation of motion of a hydraulic cylinder can be written as

$$m\ddot{x}_p = p_1 A_1 - p_2 A_2 - F_f \quad (16)$$

where $\ddot{x}_p$ is the acceleration of the cylinder piston, m is the load mass, p_1 and p_2 are the pressures in the cylinder chambers, A_1 and A_2 are the piston-side and rod-side areas, respectively, and F_f is the cylinder friction force. In turn, the friction formed in the cylinder can be represented using the LuGre friction model [28], [29]

$$\begin{cases} F_f = \sigma_0 z + \sigma_1 \dot{z} + k_\nu \dot{x}_p \\ \dot{z} = \dot{x}_p - \dfrac{|\dot{x}_p|}{g(\dot{x}_p)} z \\ g(\dot{x}_p) = \dfrac{1}{\sigma_0}\left(F_C + (F_{st} - F_C)\exp\left(-\left(\dfrac{\dot{x}_p}{v_{st}}\right)^2\right)\right) \end{cases} \quad (17)$$

where σ_0 is the flexibility coefficient, σ_1 is the damping coefficient, k_ν is the friction coefficient, F_C is the Coulomb friction, F_{st} is the Stribeck friction, and v_{st} is the Stribeck velocity. More specifically, z represents the nonmeasurable internal state, $g(\dot{x}_p)$ describes the friction behavior during constant velocity motion, and $k_\nu \dot{x}_p$ is the viscous friction.

The internal leakage flow Q_{Li} (m^3/s) between the cylinder chambers can be approximated as

$$Q_{Li} = L_i(p_1 - p_2) \quad (18)$$

where L_i is the laminar leakage flow coefficient.

TABLE II
CIRCUIT 2 PARAMETERS

m	210 kg	L_i	$1.72{\cdot}10^{-13}$ m^3/sPa
A_1	$8.04{\cdot}10^{-4}$ m^2	$C1$	$4.65{\cdot}10^{7}$
A_2	$4.24{\cdot}10^{-4}$ m^2	$C2$	$-1.79{\cdot}10^{4}$
V_{01}	$1.0{\cdot}10^{-3}$ m^3	$C3$	$4.0{\cdot}10^{11}$
V_{02}	$1.0{\cdot}10^{-3}$ m^3	$C5$	$8.0{\cdot}10^{5}$ Pa
C_ν	$2.31{\cdot}10^{-9}$ m^3/sV$\sqrt{Pa}$	V_3	$1.0{\cdot}10^{-5}$ m^3
H	1 m	U_{db}	2 V
p_s	$1.4 \cdot 10^{7}$ Pa	E_{max}	$1.8{\cdot}10^{9}$ Pa
p_t	$9.0 \cdot 10^{5}$ Pa	p_{max}	$2.8{\cdot}10^{7}$ Pa
K_v	$9.9{\cdot}10^{-1}$	σ_0	$3.2{\cdot}10^{2}$ N/m
ω_n	$3.31{\cdot}10^{2}$ rad/s	σ_1	6.3 Ns/m
ζ	$6.2{\cdot}10^{-1}$	k_ν	$1.28{\cdot}10^{3}$ Ns/m
a_1	0.5	F_C	$2.15{\cdot}10^{6}$ N
a_2	90	F_{st}	$1.13{\cdot}10^{10}$ N
a_3	3	v_{st}	$3.47{\cdot}10^{2}$ m/s

The pressures that are building up in the circuit can be calculated from

$$\begin{cases} \dfrac{V_1}{\beta_{e1}}\dot{p}_1 = Q_1 - A_1\dot{x}_p + Q_{Li} \\ \dfrac{V_2}{\beta_{e2}}\dot{p}_2 = -Q_2 + A_2\dot{x}_p - Q_{Li} \\ \dfrac{V_3}{\beta_{e3}}\dot{p}_3 = Q_3 - Q_4 \end{cases} \quad (19)$$

where the chamber volumes V_1 and V_2 are calculated as

$$\begin{cases} V_1 = A_1 x_p + V_{01} \\ V_2 = A_2(H - x_p) + V_{02} \end{cases}. \quad (20)$$

Here, H is the cylinder stroke and V_{01}, V_{02} are the dead volumes connected to the respective ports. In (19), the compressibility of hydraulic oil is accounted for by the effective bulk modulus β_{ei} $(i = 1, 2, 3)$. The effective bulk modulus for each part of the system is calculated regarding the local pressure using the empirical formula [30]

$$\beta_{ei} = a_1 E_{\text{max}} \log\left(a_2 \frac{p_i}{p_{\text{max}}} + a_3\right) \quad (21)$$

where E_{max} denotes the maximum bulk modulus of the oil, p_{max} is the maximum pressure in the system, and a_i $(i = 1, 2, 3)$ are the empirical constants. The values of parameters used in the hydraulic model described in this section are listed in Table II.

Equations (13)–(21) make up the mathematical model of Circuit 2. The presence in the model of the pressurized small volume makes the mathematical equations stiff and, hence, computationally costly.

III. Pseudodynamic Solver of Pressure in Small Volumes

The main idea of the pseudodynamic solver proposed in [16] lies in searching for a steady-state solution for pressures related to small volumes in fluid power circuits. At the same time, the pressures built up in larger volumes are solved with the conventional integration algorithms. Thus, the pseudodynamic solver includes two integration loops: the main loop, which

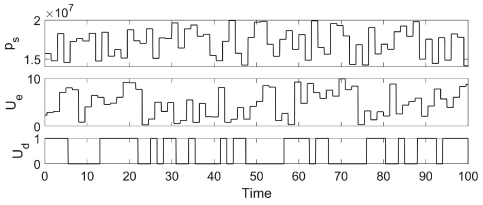

Fig. 4. Input signals for Circuit 1.

contains algebraic and differential equations related to larger volumes, and the inner loop. The inner loop, using artificially enlarged fluid volume, searches for the steady-state value of pressure passing by the transition process of pressure formation. The steady-state value of pressure is sought out during the single time step of the main loop.

The pressure inside the inner loop can be calculated from the classical continuity equation using artificially enlarged fluid volume as follows:

$$\dot{p} = \frac{B_e}{V_{\text{pseudo}}}(Q_{\text{in}} - Q_{\text{out}}) \tag{22}$$

where V_{pseudo} is the artificial pseudovolume, B_e is the effective bulk modulus of the oil, and Q_{in} and Q_{out} are the inlet and outlet volume flows, respectively. According to [21], the pseudovolume is recommended to be set at least ten times higher than the actual volume. Inlet and outlet volume flows can be expressed as a function of pressure drop as follows:

$$Q = f(\Delta p). \tag{23}$$

The integration of differential equation (22) inside the inner loop occurs by using an explicit fixed-step fourth-order Runge–Kutta integration routine with independent sufficiently small time step t_i. The integration routine continues until the convergence criterion is reached. The criterion is a predefined user parameter, which represents the first derivative of the pressure. It is important to note that the activation of the inner loop suspends the main loop until the steady-state pressure value is found.

IV. Development of the AdvPDS With Adaptive Criterion

To study the characteristics of the pseudodynamic solver described in Section III, a simple fluid power system (Circuit 1) was employed. Circuit 1 is a more complicated variant of the fluid power circuit used in [21]. The three random signals in the form of pseudorandom multilevel signals were supplied as the inputs: supply pressure p_s in the range 14–20 MPa, control voltage to the control throttle U_e in the range -10 to +10 V, and directional valve control signal U_d, which took either 1 when it is open or 0 when it is closed (see Fig. 4). The signals were supplied asynchronously with a period of 0.5 s. The system was simulated using a conventional fourth-order Runge–Kutta integrator with sufficiently small time step of 10^{-6} s for 100.5 s. During the simulation, the small volume V_1 is equal to 10^{-5} m^3. The simulation took about 5 h using the following simulation environment: MATLAB 2018b, Intel Core i5-4590 3.30 GHz

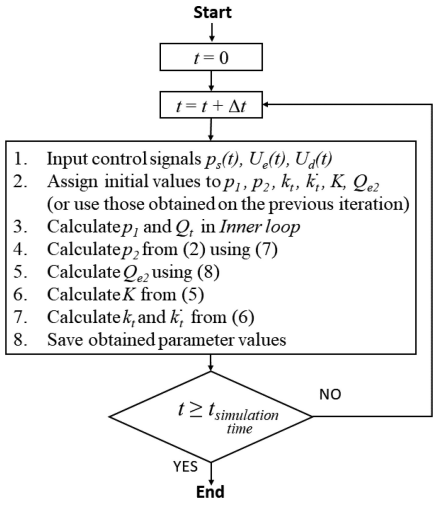

Fig. 5. Main loop sequence for Circuit 1.

with 16 GB of RAM, running OS Windows 7 64-b. The fourth-order Runge–Kutta solver is considered further in this work as a reference solver and the solutions obtained with its help thus also considered as a reference. The solution for the pressure p_1 was obtained under such conditions and was used as a reference in the case of Circuit 1.

The classical pseudodynamic solver (described in Section III) was introduced in the same simulation using recommended parameters. Unfortunately, it could not achieve a stable solution compromising its speed and accuracy. While studying the reasons for such a behavior, it was discovered that the solver becomes numerically unstable in areas of sudden pressure change owing to fixed Q_{out} in (22) during integration in the inner loop. To stabilize the numerical solution it was decided to move the calculation of Q_{out} into the inner loop. Thus, in terms of Circuit 1, the pressure build-up in the small volume (1) as well as inlet and outlet volume flows described by (3) and (4), respectively, are calculated in the inner loop. However, it was also found that the calculation of other system elements such as K and k_t inside the inner loop does not have much of an effect on the solution accuracy, moreover it makes the simulation longer. These findings formed the basis for the AdvPDS.

Further, in order to describe the operating principle of the AdvPSD Circuit 1 is used as an implementation example. Similar to the classical pseudodynamic solver, the AdvPDS consists of two integration loops.The main loop (see Fig. 5) begins with the reading of the current control signals $p_s(t)$, $U_e(t)$, and $U_d(t)$. Then, the initial values of pressures p_1 and p_2, as well as current control signal $p_s(t)$ are sent to the inner loop, and the inner loop starts to execute. Initial values of pressures, volume flows, and flow coefficients are used in the main and inner loops during the first iteration. In the following iterations, the pressure and flow values are updated every time step. The inner loop (see

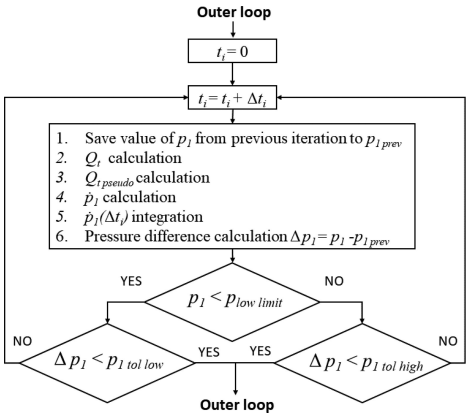

Fig. 6. Inner loop sequence for Circuit 1.

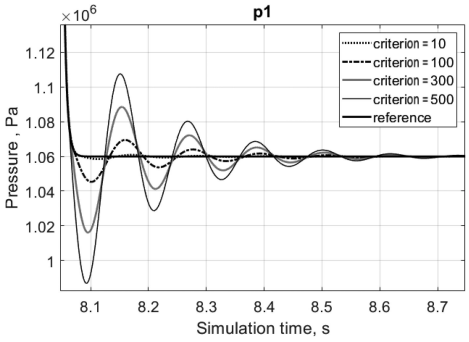

Fig. 7. Effect of the criterion value on the low-pressure calculation using the AdvPDS.

Fig. 6) first saves the previous value of the pressure p_1. The value of pressure should be saved every iteration to calculate the rate of pressure change between the adjacent iterations. The running of the inner loop occurs at its own integration time step Δt_i that may differ from the main loop time step Δt. It is important to note that the main loop is suspended during the execution of the inner loop. Further calculation of the volume flows through the pressure compensator ($Q_{1\text{pseudo}}$) and control throttle (Q_t) is performed only inside the inner loop using (3) and (4), respectively. Next, the pressure p_1 is integrated from (1). Note, that the small volume from (1) is substituted with the pseudovolume as in (22). Obtained pressure value is used to calculate the pressure difference, which is further compared to the convergence criterion value.

In the classical pseudodynamic solver the single convergence criteria was used. The criteria was based on the rate of pressure change between the iterations in the inner loop. The rate of pressure change between the iterations Δp_1 can be written as

$$\Delta p_1 = p_1 - p_{1\text{prev}} \tag{24}$$

where p_1 is the pressure from the current iteration, and $p_{1\text{prev}}$ is the pressure from the previous iteration of the inner loop. The rate of pressure change is compared with the convergence criterion value to detect the beginning of the steady-state process of the pressure. The captured steady-state value is further passed to the main loop.

The effect of the single criterion value in the inner loop of the AdvPDS on the solution accuracy was also studied. It was discovered that applying a smaller convergence criterion in the inner loop produces a more numerically stable result when the pressure approaches its lower values during the simulation. In Fig. 7, the effect of the criterion value on the calculation of the low pressures using the AdvPDS is shown. At the same time, it was noticed that the computational time of the simulation increases with the criterion decrease owing to the large number of iterations performed inside the inner loop. Thus, the adaptive convergence criterion was proposed. The idea behind the adaptive criterion is that depending on the pressure level, the criterion with the most suitable time-efficient and numerically stable effect on the pressure is automatically selected during the fluid power circuit simulation. According to Fig. 6 when the pressure difference between the iterations Δp_1 is calculated using (24) the current pressure level p_1 is compared to assigned low-pressure level $p_{\text{low limit}}$. If the current pressure level is low the smaller criteria is used, i.e., inner loop continues to iterate until the change in the pressure is less then $p_{1\,\text{tol low}}$. If $p_1 > p_{\text{low limit}}$ the inner loop proceeds with criteria $p_{1\,\text{tol high}}$. In other words, at low pressure levels in the system, the smaller criterion is implemented to achieve a more numerically stable result. At pressure levels higher than the low-pressure limit, the bigger criterion is used to reduce the computational time of the simulation. The low-pressure level was defined experimentally and for both Circuits 1 and 2 it was 22 bar. Both criteria have to be predefined by the user before the simulation, based on the recommendations given further in this work. When the criterion is satisfied, the value of pressure p_1 and flow Q_t are updated for subsequent calculations in the main loop. The main loop further updates the pressure p_2, and flows Q_{e1} and Q_{e2} according to (2), (7), and (8), respectively. Then calculation of flow coefficients (K and k_t) according to (5) and (6) is performed. The next iteration of the main loop begins at the next time step Δt. The process continues for all specified simulation time.

V. Results and Discussion

In this section, the results of the simulation of the two fluid power circuits described in Section II-B are presented. The results are represented through a comparison of the responses of the considered fluid power circuits obtained using the reference solver and the AdvPDS. The results demonstrate the features of the proposed method and its advantages compared with the traditional method of fluid power system modeling and simulation.

A. Circuit 1 Simulation

Circuit 1 was simulated for 100.5 s using the AdvPDS and the reference solver with the inputs described in Section IV.

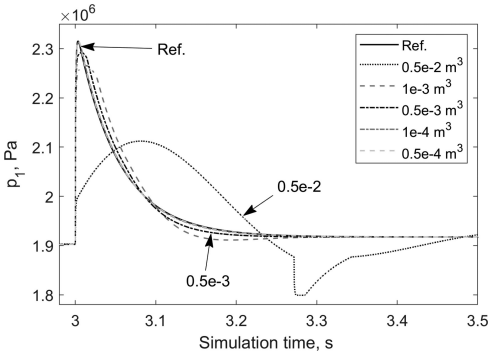

Fig. 8. Sensitivity analysis of p_1 solution to the changes in V_{pseudo}.

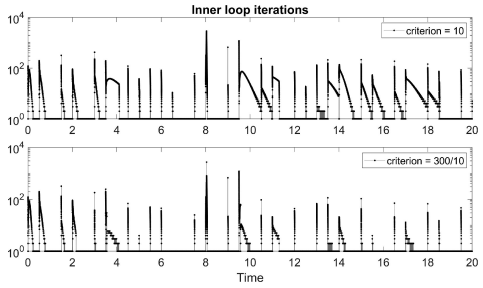

Fig. 9. Number of iterations performed by the AdvPDS in the inner loop during the first 20 s of the simulation with 10 (upper plot) and 300/10 (lower plot) criteria.

The presence of the small volume ($V_1 = 10^{-5}$ m^3) in the circuit between the pressure compensator and control throttle increased the stiffness of the whole system, and also determined the selection of the integration time step for the reference solver. The integration time step of the reference system was set to the largest possible value of 1×10^{-6} s, at which the solution for the pressure appeared numerically stable.

The use of the AdvPDS with Circuit 1 allows the stiffness of the system to be reduced owing to substitution of the small volume by the larger artificial volume. In the mathematical model of Circuit 1 the artificial volume V_{pseudo} substitutes the real volume V_1 in (1). This volume directly affects the resulting pressure p_1. In order to analyze how the size of the artificial volume affects the respective pressure solution a simple sensitivity analysis was carried out. The sensitivity analysis was performed in a way that Circuit 1 is simulated five times with the same input signals and parameter values except for the pseudovolume value. In the experiment V_{pseudo} took the following values: 0.5×10^{-2} m^3, 1×10^{-3} m^3, 0.5×10^{-3} m^3, 1×10^{-4} m^3, and 0.5×10^{-4} m^3. The upper bound of the pseudovolume range was limited by the system stability while holding the condition $\Delta t_i = 10^{-5}$ s. In Fig. 8, the results of five simulations are presented. For better visibility only short range of the simulation time is shown in the figure. It should be noted that the biggest difference in the pressure solutions of five simulations is observed in the transition areas, when one of the control signals was changed. One of such areas is shown in Fig. 8. It can be seen from the figure that the four solutions that refer to the smaller pseudovolumes are rather close to the reference one. Only the solution obtained using the biggest volume 0.5×10^{-2} m^3 compromised the accuracy. Taking into account the obtained results the artificial volume was set to $V_{\text{pseudo}} = 1 \times 10^{-3}$ m^3. On the one hand, the pseudovolume of this size ensured quite high accuracy of the solution. On the other hand, it allowed the integration time steps for the main and inner loops to be increase significantly and to be set to the values of 10^{-4} s and 10^{-5} s, respectively.

As it was previously mentioned, the number of iterations performed in the inner loop at each time step has also a direct effect on the simulation time. The transition process is more oscillatory, and the larger the pressure changes, the more iterations are performed in the inner loop. At the same time, the number of iterations is dependent on the chosen convergence criterion. It was found experimentally that the larger criterion is associated with the smaller number of iterations. Thus, to speed up the simulation of the AdvPDS-based system, the adaptive convergence criterion 300 Pa/10 Pa was selected based on experimental results. In Fig. 9, the number of iterations performed by the AdvPDS using a single convergence criterion in comparison with the use of the adaptive criterion is shown for the first 20 s of the simulation. It can be seen from the figures that the AdvPDS executed a higher number of iterations in transition areas with the single criterion than with the adaptive criterion, which resulted in a shorter simulation time.

Fig. 10 shows the pressure responses p_1 of Circuit 1, obtained with the reference solver and the AdvPDS. One can observe that the two curves are highly coincident with each other. Now the high accuracy of the AdvPDS-based system was also achieved on the low-pressure areas. The accuracy of the system was represented through root-mean-square error (rmse). The overall error was rmse $= 1.12 \cdot 10^4$Pa, which is insignificant for such high pressure levels in the system.

Thus, the use of larger integration time steps together with the adaptive convergence criteria allowed the computational time of the simulation to be reduced compared with the reference system. The simulation time with the reference solver was about 5 h, whereas only 147.983 s was spent for the same simulation using the AdvPDS. Moreover, it should be noted that the system with the AdvPDS (in contrast to the use of the classical pseudo-dynamic solver) is numerically stable during the whole 100.5 s of simulation (i.e., the solver kept the same pressure level as the reference system).

B. Circuit 2 Simulation

Circuit 2 was simulated for 10 s with input signals, which are a constant supply pressure of 14 MPa and voltage signal for the directional control valve that varies from -5 to 8 V with 1 s period. The simulation of the system in the presence

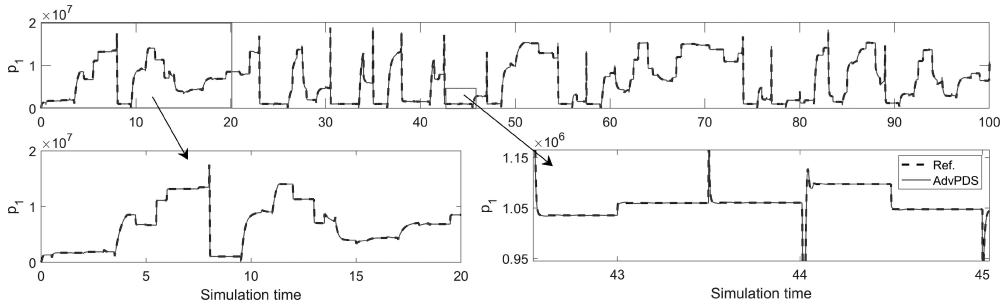

Fig. 10. Pressure responses of Circuit 1 obtained using the reference solver and AdvPDS (with enlarged areas).

TABLE III
RELATIONSHIP BETWEEN CRITERIA VALUE, SIMULATION TIME, AND CALCULATION ACCURACY FOR THE ADVPDS WITH A SINGLE CRITERION

Criteria, Pa	Simulation time, s	RMSE $\times 10^{-4}$, m
10	115.593	4.2950
20	101.847	4.3251
50	63.766	4.3554
70	46.558	4.3720
100	27.546	4.3939
200	25.222	4.4529
300	24.307	4.5051
400	23.609	4.5480
500	22.815	4.5897
600	22.638	4.6339
700	21.829	4.6704
800	22.084	4.7151
900	22.400	4.7496
1000	21.043	4.7881

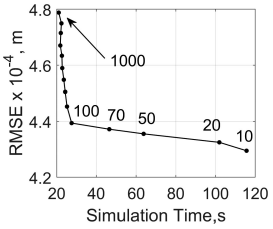

Fig. 11. Dependence between simulation time and rmse using AdvPDS with a single criterion value.

of the small volume between the pressure compensator and directional control valve using the reference solver was run with the safe integration time step of 10^{-5} s. Such time step ensured a numerically stable solution for the system.

The adaptive criterion values for the AdvPDS under the condition of tradeoff between the accuracy and simulation time was experimentally chosen using Circuit 1. In order to verify the applicability of the chosen criterion values to other fluid power circuits which also include small volumes Circuit 2 with the AdvPDS was used in another experiment. In the experiment the circuit was simulated 14 times with the different values of the criterion of the AdvPDS while the simulation times and solution accuracy for the cylinder position piston x_p (against the responses obtained with the reference solver) were measured. The use of AdvPDS for the solution of the system allowed the integration time step to be increased to 10^{-4} seconds for both the main and inner loops. The single criteria value was used in order to the dependence (criterion value/accuracy versus simulation time) showed itself more clearly. The experimental results are summarized in Table III and graphically illustrated by Fig. 11. It can be seen from the figure that the calculation accuracy and simulation time have exponential dependence. Thus, it can be concluded that a larger criterion reduces the simulation time but decrease the calculation accuracy, which is expressed by an increased rmse. In this case, the criterion equal to 100 can be considered as optimal. However, according to the results, as the increase in overall accuracy was not significant in contrast with the decrease in simulation time, which in our work is the more advantageous system performance. While also taking into account the solution problems in the low-pressure areas, which were solved by use of a smaller criterion, it became clear that the adaptive criteria 300/20 Pa was the most suitable choice. Consequently, the simulation time was 27.572 s, which is a better result compared with the reference system and with systems having a single convergence criterion. The response of the pressure p_3 built up in the small volume as well as the cylinder position piston x_p against the responses obtained with the reference solver can be observed in Fig. 12. The obtained responses of the AdvPDS-based system in pressure and cylinder piston position were accurate and differed from the reference responses with rmses of $1.12 \cdot 10^5$ Pa and only $4.24 \cdot 10^{-4}$ m for the pressure and piston position, respectively. The obtained accuracy of the responses was ensured, in particular, by the adaptive criteria, which provided more precise solution in the low-pressure areas. In Table IV, the resulting simulation times for both circuits using reference solver and AdvPDS are presented. The appropriateness of the adaptive criterion chosen was confirmed by a number of experiments that were carried out also with Circuit 2.

C. Real-Time Implementation

To investigate the possibilities of the use of the developed method in real-time and faster than real-time implementations,

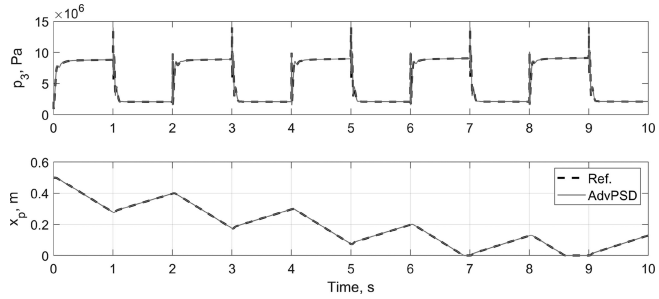

Fig. 12. Circuit 2 responses in pressure p_3 and cylinder piston position x_p using the reference solver and the AdvPDS.

TABLE IV
SIMULATION TIME OF CIRCUIT 1 AND CIRCUIT 2 USING THE REFERENCE SOLVER AND THE ADVPDS

Circuit	Solver	Real Time, seconds	Time Step (s) (global/inner)	Simulation Time	Adaptive Criterion	RMSE w.r.t. Ref.
1	Ref.	100.5	$10^{-6}/-$	$\sim$ 5 h	–	–
	AdvPDS	100.5	$10^{-4}/10^{-5}$	147.983 s	300/10	$RMSE_{p1} = 1.12 \cdot 10^{4}$ Pa
2	Ref.	10	$10^{-5}/-$	200.350 s	–	–
	AdvPDS	10	$10^{-4}/10^{-4}$	27.572 s	300/20	$RMSE_{p3} = 1.89 \cdot 10^{5}$ Pa $RMSE_{xp} = 4.24 \cdot 10^{-4}$ m

MATLAB codes for Circuit 2 with the reference solver and the AdvPDS were translated into standalone C code using MATLAB Coder 4.1. Both codes were compiled and run outside MATLAB on a PC with an Intel Core i5-4590 3.30 GHz with 16 GB RAM. As a result, to simulate an interval of 10 s of real time, it took 219 ms for the reference system, whereas for the AdvPDS-based system it took only 47 ms to simulate the same time interval. Thus, the introduction of the developed AdvPDS solver allowed Circuit 2 to be simulated 4.7 times faster in comparison with the use of the reference solver usage. It should be noted that in our case, both implementations were calculated much faster than real time. However, in virtual prototypes the fluid power system are usually employed in conjunction with mechanical components (i.e., multibody dynamic representation of the mobile machine structure). Thus, the mechanical component should also be calculated at each time step of the real-time simulation. Based on the results, it can be concluded that the use of the AdvPDS for the solution of the real-time and faster than real-time systems, which include fluid power components with the small volumes, can be more beneficial than the reference solver application.

VI. CONCLUSION

In this article, the AdvPDS with adaptive criterion has been proposed for the efficient solution of fluid power systems with singularities originating (in particular) from the presence in the system of small volumes. Based on the results of the experiments performed with two test fluid power circuits, which contained small volumes in their structure, the model for the AdvPDS was formulated. There are two main differences of the AdvPDS in comparison with the classical pseudodynamic solver. First, the calculation of the outlet volume flow rate related to the small volume is included into the inner loop of the solver, which allowed the numerical stability of the solution to be increased. Second, the adaptive convergence criterion is introduced, which allowed the simulation time to be decreased and the calculation accuracy to be increased. Side-by-side simulation results confirmed that the proposed solver is much more efficient in solution of the fluid power circuits than the conventional method as well as the classical pseudodynamic solver. The main advantage of the proposed solver is that it produces the lower error than the classical pseudodynamic solver with single criteria. In addition, the AdvPDS-based model can be calculated faster than the conventional model of the fluid power circuit with small volumes owing to the possibility of the application of a larger integration time step. Moreover, the AdvPDS solver can be the preferable method in modeling of more-detailed fluid power circuits, especially in such cases when the classical pseudodynamic solver may show numerically unstable and slow response. The described advantages in solution of the fluid power systems with small volumes of the developed solver allow to use AdvPDS in simulations of mobile machines in the real time and faster than real-time applications. Moreover, mechatronic applications such as [4], [6], and [7] can directly benefit from the usage of the developed solver. In these applications in particular, the solver can ensure the accurate real-time or faster than real-time simulation of the multibody systems with the fluid power actuation. Future studies will be associated with the use of the AdvPDS-based fluid power model as a part of the simulation model of a mobile machine for the real-time applications.

REFERENCES

[1] A. Mikkola and H. Handroos, "Modelling and simulation of a flexible hydraulic driven log crane," in *Proc. 9th Bath Int. Fluid Power Workshop*, Sep. 1996, pp. 431–442.

[2] S. Esqué, A. Raneda, and A. Ellman, "Techniques for studying a mobile hydraulic crane in virtual reality," *Int. J. Fluid Power*, vol. 4, no. 2, pp. 25–35, 2003.
[3] K. Liu, C. Zhang, and Z. Sun, "Independent pressure and flow rate control enabled by hydraulic free piston engine," *IEEE/ASME Trans. Mechatronics*, vol. 24, no. 3, pp. 1282–1293, Jun. 2019.
[4] V. Zhidchenko, I. Malysheva, H. Handroos, and A. Kovartsev, "Faster than real-time simulation of mobile crane dynamics using digital twin concept," *J. Phys., Conf. Ser.*, vol. 1096, Sep. 2018, Art. no. 012071.
[5] Y. Zheng, T. Ge, and J. Liu, "Kinematics modeling and control simulation for a logging harvester in virtual environments," *Adv. Mech. Eng.*, vol. 7, no. 10, pp. 1–10, 2015.
[6] J. Rahikainen, M. Kiani, J. Sopanen, P. Jalali, and A. Mikkola, "Computationally efficient approach for simulation of multibody and hydraulic dynamics," *Mechanism Mach. Theory*, vol. 130, pp. 435–446, 2018.
[7] I. Malysheva, H. Handroos, V. Zhidchenko, and A. Kovartsev, "Faster than real-time simulation of a hydraulically actuated log crane," in *Proc. Glob. Fluid Power Soc. Ph.D. Symp.*, 2018, pp. 1–6.
[8] M. M. Pedersen, M. R. Hansen, and M. Ballebye, "Developing a tool point control scheme for a hydraulic crane using interactive real-time dynamic simulation," *Model., Identification Control*, vol. 31, no. 4, pp. 133–143, 2010.
[9] A. Mikkola, "Studies on fatigue damage in a hydraulically driven boom system using virtual prototype simulations," D.Sc. thesis, Dept. Mech. Eng., Lappeenranta Univ. Technol., Lappeenranta, Finland, 1997.
[10] J. Yao, Z. Jiao, D. Ma, and L. Yan, "High-accuracy tracking control of hydraulic rotary actuators with modeling uncertainties," *IEEE/ASME Trans. Mechatronics*, vol. 19, no. 2, pp. 633–641, Apr. 2014.
[11] C.-G. Park, S. Yoo, H. Ahn, J. Kim, and D. Shin, "A coupled hydraulic and mechanical system simulation for hydraulic excavators," *Proc. Institution Mech. Eng., I, J. Syst. Control Eng.*, vol. 234, no. 4, pp. 527–549, 2020.
[12] J. A. Ferreira, F. G. Almeida, M. R. Quintas, and J. P. E. de Oliveira, "Hybrid models for hardware-in-the-loop simulation of hydraulic systems part 2: Experiments," *Proc. Institution Mech. Eng., I, J. Syst. Control Eng.*, vol. 218, no. 6, pp. 475–486, 2004.
[13] D. E. Bowns and L. M. Wang, "The digital computation of pressures in hydraulic pipes with small volume using an iterative technique," *Proce. Institution Mech. Eng., C, Mech. Eng. Sci.*, vol. 204, no. 1, pp. 29–36, 1990.
[14] A. Ellman and R. Piché, "A modified orifice flow formula for numerical simulation of fluid power systems," in *Proc. ASME Int. Mechan. Eng. Congr. Expo., Fluid Power Syst. Technol.*, vol. 3, Nov. 1996, pp. 59–63.
[15] A. Ellman and R. Piché, "A two regime orifice flow formula for numerical simulation," *J. Dyn. Syst., Meas., Control*, vol. 121, no. 4, pp. 721–724, 1999.
[16] R. Åman, H. Handroos, and T. Eskola, "Computationally efficient two-regime flow orifice model for real-time simulation," *Simul. Model. Pract. Theory*, vol. 16, no. 8, pp. 945–961, 2008.
[17] E. Hairer and G. Wanner, *Stability Analysis for Explicit RK Methods*. Berlin, Germany: Springer, 1996, pp. 15–39.
[18] S. Esqué, "A new approach for numerical simulations of fluid power circuits using Rosenbrock methods," Ph.D. dissertation, Dept. Automat. Tech. Mech. Eng., Tampere Univ. Technol., Tampere, Finland, 2008.
[19] R. Piché and A. Ellman, "Numerical integration of fluid power circuit models using two-stage semi-implicit Runge-Kutta methods," *Proc. Institution Mech. Eng., C, J. Mech. Eng. Sci.*, vol. 208, no. 3, pp. 167–175, 1994.
[20] R. Åman and H. Handroos, "Pseudo-dynamic solution of pressures in small volumes in fluid power circuit simulation," in *Proc. 5th FPNI PhD Symp.*, Jul. 2008, pp. 406–416.
[21] R. Åman and H. Handroos, "Comparison of numerical effectiveness of three methods for modelling 2-way flow control valves," in *Proc. 7th Int. Conf. Fluid Power Transmiss. Control*, Apr. 2009, pp. 711–715.
[22] R. Åman and H. Handroos, "Optimization of parameters of pseudo-dynamic solver for real-time simulation of fluid power circuits," in *Proc. Workshop 7th Int. Fluid Power Conf.*, Mar. 2010, vol. 1, pp. 495–507.
[23] M. Kiani-Oshtorjani, A. Mikkola, and P. Jalali, "Numerical treatment of singularity in hydraulic circuits using singular perturbation theory," *IEEE/ASME Trans. Mechatronics*, vol. 24, no. 1, pp. 144–153, Feb. 2019.
[24] J. Rahikainen, "On the dynamic simulation of coupled multibody and hydraulic systems for real-time applications," D.Sc. thesis, Dept. Mech. Eng., Lappeenranta-Lahti Univ. Technol., Lappeenrata, Finland, 2019.
[25] B. Xu, R. Ding, J. Zhang, L. Sha, and M. Cheng, "Multiphysics-coupled modeling: Simulation of the hydraulic-operating mechanism for a sf6 high-voltage circuit breaker," *IEEE/ASME Trans. Mechatronics*, vol. 21, no. 1, pp. 379–393, Feb. 2016.
[26] H. E. Merritt, *Hydraulic Control Systems*. New York, NY, USA: Wiley, 1967.
[27] H. Handroos and M. Vilenius, "Flexible semi-empirical models for hydraulic flow control valves," *J. Mech. Des.*, vol. 113, no. 3, pp. 232–238, 1991.
[28] C. Canudas de Wit, H. Olsson, K. J. Åström, and P. Lischinsky, "A new model for control of systems with friction," *IEEE Trans. Autom. Control*, vol. 40, no. 3, pp. 419–425, Mar. 1995.
[29] H. Olsson, "Control systems with friction," Ph.D. dissertation, Dept. Autom. Control, Lund Inst. Technol., Lund, Sweden, 1996.
[30] M. Jelali and A. Kroll, *Hydraulic Servo-Systems: Modelling, Identification and Control* (Advances in Industrial Control Series). London, U.K.: Springer-Verlag, 2002.

Julia Malysheva received the M.Sc. degree in computational engineering and technical physics with an emphasis in computer vision and pattern recognition from the Lappeenranta-Lahti University of Technology (LUT), Lappeenranta, Finland, in 2017.

She is currently working as a Researcher with the Laboratory of Intelligent Machines, LUT University. Her current research interests include simulation of multibody systems with hydraulic components and deep neural networks.

Stanislav Ustinov received the B.Sc. degree in mechanical engineering and production technology from the Saimaa University of Applied Sciences, Lappeenranta, Finland, in 2016, and the M.Sc. degree in mechatronic system design from Lappeenranta-Lahti University of Technology (LUT), Lappeenranta, Finland, in 2018.

He is currently working as a Researcher with the Laboratory of Intelligent Machines, LUT University. His research interests include fluid power systems, real-time simulation of multibody systems, and artificial intelligence.

Heikki Handroos (Member, IEEE) received the M.Sc. and D.Sc. degrees in hydraulics and automation from the Tampere University of Technology, Tampere, Finland, in 1985 and 1991, respectively.

He has been a Professor of machine automation with the Lappeenranta-Lahti University of Technology, Lappeenranta, Finland, since 1993. He has authored or coauthored about 250 scientific journal and conference papers. His research interests include mechatronic systems to off-road vehicle transmissions and robotics.

Mr. Handroos is a Member of the ASME and has served in several editorial boards of journals and conferences in the field of mechatronics.

Publication II

Kiani-Oshtorjani, M., Ustinov, S., Handroos, H., Jalali, P., and Mikkola, A.
Real-Time Simulation of Fluid Power Systems Containing Small Oil Volumes, Using the Method of Multiple Scales

Reprinted with permission from
IEEE Access
Vol. 8, pp. 196940-196950, 2020

IEEE Access
Multidisciplinary ⋮ Rapid Review ⋮ Open Access Journal

Received October 7, 2020, accepted October 27, 2020, date of publication October 29, 2020, date of current version November 10, 2020.

Digital Object Identifier 10.1109/ACCESS.2020.3034698

Real-Time Simulation of Fluid Power Systems Containing Small Oil Volumes, Using the Method of Multiple Scales

MEHRAN KIANI-OSHTORJANI[1], STANISLAV USTINOV[2], HEIKKI HANDROOS[2], (Member, IEEE), PAYMAN JALALI[1], AND AKI MIKKOLA[2]
[1]Laboratory of Thermodynamics, School of Energy Systems, LUT University, 53850 Lappeenranta, Finland
[2]Department of Mechanical Engineering, School of Energy Systems, LUT University, 53850 Lappeenranta, Finland

Corresponding author: Mehran Kiani-Oshtorjani (mehran.kiani@lut.fi)

This work was supported by the SIM-Platform at LUT University.

ABSTRACT Machinery devices often consist of mechanical mechanisms that are actuated by fluid power systems. In many applications, the mechanical system can be modelled and analysed in terms of the multi-body system dynamics. Fluid power systems, in turn, can be analysed via the lumped-fluid theory, with which simulation of fluid power systems requires smaller integration time steps than needed by multi-body solvers. This leaves simulation of the entire machinery device beyond reach for a real-time framework, with the main reason for the very small time steps in modelling of fluid power systems being the presence of a small hydraulic volume, which creates a numerical stiffness problem. The stiffness issue may arise from numerical singularity emerging in the fluid power system, which implies that solving the governing equations involves different time scales – small and large. To resolve the numerical singularity in hydraulic circuits, the authors developed a perturbed model to alleviate the stiffness problem demonstrated that it can increase the integration time step by an order of magnitude. Since the perturbed model does necessitate a correction factor for the volumetric flow rate, the method of multiple scales is applied to compute the pressure within the small volume to second-order accuracy, $O(\varepsilon^2)$, in comparison with the perturbed model's $O(\varepsilon)$. The results reveal that if the correction parameter is not set, the perturbed model's cumulative error leads to considerable deviation in piston position with respect to the reference model, whereas the multiple-scale model eliminates the issue of cumulative error without demanding any flow-rate correction factor.

INDEX TERMS Fluid power system, real-time simulation, singular perturbed model, small volumes.

I. INTRODUCTION

Fluid power systems have been widely used for decades in such mechanical-engineering applications as mechatronics, robotics, manufacturing, and road machinery, in which using fluid power systems still remains the most commonly employed method of power transmission. The design of machines of this nature is strongly linked with real-time simulation, a tool necessary for improving the controllability of the machine, its work conditions, and the specification process, by means of online feedback from simulations. This concept is frequently referred to as using a 'digital twin', referring to two-way coupling of a physical machine with a 'twin' to improve its functionality [1], [2].

When considering a machinery device as a combination of mechanical mechanisms and fluid power systems, one finds that the mechanical mechanisms can be modelled in a straightforward manner in terms of multi-body system dynamics [3], whereas a fluid power system is often modelled via the theory of lumped fluids, in which the system gets divided into hydraulic volumes with evenly distributed pressure [4]. The integration time step applied for a fluid power system is usually smaller than that in a multi-body solver [5]–[7], so managing fast response for the fluid power system is crucial to real-time simulation for vehicles [8]. There are two popular approaches to dealing with assemblies comprising a mechanical mechanism and fluid power system, known as the unified approach and the multi-rate integration approach [8]. In the unified approach [3], [9] the hydraulic and mechanical equations are combined into a single set of equations to be solved via an identical-integration scheme with a single time step. In contrast, in the multi-rate integration approach [10], [11], a distinct time step is used for each mechanical or hydraulic subsystem. The multi-rate

The associate editor coordinating the review of this manuscript and approving it for publication was Zheng Chen.

integration method can be less computationally expensive, as fluid power system simulations usually require a smaller time step [12] than mechanical parts do. The computation cost connected with fluid power is mainly due to three parameters: the orifice model, the presence of a small hydraulic-oil volume in the circuit, and bulk modulus models. These increase the system's numerical stiffness and render the set of equations numerically singular.

If the pressure drop approaches zero, the traditional turbulent-flow orifice equation is inefficient because of the infinity value of the volumetric flow-rate derivative. To overcome this difficulty, Ellman and Piché [13], [14] proposed several orifice models involving laminar- and turbulent-orifice equations. Then, a computationally efficient solution was offered by Åman *et al.* [15], who posited that a polynomial relationship exists between flow rate and pressure drop for small pressure drops. This is a so-called two-regime flow-rate model, in which a third-order polynomial is utilised for describing the laminar- and transition-flow area while the traditional square-root relation of flow rate is kept for the turbulence regime. To obtain the constants for the model, one considers the boundary conditions where the laminar and turbulent model meet. This method provides a continuous finite partial derivative of flow rate with respect to the pressure drop in all conditions. In addition, some experimental orifice models have been presented in the literature. For instance, Borutzky *et al.* [16] proposed an empirically obtained polynomial function for the orifice volumetric flow rate that displays a smooth transition between the laminar- and turbulent-flow regime. With this approach, numerical singularities can be avoided when the pressure difference approaches zero.

The most significant problem with the lumped-fluid theory in dynamic simulation of fluid power circuits is numerical stiffness connected with the pressure-governing differential equations, due to either the presence of a small volume in the system or the highly stiff oil (high bulk modulus values). The presence of different orders of hydraulic volume in a fluid power circuit is the reason that the response terms are on different time scales, making the system numerically singular and stiff. Consequently, classical integrators cannot resolve the integration-related numerical difficulties in generating a stable response with high integration time steps, so the simulation gets slowed down by setting of quite small time steps [17]. Therefore, the solution for systems with small volumes should be derived by means of specific numerical solvers if one wishes to avoid the problem of instability in dynamic models for a fluid power circuit. Implementation of bespoke integrators to handle numerical singularities, iterative methods, machine-learning algorithms, and use of a perturbed model can be highlighted as the approaches that alleviate the numerical stiffness of hydraulic systems.

The accuracy and instability of various two-stage semi-implicit Runge–Kutta methods were investigated by Piché and Ellman [17], who recognised that it is hard to solve ordinary differential equations governing different volume sizes. They proposed an L-stable integrator as the most suitable tool. Later, Esqué *et al.* [18] studied real-time simulation of a hydraulic crane in terms of an L-stable Rosenbrock integration scheme. They found that the maximum integration time step should be selected on the basis of stability and computation-time criteria. These two factors led them to choose a 0.1 ms time step for their application.

Iterative methods have been investigated by many researchers too. Bowns and Wang [19], reporting on difficulties that arise in simulation of hydraulic pipe systems with small volumes, indicated that if the volume of one or several pipes is small, the required simulation time steps grow very small. To overcome this problem, they proposed iterative models; however, these methods are computationally costly and similar to applying small time steps in the integration. Another iterative method introduced and studied is the 'pseudo-dynamic one' [20]–[22]. The goal with this algorithm is to reduce the numerical problems by seeking a steady-state pressure value within the small volume. The main idea is to replace the small volume in traditional continuity equations with an artificial one that is large enough for producing a stable response of pressure. Then, the pressure is integrated in a separate loop until the convergence criterion is met. Although this algorithm provides a suitable response, its inherently iterative nature renders it costly, in that several iterations are needed at each time step.

In addition to the above-mentioned models intended to alleviate the numerical stiffness of hydraulic systems, there have been several efforts to model hydraulic components by using machine-learning tools, such as a neural network [23]–[25]. However, these tools would seem time-consuming, as the number of neuron layers increases in line with response resolution and the complexity of the system. Moreover, these models have significantly restricted operating conditions, depending on the algorithms' training data. In addition, the lack of physical modelling and treatment of the fluid power system as a black box imposes hurdles to system development related to neural-network models.

Kiani-Oshtorjani *et al.* [4] introduced an algorithm based on singular perturbation theory, to increase the simulation time step in circumstances wherein a small volume is found in the circuit. As they mentioned, this algorithm substitutes an algebraic equation for a non-linear differential equation for pressure. In consequence, the perturbed model can function with a larger time step while maintaining the stability of the system. Although this model is fast and stable for various hydraulic circuits, its accuracy is limited to an order of magnitude as $O(\varepsilon^1)$. This model requires a correction factor for adjusting the rate of flow from the small volume.

In contrast to singular perturbation theory, which rules out the fast response of the system, a method involving multiple scales can maintain any level of accuracy. This method of multiple scales, or MMS, is a mathematical tool that can address non-linear singular systems on both small and large time scales. The approach has been widely implemented in vibration [26], [27], hydraulic [28], [29] and pneumatic [30], fluid [31], [32], and thermal [33], [34] analyses to determine

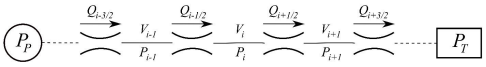

FIGURE 1. Orifice and pipe hydraulic circuit schematic.

a system's non-linear behaviour. For instance, Nayfeh and Bouguerra [35] used this method to model the non-linear response of a relief valve.

To eliminate the need for a correction factor such as that described above for the perturbed model, this paper introduces an MMS technique for fluid power systems. The model does not require any flow-rate modifications and can resolve the numerical stiffness problem associated with a small hydraulic volume, for calculation of its pressure to second-order accuracy, $O(\varepsilon^2)$, within a real-time framework. To demonstrate this, we derive the multi-scale hydraulic model in Section II and present its implementation for a fluid power system in Section III. Further on in Section III, stability analysis for fluid power system is investigated, to shed some light on the factors that lead to a numerically stiff circuit. Section IV presents the results, and some concluding thoughts, in Section V, round out the paper.

II. HYDRAULIC FORMULATION

The lumped-fluid theory is an essential tool for modelling and simulation of fluid power system. However, it either fails to simulate hydraulic circuits that contain small volumes or demands small time steps that are infeasible for real-time platforms. For overcoming this difficulty, the perturbed hydraulic system was recently proposed [4], and this is where we begin our discussion. We start by detailing the lumped-fluid theory and perturbed model and, in turn, derive the multiple-scale hydraulic model's equations.

A. THE LUMPED-FLUID THEORY

The theory of lumped fluids is often used in modelling of hydraulic systems. In the lumped-fluid theory, the hydraulic circuit is divided into volumes in which the pressure is assumed to be evenly distributed. Differential equations are formed for the volumes with which the pressure of the system at a certain time can be solved for, directly or indirectly. Individual volumes are assumed to be separated by a throttling mechanism through which the fluid can flow. For the model, the directional, pressure, and flow-control valves are replaced with throttles that control the rate of flow between the various volumes, as are the long pipelines used in real-world systems.

Figure 1 illustrates a set of orifices connecting hydraulic pump p_P to tank p_T. The pressure in a volume within the hydraulic circuit can be calculated by means of differential equations as:

$$\dot{p}_i = \frac{B_e}{V_i}(Q_{i-\frac{1}{2}} - Q_{i+\frac{1}{2}} - \frac{dV_i}{dt}) \tag{1}$$

where the t term is time, p_i is the pressure in the ith orifice, B_e is the effective bulk modulus, V_i is the hydraulic volume, $Q_{i-\frac{1}{2}}$ and $Q_{i+\frac{1}{2}}$ are the incoming and out-bound volumetric flow, and $\frac{dV_i}{dt}$ is the change in volume over time. The effective bulk modulus represents the fluid bulk modulus such that the effects of the container flexibility and any dissolved and entrained air are taken into account.

The volumetric turbulent-flow rate $Q_{i+\frac{1}{2}}$ across a throttle can be written in the following form [16], [36]:

$$Q_{i+\frac{1}{2}} = K\sqrt{p_i - p_{i+1}} \tag{2}$$

where $K = C_d A_t \sqrt{\frac{2}{\rho}}$, C_d denotes the discharge coefficient, A_t is the valve cross-section area, and ρ is the fluid density. The volumetric flow rate is usually described through semi-empirical methods in which the valve parameters are determined from data collected in manufacturer experiments. Our work follows a valve specified in the literature [37].

B. THE SINGULAR PERTURBED MODEL

In singular perturbation problems, a small-valued parameter appearing in the governing equation plays a key role. Cases of regular perturbation involve problems in which one can obtain the solution by equating that small parameter to zero, whereas in singular perturbation problems it cannot be neglected without a significant loss of accuracy in the results. If the hydraulic volume divided to the bulk modulus is small, the pressure-variation equations of the lumped-fluid theory fall into the latter category. A well-known approach for perturbation problems of this type is the singular perturbation technique. As scholars have noted [4], this approach takes the ordinary differential equations that contain the infinitesimal parameter ε and transfer them into a quasi-steady-state model based on Tikhonov's theorem [38]. Consider the following system of singular equations:

$$\dot{\phi} = f(\phi, \psi, t, \varepsilon) \quad \phi(t_0) = \zeta(\varepsilon) \tag{3a}$$
$$\dot{\psi} = g(\phi, \psi, t, \varepsilon) \quad \psi(t_0) = \xi(\varepsilon) \tag{3b}$$

where $\phi \in R^m$ and $\psi \in R^n$, with ε being an infinitesimal parameter. The quasi-steady-state model of the above system [39] is

$$\dot{\bar{\phi}} = f(\bar{\phi}, h(t, \bar{\phi}), t, \varepsilon) \quad \bar{\phi}(t_0) = \zeta(\varepsilon) \tag{4a}$$
$$\bar{\psi}(t) = h(t, \bar{\phi}) \tag{4b}$$

The over-bar denotes the perturbed variables, and h is an algebraic equation that is determined during the order reduction. The ith volume in Figure 1 is considered a small volume in comparison with the neighbouring ones. In consequence, as the literature explains [4], applying singular perturbation theory to this volume yields

$$p_i = \frac{p_{i+1} + \alpha p_{i-1}}{1 + \alpha} \tag{5}$$

where $\alpha = \left(\frac{A_{i-1}}{A_{i+1}}\right)^2$.

C. THE METHOD OF MULTIPLE SCALES

The singular perturbation method only gives the solution corresponding to the largest time scale, leaving out other time scales, corresponding to other dynamic behaviours. Each scale can be treated as an independent variable reproducing a set of equations instead of a single equation. For instance, t and εt can be treated as two independent variables, each

of them representing a scale of time. Although the perturbed hydraulic model returns the steady-state response, the error arising from the smaller scales can accumulate over time to create a substantial deviation from the precise response actually involved, especially for those circumstances in which the dynamic behaviour of systems should not be simply ignored. The error of perturbed model should be compensated for through the correction factor mentioned above [4]. However, another option is to introduce a more accurate model, one not needing any modification. To this end, the MMS can be used to derive the hydraulic model governing small hydraulic oil volumes. In this method, the new independent time variables are introduced as

$$T_n = \varepsilon^n t \quad n = 0, 1, 2, \ldots \tag{6}$$

Therefore, the time derivative can be expressed in terms of the chain rule thus:

$$\frac{d}{dt} = \frac{dT_0}{dt}\frac{\partial}{\partial T_0} + \frac{dT_1}{dt}\frac{\partial}{\partial T_1} + \ldots \tag{7}$$

In addition, one may assume that the solution to Equation 1 can be written as

$$p_i(t, \varepsilon) = p_0(T_0, T_1, \ldots) + \varepsilon p_1(T_0, T_1, \ldots) + O(\varepsilon^2) \tag{8}$$

It is worth mentioning that the number of time scales is a function of the accuracy required. If we want to expand the solution up to the second order, $O(\varepsilon^2)$, the T_0 and T_1 time scales are required. Substituting Equation 8 into 7 and then plugging the result into Equation 1 yields

$$\left(\frac{\partial}{\partial T_0} + \varepsilon\frac{\partial}{\partial T_1} + \varepsilon^2\frac{\partial}{\partial T_2}\right)(p_0 + \varepsilon p_1 + \varepsilon^2 p_2) = \frac{\beta_e}{V_i}\left(Q_{i-\frac{1}{2}} - Q_{i+\frac{1}{2}}\right) \tag{9}$$

On the other hand, the flow rates $Q_{i-\frac{1}{2}}$ and $Q_{i+\frac{1}{2}}$ are functions of the pressure in the small volume. If these flow rates are calculated in line with the perturbed pressure, errors are going to arise. Consequently, they have to be calculated with reference to the true, exact value of p_i. Considering Equation 2, one can obtain $Q_{i+\frac{1}{2}}$ as

$$Q_{i+\frac{1}{2}} = C_c A\sqrt{p_i - p_{i+1}} = C_c A\sqrt{p_0 - p_{i+1} + \varepsilon p_1 + \varepsilon^2 p_2} \tag{10}$$

Therefore, by getting $p_0 - p_{i+1}$ from the square-root function and implementing Taylor series for $\sqrt{1+x} \approxeq 1 + \frac{x}{2} - \frac{x^2}{8}$ in which $x < 1$, we have

$$\begin{aligned} Q_{i+\frac{1}{2}} &= C_c A\sqrt{p_0 - p_{i+1}}\left(1 + \frac{p_1\varepsilon + p_2\varepsilon^2}{2(p_0 - p_{i+1})} - \frac{p_1^2\varepsilon^2}{8(p_0 - p_{i+1})^2}\right) \\ &= \bar{Q}_{i+\frac{1}{2}}\left(1 + \frac{p_1\varepsilon + p_2\varepsilon^2}{2(p_0 - p_{i+1})} - \frac{p_1^2\varepsilon^2}{8(p_0 - p_{i+1})^2}\right) \end{aligned} \tag{11}$$

Here, $\bar{Q}_{i+\frac{1}{2}} = C_c A\sqrt{p_0 - p_{i+1}}$ is the flow rate calculated on the basis of the perturbed pressure, referred to as the perturbed flow rate from here on. The same logic is valid for $Q_{i-\frac{1}{2}}$, resulting in the following relation:

$$Q_{i-\frac{1}{2}} = \bar{Q}_{i-\frac{1}{2}}\left(1 - \frac{p_1\varepsilon + p_2\varepsilon^2}{2(p_{i-1} - p_0)} - \frac{p_1^2\varepsilon^2}{8(p_{i-1} - p_0)^2}\right) \tag{12}$$

Substituting the flow rates calculated via equations 11 and 12 into Equation 9 and separating the equations for $O(\varepsilon^0)$, $O(\varepsilon^1)$, and $O(\varepsilon^2)$ produces the following set of equations:

$$O(\varepsilon^0): \frac{\partial p_0}{\partial T_0} = \frac{\beta_e}{V_i}\left(\bar{Q}_{i-\frac{1}{2}} - \bar{Q}_{i+\frac{1}{2}}\right) \tag{13}$$

$$O(\varepsilon^1): \frac{\partial p_1}{\partial T_0} + \frac{\beta_e}{V_i}p_1\left(\frac{\bar{Q}_{i-\frac{1}{2}}}{2(p_{i-1} - p_0)} + \frac{\bar{Q}_{i+\frac{1}{2}}}{2(p_0 - p_{i+1})}\right) = -\frac{\partial p_0}{\partial T_1} \tag{14}$$

along with

$$\begin{aligned} O(\varepsilon^2): &\frac{\partial p_2}{\partial T_0} + \frac{\beta_e}{V_i}p_2\left(\frac{\bar{Q}_{i-\frac{1}{2}}}{2(p_{i-1} - p_0)} + \frac{\bar{Q}_{i+\frac{1}{2}}}{2(p_0 - p_{i+1})}\right) \\ &= \frac{\beta_e}{V_i}\left(\frac{\bar{Q}_{i+\frac{1}{2}}p_1^2}{8(p_0 - p_{i+1})^2} - \frac{\bar{Q}_{i-\frac{1}{2}}p_1^2}{8(p_{i-1} - p_0)^2}\right) - \frac{\partial p_1}{\partial T_1} - \frac{\partial p_0}{\partial T_2} \end{aligned} \tag{15}$$

Equation 13 is equivalent to the perturbed model because of the presence of small volume V_i, giving us the perturbed pressure as obtained in Equation 5, as $p_0 = \frac{p_{i+1} + \alpha p_{i-1}}{1+\alpha}$. As a result, $\frac{\partial p_0}{\partial T_1} = 0$, and when we recall the $\bar{Q}_{i-\frac{1}{2}}$ and $\bar{Q}_{i+\frac{1}{2}}$ relations, Equation 14 can be solved as

$$p_1 = \Lambda(T_1) exp\left(-\int_0^{T_0}\frac{\beta_e}{V_i}\left[\frac{\bar{Q}_{i-\frac{1}{2}}}{2(p_{i-1} - p_0)} + \frac{\bar{Q}_{i+\frac{1}{2}}}{2(p_0 - p_{i+1})}\right]dT_0\right) \tag{16}$$

Considering $\frac{dp_1}{p_1} = \frac{d(\varepsilon p_1)}{\varepsilon p_1}$ and assuming a constant pressure drop through the small volume $\sqrt{p_{i-1} - p_{i+1}}$, one can solve Equation 16 thus:

$$\begin{aligned} &\frac{\partial p_2}{\partial T_0} + \frac{\beta_e}{V_i}p_2\left(\frac{\bar{Q}_{i-\frac{1}{2}}}{2(p_{i-1} - p_0)} + \frac{\bar{Q}_{i+\frac{1}{2}}}{2(p_0 - p_{i+1})}\right) \\ &= \frac{\beta_e}{V_i}\left(\frac{\bar{Q}_{i-\frac{1}{2}}}{8(p_{i-1} - p_0)} + \frac{\bar{Q}_{i+\frac{1}{2}}}{8(p_0 - p_{i+1})}\right)\Lambda^2 \\ &\quad \times exp\left(-2\int_0^{T_0}\frac{\beta_e}{V_i}\left[\frac{\bar{Q}_{i-\frac{1}{2}}}{2(p_{i-1} - p_0)} + \frac{\bar{Q}_{i+\frac{1}{2}}}{2(p_0 - p_{i+1})}\right]dT_0\right) \\ &\quad - \frac{\partial\Lambda}{\partial T_1} exp\left(-\int_0^{T_0}\frac{\beta_e}{V_i}\left[\frac{\bar{Q}_{i-\frac{1}{2}}}{2(p_{i-1} - p_0)} + \frac{\bar{Q}_{i+\frac{1}{2}}}{2(p_0 - p_{i+1})}\right]dT_0\right) \end{aligned} \tag{17}$$

The terms on the right-hand side in Equation 17 are secular, meaning that they can grow to infinity over time. To avoid such infinities, one must set these terms to zero. Therefore, we have

$$\begin{aligned} &\frac{\partial\Lambda}{\partial T_1} - \Lambda^2\frac{\beta_e}{V_i}\left(\frac{\bar{Q}_{i-\frac{1}{2}}}{8(p_{i-1} - p_0)} + \frac{\bar{Q}_{i+\frac{1}{2}}}{8(p_0 - p_{i+1})}\right) \\ &\times exp\left(-\int_0^{T_0}\frac{\beta_e}{V_i}\left[\frac{\bar{Q}_{i-\frac{1}{2}}}{2(p_{i-1} - p_0)} + \frac{\bar{Q}_{i+\frac{1}{2}}}{2(p_0 - p_{i+1})}\right]dT_0\right) = 0 \end{aligned} \tag{18}$$

This yields

$$\Lambda = -\frac{1}{fT_1} \tag{19}$$

in which $f = \frac{\beta_e}{V_i}\left(\frac{\bar{Q}_{i-\frac{1}{2}}}{8(p_{i-1}-p_0)} + \frac{\bar{Q}_{i+\frac{1}{2}}}{8(p_0-p_{i+1})}\right)exp\Big(- \int_0^{T_0}\frac{\beta_e}{V_i}\left[\frac{\bar{Q}_{i-\frac{1}{2}}}{2(p_{i-1}-p_0)} + \frac{\bar{Q}_{i+\frac{1}{2}}}{2(p_0-p_{i+1}}\right]dT_0\Big)$. Substituting Equation 19 into Equation 16 gives us

$$p_1 = -\frac{1}{T_1}\frac{8V_i}{\beta_e}\left(\frac{\bar{Q}_{i-\frac{1}{2}}}{(p_{i-1}-p_0)} + \frac{\bar{Q}_{i+\frac{1}{2}}}{(p_0-p_{i+1})}\right)^{-1} \tag{20}$$

By considering $T_1 = \varepsilon t$ and combining p_0 and εp_1 in accordance with Equation 8, we can express small-volume pressure p_i as

$$p_i = \frac{p_{i+1}+\alpha p_{i-1}}{1+\alpha} - \frac{1}{t}\frac{8V_i}{\beta_e}\left(\frac{\bar{Q}_{i-\frac{1}{2}}}{(p_{i-1}-p_0)} + \frac{\bar{Q}_{i+\frac{1}{2}}}{(p_0-p_{i+1})}\right)^{-1} \tag{21}$$

This equation reveals that the deviation from the exact solution under the perturbed model depends primarily on the pressure drop through the small volume $p_{i-1} - p_{i+1}$, bulk modulus β_e, and volume V_i. If said pressure drop approaches zero, $p_{i-1} - p_{i+1} \rightarrow 0$, meaning that there is no pressure change from p_{i-1} to p_{i+1}, then $\varepsilon p_1 \rightarrow 0$, and hence the perturbed model yields results identical to exact-solution procedures.

The same logic is valid for the bulk modulus and the volume size. Obviously, the perturbed model is more accurate as the size of the small volume approaches zero, as $\varepsilon p_1 \rightarrow 0$ if $V_i \rightarrow 0$.

III. A NUMERICAL EXAMPLE

The fluid power circuit depicted in Figure 2 is a practical example of a hydraulic actuator that considers real-world valve leakage. The circuit contains a 4/3 proportional directional control valve, a pressure compensator, and a two-chamber double-acting hydraulic cylinder. The mobile mass m is attached to the end of a horizontal cylinder rod. The system has an ideal tank and pump working at a constant pressure of $p_t = 9$ bar and $p_p = 200$ bar, respectively. The small volume V_p is situated between the pressure-compensator throttle and the orifice of the directional control valve.

A. HYDRAULIC CIRCUIT MODEL

The hydraulic circuit was modelled and simulated in the Simulink R2018 environment. The initial values and constants for the system are presented in Table 1. The mathematical model of the fluid power circuit considered is fully represented by a set of algebraic and differential equations. The flow Q_p through the pressure compensator's throttle is calculated in accordance with a semi-empirical approach presented in the literature [40]:

$$\begin{aligned} Q_p &= K\sqrt{p_s - p_p}, \\ \dot{K} &= \frac{1}{C3}(C5 - p_p + p_{shuttle} - (C1 + C2(p_s - p_p))K) \end{aligned} \tag{22}$$

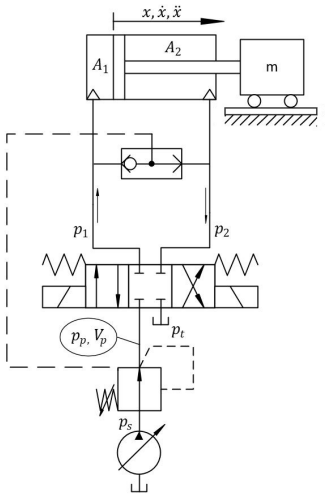

FIGURE 2. Schematic representation of the practical fluid power circuit.

where K is a semi-empirical flow coefficient; $C1$, $C2$, $C3$, and $C5$ are empirical constants [40]; p_s is pump pressure; and p_p is the pressure in the small volume. The output pressure of the shuttle valve between points A and B $p_{shuttle}$ is dependent on the maximum value of pressures p_1 and p_2 and can be expressed as $p_{shuttle} = max(p_1, p_2)$.

The 4/3 proportional directional valve's volume flow rates Q_1 and Q_2 are presented by means of a turbulent-orifice model with a triangular groove cross-section as follows:

$$Q_1 = \begin{cases} C_v(U_s - U_d)\sqrt{|p_p - p_1|}sign(p_s - p_1), & U_s \geq U_d \\ C_v(U_s - U_d)\sqrt{|p_1 - p_t|}sign(p_1 - p_t), & U_s \leq -U_d \\ 0 & \text{otherwise} \end{cases}$$

$$Q_2 = \begin{cases} -C_v(U_s - U_d)\sqrt{|p_2 - p_t|}sign(p_2 - p_t), & U_s \geq U_d \\ -C_v(U_s - U_d)\sqrt{|p_p - p_2|}sign(p_s - p_2), & U_s \leq -U_d \\ 0 & \text{otherwise} \end{cases} \tag{23}$$

where C_v is the flow constant that accounts for cross-sectional areas and the geometry of the valve orifices; U_d is the insensitivity area for the signal applied; and p_1, p_2, p_p, and p_t are the pressures in, respectively, the two cylinder chambers, the small volume V_p, and the tank.

The pressures in this example fluid power circuit are integrated from the following pressure-continuity equations:

$$\begin{aligned} \dot{p}_p &= \frac{B_e}{V_p}(Qp - Q_3) \\ \dot{p}_1 &= \frac{B_e}{V_1}(Q_1 - A_1\dot{x}) \\ \dot{p}_2 &= \frac{B_e}{V_2}(-Q_2 + A_2\dot{x}) \end{aligned} \tag{24}$$

TABLE 1. Fluid power circuit constants and initial conditions.

para.	*val.*	*unit*	*para.*	*val.*	*unit*
p_s	200×10^5	Pa	A_1	12.56×10^{-4}	m^2
p_1	9×10^5	Pa	A_2	7×10^{-4}	m^2
p_2	9×10^5	Pa	V_p	10^{-6}	m^3
p_p	9×10^5	Pa	V_{dead}	10^{-4}	m^3
p_t	9×10^5	Pa	B_e	10^9	Pa
C_1	4.65×10^7	–	S_c	1	m
C_2	-1.79×10^4	–	F_c	$6720\ \sigma_0$	N
C_3	4.0×10^{11}	–	F_s	$5290\ \sigma_1$	N
C_5	10^6	–	k_v	$201\ \sigma_1$	N.s/m
K	10^{-6}	–	v_s	347	m/s
σ_0	320	N/m	x_0	0.75	m
σ_1	$0.0199\ \sigma_0$	N.s/m	m	100	kg

where p_p is the pressure in the pipeline between the pressure compensator and directional control valve, p_1 and p_2 are the pressures in the two cylinder chambers, V_p is the small volume between the pressure compensator and directional control valve, V_1 and V_2 are the volumes of the pipelines and chamber for path A and B, B_e is the effective bulk modulus of oil, A_1 and A_2 are the cross-sectional areas of the chambers of the cylinder, and $\dot{x}$ is the sliding velocity of the piston. The outlet flow Q_3 is determined by the following relation:

$$Q_3 = \begin{cases} Q_1, & U_s \geq U_d \\ -Q_2, & U_s \leq -U_d \\ 0 & \text{otherwise} \end{cases} \tag{25}$$

The volumes in the circuit can be calculated thus:

$$\begin{aligned} V_1 &= A_1 x + V_{dead} \\ V_2 &= A_2(S_c - x) + V_{dead} \end{aligned} \tag{26}$$

where S_c is a full stroke of the cylinder; x is the position of the piston; A_1 and A_2 are the area of the first and of the second chamber, respectively; and V_{dead} is the dead volume, which represents the volume of the pipelines from directional control valve to cylinder.

The total force generated by the piston is described by the system-force equation as follows:

$$F_{tot} = p_1 A_1 - p_2 A_2 - F_\mu = m\ddot{x} \tag{27}$$

Here, F_μ denotes the friction between the walls of the cylinder and the piston, m is the load mass, and $\ddot{x}$ is the acceleration of the piston.

The friction model applied for the simulation is based on the LuGre friction model [41]–[43]. This model can be introduced by the following set of equations:

$$\begin{aligned} \dot{z} &= \dot{x} - \frac{|\dot{x}|}{g(\dot{x})} z \\ g(\dot{x}) &= \frac{1}{\sigma_0}\left(F_c + (F_s - F_c) e^{(-|\frac{\dot{x}}{v_s}|)^2}\right) \\ F_\mu &= \sigma_0 z + \sigma_1 \dot{z} + k_v \dot{x} \end{aligned} \tag{28}$$

where F_μ is total friction force, z denotes a non-measurable internal state, F_c is the force of Coulomb friction, $\dot{x}$ is the sliding velocity of the piston, v_s is the sliding speed coefficient, and F_s is static friction. The viscous friction coefficient is included as k_v, and σ_0 and σ_1 are the flexibility and damping coefficient, respectively.

TABLE 2. State variables.

state var.	definition	explanation
x_1	$\sqrt{p_s - p_p}$	pressure drop Δp_1
x_2	$\sqrt{p_2 - p_t}$	pressure drop Δp_2
x_3	$\sqrt{p_p - p_1}$	pressure drop Δp_3
x_4	$\sqrt{\dot{x}}$	velocity $\dot{x}$
x_5	$\sqrt{x}$	position x

B. STABILITY AND NUMERICAL STIFFNESS ANALYSIS

The numerical singularity problem occurs in circumstances wherein both a 'fast' term and 'slow' ones contribute to the solution for independent variables. The eigenvalues associated with a set of differential equations determine how quickly their corresponding terms develop. Therefore, the comparison of extremum eigenvalues will determine the speed of the 'fastest' term relative to the 'slowest'. Consequently, the system is numerically stiff whenever the ratio of the largest to the smallest eigenvalues obtained from the Jacobian is large. The set of equations represented as Equation 24 and the one for motion, Equation 31, together form the set of equations for stability analysis. This set of equations is transformed to the state space by means of the state variables in Table 2 in the following manner:

$$\begin{aligned} 2x_1\dot{x}_1 &= \frac{B_e}{V_p}\left(C_v U x_3 - K x_1\right) \\ 2x_2\dot{x}_2 &= \frac{B_e}{A_2(S_c - x_5^2) + V_{dead}}\left(C_v U x_3 + A_2 x_4^2\right) \\ 2x_3\dot{x}_3 &= \frac{B_e}{A_1 x_5^2 + V_{dead}}\left(A_1 x_4^2 - C_v U x_3\right) \\ 2x_4\dot{x}_4 &= -\frac{A_1}{m}\left(x_1^2 + x_3^2\right) - \frac{A_2}{m}x_2^2 - \frac{k_v}{m}x_4^2 + \frac{A_1}{m}p_s - \frac{A_2}{m}p_t \\ 2x_5\dot{x}_5 &= x_4^2 \end{aligned} \tag{29}$$

in which the flow coefficient for the pressure compensator (K) is assumed to be constant and the friction model is overlooked for purposes of simplifying the Jacobian matrix derivation. It should be highlighted that the set of state-space equations presented is a representation of the system with a positive valve position ($U >= 0$). Stability analysis for a negative valve position ($U < 0$) follows the same approach apart from minor changes in the equations.

After the Jacobian matrix is formed through taking the partial derivative of the state equations with respect to the state variables as $J = \frac{\partial F}{\partial x}$, the eigenvalues of the system can be calculated (five eigenvalues for a 5×5 Jacobian matrix). For investigation of the system numerical stiffness, a condition number, κ, is computed:

$$\kappa(J) = \frac{|\lambda_{max}(J)|}{|\lambda_{min}(J)|} \tag{30}$$

This measures the 'speed' of the 'fastest' term (corresponding to the maximum eigenvalue λ_{max}) of the solution relative to that of the 'slowest' one (corresponding to the minimum eigenvalue λ_{min}). Note that a higher condition number at the given operating point implies that the system is more numerically stiff.

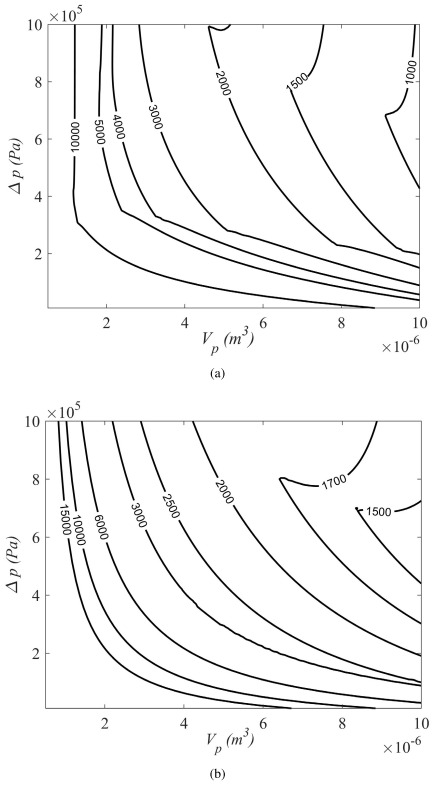

FIGURE 3. Stability analysis curves showing the condition number (κ) contours in the $\Delta p - V_p$ plane for $x = [\Delta p \ \ \Delta p \ \ \Delta p \ \ 0.2 \ \ 0.5]$ (a) and for $x = [\Delta p \ \ 5 \times 10^5 \ \ 5 \times 10^5 \ \ 0.2 \ \ 0.5]$ (b).

For conditions of an identical pressure drop over all three hydraulic volumes, $\Delta p_1 = \Delta p_2 = \Delta p_3 = \Delta p$, the state variables $x = [x_1 \ x_2 \ x_3 \ x_4 \ x_5]$ are set to $[\Delta p \, \Delta p \, \Delta p \ 0.2 \ 0.5]$, and the corresponding stability graph is plotted in Figure 3a. The x-axis of this figure shows the small hydraulic volume varying between 0 and 10^{-5} m^3, for depicting the effects of the pressure drop on the condition number, κ. As this figure suggests, where there is a constant pressure drop, the smaller volume V_p produces a higher κ value: the system becomes more numerically stiff. On the other hand, for a fixed volume smaller than 6.5×10^{-6} m^3, less of a pressure drop makes for a higher condition number and greater numerical stiffness of the system. One can conclude that a small hydraulic volume or a small pressure drop through the volumes increase the numerical stiffness.

We can perform the same analysis while varying only the pressure drop through the small volume Δp_1 and setting $\Delta p_2 = \Delta p_3 = 5 \times 10^5$ Pa. In this case, the state variables become $x = [\Delta p \ 5 \times 10^5 \ 5 \times 10^5 \ \ 0.2 \ 0.5]$. The corresponding stability graph is depicted in Figure 3b.

TABLE 3. The simulation results.

input	time step (s)			error %	
$\frac{U}{U_d}$	$ref.$	$pert.$	MMS	$pert.$	MMS
$sin(0.25t)$	10^{-4}	10^{-4}	4×10^{-4}	10.9	1.0
$sin(0.25t)$	10^{-4}	10^{-4}	5×10^{-4}	10.9	1.64
$sin(0.75t)$	10^{-4}	10^{-4}	4×10^{-4}	10.6	0.6
$u(t)$	5×10^{-5}	10^{-4}	10^{-3}	13.2	0.09

This figure exhibits the same trend visible in Figure 3a with regard to the volume and pressure drop. There is a difference, however, in that, for a certain volume and pressure drop, Figure 3b predicts a more numerically stiff system than does Figure 3a.

IV. RESULTS AND DISCUSSION

This section describes the results of fluid power circuit simulation. The results are represented through comparison of three simulation models – namely, a model that addresses the small volume in terms of the lumped-fluid theory, with a relatively small integration time step; the perturbed model, based on singular perturbation theory; and our multiple-scale model derived by means of the MMS. The first of these is a reference model that, while yielding the exact solution, is computationally expensive since the integration time step used should be very small. For the comparison, we set the time step for that original model to the largest value that does not render the system unstable. Below, we will demonstrate the advantages of the proposed MMS model over both this traditional one and the perturbation method in circumstances wherein the presence of small volumes creates challenges for the real-time simulation of fluid power systems.

We performed the simulation for a time interval of 200 s, with three distinct input signals: $\sin(0.25t)$, $\sin(0.75t)$, and $u(t)$. For all three models, input sine excitation of $sin(0.25t)$ was used for the opening of the valve in the simulation conditions. The differences in simulation time step and the corresponding error values are presented in Table 3. For the original model, the largest possible time step proved to be 10^{-4} s, while for the MMS model we can make it four times greater with only 1% error. As Figure 4a illustrates, the perturbed model, in contrast, accumulates nearly 10.9% error by the end of the period. Recall that appropriate operation of the perturbed model demands correction of the flow rate from the small volume, to prevent cumulative error from rendering the results inaccurate, while the MMS model does not require such a factor and maintains second-order accuracy, $O(\varepsilon^2)$. The error values shown in Figure 4b for the perturbed and MMS model with respect to the reference model were calculated by means of the following relation:

$$error\% = \frac{100}{S_c}\sqrt{\frac{1}{N}\sum_{i=1}^{N}(x_i^p - x_i^r)^2} \tag{31}$$

where x_i^r and x_i^p are the reference- and the perturbed-model signal, each broken down into N data points. The pressures in chamber 1 and in chamber 2 are presented in figures 4c and 4d, respectively, which show the MMS to be in good

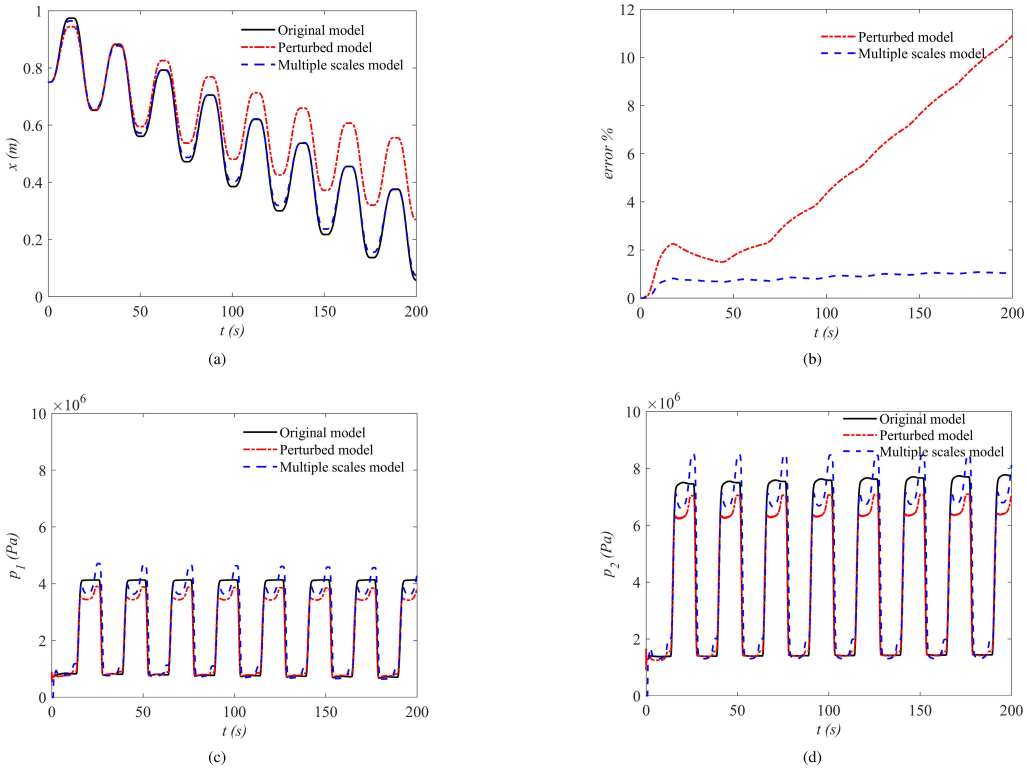

FIGURE 4. The results corresponding to the input signal of sin(0.25t). a) Comparison of piston position among the original model (solid black line), perturbed model (dashed red line), and multiple-scale model (blue dot-dashed line). b) Their relative error. c) The pressure in chamber 1 (p_1) and d) the pressure in chamber 2 (p_2).

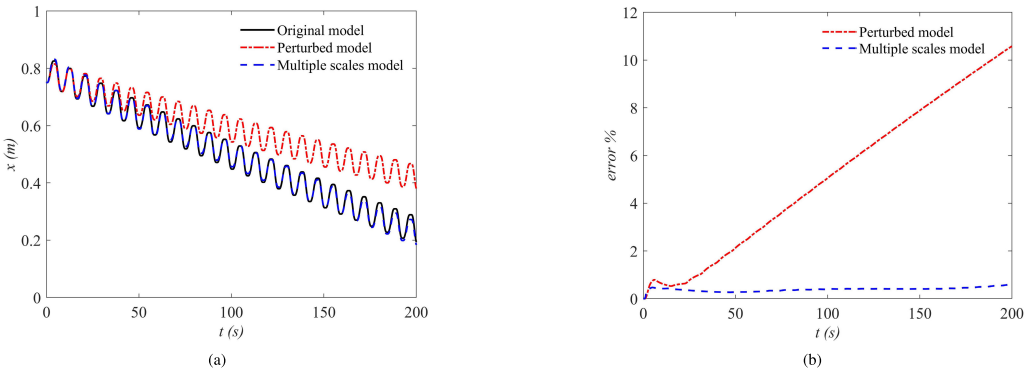

FIGURE 5. The results corresponding to the input signal of sin(0.75t): a) Comparison of piston position among the original, perturbed, and multiple-scale model (denoted as in the previous figure). b) Their relative error.

agreement with the original model whereas the pressure values obtained via the perturbed model are underestimated. It is worth highlighting the possibility of increasing the integrator's time step under the MMS model, while the largest one possible was used for the reference model. For instance, when this simulation is performed with the same input signal,

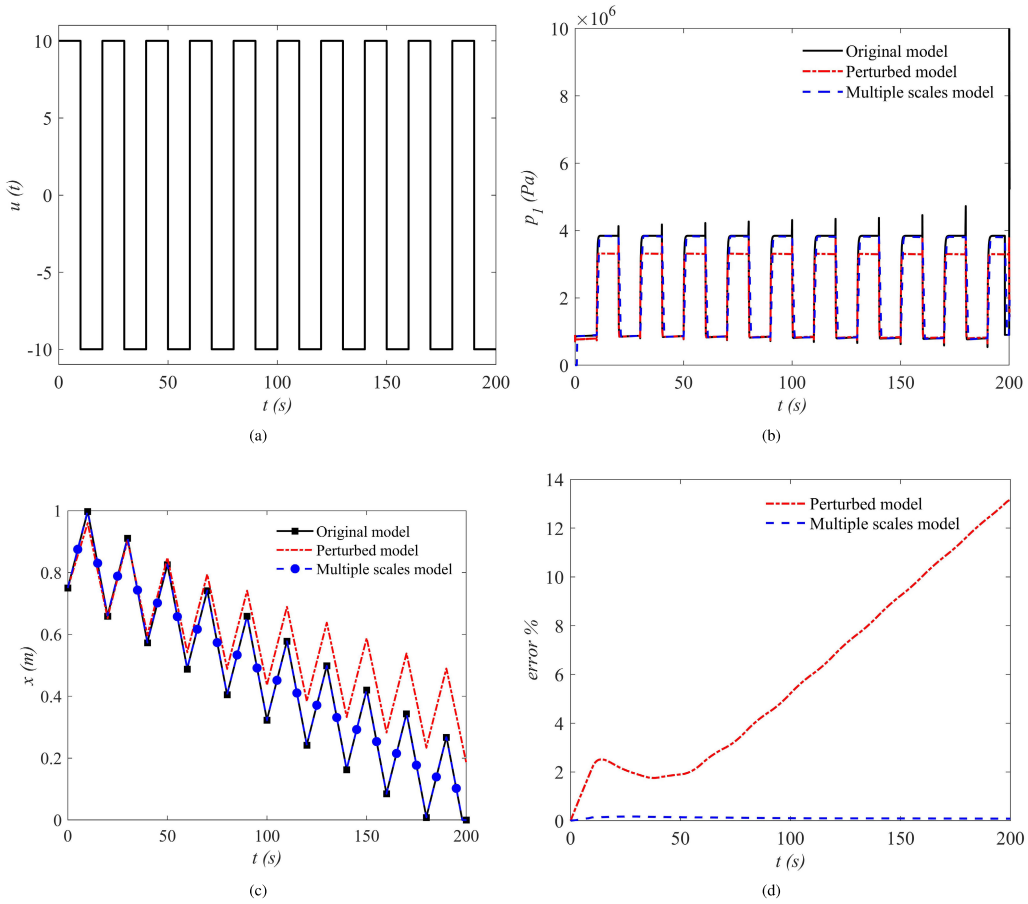

FIGURE 6. a) Pulse input $u(t)$; b) its corresponding pressure in chamber 1, p_1; c) the piston position obtained with the small time step in what is referred to as the original model (black line with squares), the perturbed model (broken red line), and the multiple-scale model (dashed blue line with circles); and d) the relative error of the latter two models relative to the original model.

increasing the time step for the MMS model to 5×10^{-5} s, causes the error to rise to just 1.64%, as the second row in Table 3 indicates.

Figure 5a shows the position response of the system with a $\sin(0.75t)$ input signal under all three methods. The figure, depicting the piston position, indicates a good match across all of the models for the first 40 s, after which the perturbed model starts to diverge from the reference exact solution. According to this figure, the positions produced via the traditional and MMS model roughly coincide while the response of the perturbed model deviates from the original one. The phenomenon is visible in Figure 4b also: the relative error of the MMS model is below 1% while the perturbed model's error rises almost linearly with time.

Additionally, the methods were tested with a pulse input of $u(t)$, which signal is presented in Figure 6a. The corresponding pressure in chamber 1 is shown in Figure 6b for all three models. We found that the MMS model is entirely consistent with the original model, while there is significant deviation in the pressure response of singular perturbed model. Furthermore, one can observe from both Figure 6c and Figure 6d that the MMS model produces a stable piston-position response with relative error of 0.09% only. The deviation under the MMS model cannot be considered critical in comparison to the perturbed model, which accumulates error values as high as 13.2% after a 200 s interval. As the tabulation in Table 3 attests, the MMS model copes with a much bigger simulation time step (10^{-3} s) than do both the original model (5×10^{-5} s) and the perturbed one (10^{-4} s). Thereby, the MMS model is amenable to real-time simulation of fluid power systems while retaining acceptable accuracy.

V. SUMMARY AND CONCLUSION

With this paper, we have introduced the MMS as a suitable technique for time-efficiently arriving at accurate solutions for numerically stiff fluid power systems, specifically when small volumes appear in their modelling. Comparison of a reference exact approach, singular perturbation, and our MMS model serves to demonstrate the novel method, considered for several valve-input signals. For this purpose, a practical fluid power circuit including a two-chamber hydraulic cylinder, a 4/3 proportional directional valve, and a pressure compensator was implemented in Simulink. The same fluid power circuit was used to investigate how applying the perturbed and the MMS model to the small hydraulic volume affects the computation efficiency and integrator time step. Comparing all of the models with regard to the same fluid power system demonstrates nicely that the perturbed model cannot achieve acceptable results without a correction factor – through cumulative error, its results deviate from the exact solution otherwise. In addition, considering the MMS model alongside the exact technique demonstrates the novel model's ability to eliminate the numerical stiffness problem brought by fluid power systems and increase computation efficiency to the levels demanded by real-time simulation conditions.

REFERENCES

[1] J. Wang, L. Ye, R. X. Gao, C. Li, and L. Zhang, "Digital twin for rotating machinery fault diagnosis in smart manufacturing," *Int. J. Prod. Res.*, vol. 57, no. 12, pp. 3920–3934, Jun. 2019.

[2] Y. Lu, C. Liu, K. I.-K. Wang, H. Huang, and X. Xu, "Digital twin-driven smart manufacturing: Connotation, reference model, applications and research issues," *Robot. Comput.-Integr. Manuf.*, vol. 61, Feb. 2020, Art. no. 101837.

[3] F. Pfeiffer, M. Foerg, and H. Ulbrich, "Numerical aspects of non-smooth multibody dynamics," *Comput. Methods Appl. Mech. Eng.*, vol. 195, nos. 50–51, pp. 6891–6908, Oct. 2006.

[4] M. K. Oshtorjani, A. Mikkola, and P. Jalali, "Numerical treatment of singularity in hydraulic circuits using singular perturbation theory," *IEEE/ASME Trans. Mechatronics*, vol. 24, no. 1, pp. 144–153, Feb. 2019.

[5] O. A. Bauchau and H. Liu, "On the modeling of hydraulic components in rotorcraft systems," *J. Amer. Helicopter Soc.*, vol. 51, no. 2, pp. 175–184, Apr. 2006.

[6] M. Naya, J. Cuadrado, D. Dopico, and U. Lugris, "An efficient unified method for the combined simulation of multibody and hydraulic dynamics: Comparison with simplified and co-integration approaches," *Arch. Mech. Eng.*, vol. 58, no. 2, pp. 223–243, Jan. 2011.

[7] A. Ylinen, H. Marjamäki, and J. Mäkinen, "A hydraulic cylinder model for multibody simulations," *Comput. Struct.*, vol. 138, pp. 62–72, Jul. 2014.

[8] J. Rahikainen, M. Kiani, J. Sopanen, P. Jalali, and A. Mikkola, "Computationally efficient approach for simulation of multibody and hydraulic dynamics," *Mechanism Mach. Theory*, vol. 130, pp. 435–446, Dec. 2018.

[9] O. Brüls and M. Arnold, "The generalized-α scheme as a linear multistep integrator: Toward a general mechatronic simulator," *J. Comput. Nonlinear Dyn.*, vol. 3, no. 4, p. 41007, Oct. 2008.

[10] K. J. Bathe, *Finite Element Procedures*. Englewood Cliffs, NJ, USA: Prentice-Hall, 1996.

[11] A. Cardona and M. Geradin, "Modeling of a hydraulic actuator in flexible machine dynamics simulation," *Mechanism Mach. Theory*, vol. 25, no. 2, pp. 193–207, Jan. 1990.

[12] A. Ylinen, J. Mäkinen, and R. Kouhia, "Two models for hydraulic cylinders in flexible multibody simulations," in *Computational Methods for Solids and Fluids*. Cham, Switzerland: Springer, 2016, pp. 463–493.

[13] A. Ellman and R. Piché, "A modified orifice flow formula for numerical simulation of fluid power systems," in *Proc. ASME Int. Mech. Eng. Congr. Expo., Atlanta, Fluid Power Syst. Technol.*, vol. 3, Nov. 1996, pp. 59–63.

[14] A. Ellman and R. Piché, "A two regime orifice flow formula for numerical simulation," *J. Dyn. Syst., Meas., Control*, vol. 121, no. 4, pp. 721–724, Dec. 1999.

[15] R. Åman, H. Handroos, and T. Eskola, "Computationally efficient two-regime flow orifice model for real-time simulation," *Simul. Model. Pract. Theory*, vol. 16, no. 8, pp. 945–961, Sep. 2008.

[16] W. Borutzky, B. Barnard, and J. Thoma, "An orifice flow model for laminar and turbulent conditions," *Simul. Model. Pract. Theory*, vol. 10, nos. 3–4, pp. 141–152, Nov. 2002.

[17] R. Piché and A. Ellman, "Numerical integration of fluid power circuit models using two-stage semi-implicit runge-kutta methods," *Proc. Inst. Mech. Eng., C, J. Mech. Eng. Sci.*, vol. 208, no. 3, pp. 167–175, May 1994.

[18] S. Esqué, A. Raneda, and A. Ellman, "Techniques for studying a mobile hydraulic crane in virtual reality," *Int. J. Fluid Power*, vol. 4, no. 2, pp. 25–35, 2003.

[19] D. E. Bowns and L. M. Wang, "The digital computation of pressures in hydraulic pipes with small volume using an iterative technique," *Proc. Inst. Mech. Eng., C, Mech. Eng. Sci.*, vol. 204, no. 1, pp. 29–36, Jan. 1990.

[20] R. Åman and H. Handroos, "Pseudo-dynamic solution of pressures in small volumes in fluid power circuit simulation," in *Proc. 5th FPNI PhD Symp. Cracow*, Jul. 2008, pp. 406–416.

[21] R. Åman and H. Handroos, "Comparison of numerical effectiveness of three methods for modelling 2-way flow control valves," in *Proc. 7th Int. Conf. Fluid Power Transmiss. Control*. Beijing, China: World Publishing Corporation, Apr. 2009, pp. 711–715.

[22] R. Åman and H. Handroos, "Optimization of parameters of pseudo-dynamic solver for real-time simulation of fluid power circuits," in *Proc. 7th Int. Fluid Power Conf. Aachen Workshop*, vol. 1, Mar. 2010, pp. 495–507.

[23] M. Krishna and J. Bares, "Hydraulic system modeling through memory-based learning," in *Proc. IEEE/RSJ Int. Conf. Intell. Robots Syst. Innov. Theory, Pract. Appl.*, vol. 3, Oct. 1998, pp. 1733–1738.

[24] M. Krishna and J. Bares, "Constructing fast hydraulic robot models for optimal motion planning," Tech. Rep., Jan. 1999.

[25] G. Bidini and F. Mariani, "Simulation of hydraulic power plant transients using neural networks," *Proc. Inst. Mech. Eng., A, J. Power Energy*, vol. 211, no. 5, pp. 393–398, Aug. 1997.

[26] A. H. Nayfeh and D. T. Mook, *Nonlinear Oscillations*. Hoboken, NJ, USA: Wiley, 2008.

[27] M. Sajjadi, H. N. Pishkenari, and G. Vossoughi, "On the nonlinear dynamics of trolling-mode AFM: Analytical solution using multiple time scales method," *J. Sound Vib.*, vol. 423, pp. 263–286, Jun. 2018.

[28] M. A. Langthjem and T. Nakamura, "On the dynamics of the fluid balancer," *J. Fluids Struct.*, vol. 51, pp. 1–19, Nov. 2014.

[29] S. Ilbeigi, J. Jahanpour, and A. Farshidianfar, "A novel scheme for nonlinear displacement-dependent dampers," *Nonlinear Dyn.*, vol. 70, no. 1, pp. 421–434, Oct. 2012.

[30] B. Kalita and S. K. Dwivedy, "Dynamic analysis of pneumatic artificial muscle (PAM) actuator for rehabilitation with principal parametric resonance condition," *Nonlinear Dyn.*, vol. 97, no. 4, pp. 2271–2289, Sep. 2019.

[31] S. L. Woodruff and R. Rubinstein, "Multiple-scale perturbation analysis of slowly evolving turbulence," *J. Fluid Mech.*, vol. 565, pp. 95–103, Oct. 2006.

[32] S. W. Rienstra and W. Eversman, "A numerical comparison between the multiple-scales and finite-element solution for sound propagation in lined flow ducts," *J. Fluid Mech.*, vol. 437, pp. 367–384, Jun. 2001.

[33] P. Romanazzi, M. Bruna, and D. A. Howey, "Thermal homogenization of electrical machine windings applying the multiple-scales method," *J. Heat Transf.*, vol. 139, no. 1, Jan. 2017, Art. no. 012101.

[34] J. White, "Analysis of heat conduction in a heterogeneous material by a multiple-scale averaging method," *J. Heat Transf.*, vol. 137, no. 7, Jul. 2015, Art. no. 071301.

[35] A. H. Nayfeh and H. Bouguerra, "Non-linear response of a fluid valve," *Int. J. Non-Linear Mech.*, vol. 25, no. 4, pp. 433–449, 1990.

[36] M. Mohammadi, M. Kiani-Oshtorjani, and A. Mikkola, "The effects of oil entrained air on the dynamic performance of a hydraulically driven multibody system," *Int. Rev. Model. Simul.*, vol. 13, no. 4, pp. 214–222, 2020.

[37] H. M. Handroos and M. J. Vilenius, "Flexible semi-empirical models for hydraulic flow control valves," *J. Mech. Des.*, vol. 113, no. 3, pp. 232–238, Sep. 1991.

[38] A. N. Tikhonov, "Systems of differential equations containing small parameters in the derivatives," *Matematicheskii Sbornik*, vol. 73, no. 3, pp. 575–586, 1952.
[39] L. Noethen and S. Walcher, "Tikhonov's theorem and quasi-steady state," *Discrete Continuous Dyn. Syst.-B*, vol. 16, no. 3, pp. 945–961, 2011.
[40] H. M. Handroos and M. J. Vilenius, "Flexible semi-empirical models for hydraulic flow control valves," *J. Mech. Des.*, vol. 113, no. 3, pp. 232–238, Sep. 1991.
[41] C. C. de Wit, H. Olsson, K. J. Astrom, and P. Lischinsky, "Dynamic friction models and control design," in *Proc. Amer. Control Conf.*, Jun. 1993, pp. 1920–1926.
[42] C. C. de Wit, H. Olsson, K. J. Astrom, and P. Lischinsky, "A new model for control of systems with friction," *IEEE Trans. Autom. Control*, vol. 40, no. 3, pp. 419–425, Mar. 1995.
[43] H. Olsson, "Control systems with friction," Ph.D. dissertation, Dept. Autom. Control, Lund Inst. Technol., Lund, Sweden, 1996.

MEHRAN KIANI-OSHTORJANI is currently pursuing the Ph.D. degree with LUT University. His research interests include fluid power systems, real-time simulation, the dynamics and thermal behaviour of granular materials, and multi-phase flows. He is also an Expert in performing real-time simulations, both as an Algorithm Designer and as a Professional Scientific Programmer.

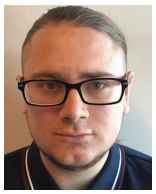

STANISLAV USTINOV received the B.Sc. degree from the Saimaa University of Applied Sciences, Lappeenranta, Finland, in 2016, within the mechanical engineering and production technology programme, and the M.Sc. degree in mechatronic system design from LUT University, in 2018. He is currently working as a Researcher with the Laboratory of Intelligent Machines, Mechanical Engineering Department, LUT University. His research interests include fluid power systems, real-time simulation of multi-body systems, and artificial intelligence.

HEIKKI HANDROOS (Member, IEEE) has been a Full Professor with LUT University since 1998. His research interests include modeling and simulation of mechatronics systems to robotics. He has served as an Associate Editor for ASME's *Journal of Dynamic Systems, Measurement and Control* from 2014 to 2020 and himself has published 161 Scopus-indexed articles. He has also served as a principal investigator for various international and domestic research projects, with a total budget of more than €15M. He has been the supervisor or co-supervisor of 24 doctoral students and participated in evaluating about a dozen doctoral dissertations, both in Finland and abroad.

PAYMAN JALALI received the Ph.D. degree in energy technology from LUT University, in 2000. He was a Postdoctoral Fellow with the US's Georgia Institute of Technology from 2001 to 2003. After working as a Researcher, he was appointed as an Adjunct Professor with LUT University in 2006 and has been held the title Associate Professor of energy technology there since 2011. He was a Visiting Professor with Duke University, USA, from 2016 to 2018. Today, his co-ordinates research in the fields of computational and experimental fluid flows, heat transfer, multi-phase flows, and complex systems, with areas of application including hydraulic circuits, gas–solid multi-phase systems in the energy-technology sector, practical physics of granular and particle systems, and biomedical research. He has written or coauthored 84 peer-reviewed articles, and he has been the principal investigator or a co-PI of four major Academy of Finland projects.

AKI MIKKOLA received the Ph.D. degree in machine design in 1997. He has been working as a Full Professor with the Department of Mechanical Engineering, LUT University, since 2002. He is currently leading the research team of that university's Laboratory of Machine Design. His research interests include machine dynamics and vibration, multi-body system dynamics, and bio-mechanics. He has been awarded five patents and has contributed to more than 90 peer-reviewed journal articles.

Publication III

Ustinov, S., Wu, H., and Handroos, H.
A Hybrid Model for Fast and Efficient Simulation of Fluid Power Circuits With Small Volumes Utilizing a Recurrent Neural Network

Reprinted with permission from
IEEE Access
Vol. 10, pp. 48824-48835, 2022

IEEE Access
Multidisciplinary ⋮ Rapid Review ⋮ Open Access Journal

Received April 13, 2022, accepted April 27, 2022, date of publication May 4, 2022, date of current version May 11, 2022.

Digital Object Identifier 10.1109/ACCESS.2022.3172662

A Hybrid Model for Fast and Efficient Simulation of Fluid Power Circuits With Small Volumes Utilizing a Recurrent Neural Network

STANISLAV USTINOV, HUAPENG WU, AND HEIKKI HANDROOS, (Member, IEEE)
Laboratory of Intelligent Machines, School of Energy Systems, Lappeenranta-Lahti University of Technology (LUT University), 53850 Lappeenranta, Finland
Corresponding author: Stanislav Ustinov (stanislav.ustinov@lut.fi)

This work was supported by the Research Foundation of the Lappeenranta-Lahti University of Technology (LUT University).

ABSTRACT The modeling and simulation of fluid power systems are essential parts of the real-time simulation of virtual prototypes of mobile working machines. In several cases in the dynamic simulation of such fluid power systems, a longer simulation time is required. This makes the traditional mathematical models inefficient for real-time simulations, particularly when simulating fluid power systems because of the small volumes in stiff differential equations of pressure. To overcome this issue, a novel hybrid model is proposed for stiff fluid power systems simulation. The main feature of the model is the utilization of a recurrent neural network instead of stiff differential equations of pressure with small volume. At the same time, the dynamics of the rest system are traditionally presented with algebraic and differential equations. The testing results of the introduced hybrid model showed that the novel method can reduce the simulation time, which makes the model suitable for real-time applications. Moreover, the accuracy of the model remains at a fairly high level compared to traditional mathematical models.

INDEX TERMS Dynamic simulation, fluid power system, real-time simulation, recurrent neural network, small volumes.

I. INTRODUCTION

Fluid power systems are widely used in the real-life modeling of various mobile machines such as logging harvesters, cranes, excavators, and industrial robots. The recent trend in modeling digital twins [1] and virtual prototypes [2]–[4] has shown that mathematical modeling of fluid power systems plays a vital role in the development of industrial simulators of such mobile working machines. For this purpose, real-time and faster than real-time techniques [5] are used to get a fast response in the system. However, fluid power circuits can contain singularities that directly affect the computational speed of the whole system and make a real-time simulation of the system impossible.

In general, there are two main problems in fluid power circuits modeling and simulation. The first problem is related to the pressure drop approaching zero. This phenomenon is associated with difficulties in the use of the traditional turbulent flow orifice equation because of the infinite value of the flow rate derivative. To solve this problem, several combined orifice models were proposed by Ellman *et al.* at the end of the 1990s [6], [7]. Another computationally efficient solution was proposed by Aman *et al.* in 2008 [8] in which the polynomial relation between flow rate and pressure drop was derived for cases when the pressure drop approaches zero. The model was named the two-regime flow model in which the third-order polynomial is used for describing the laminar and transition flow areas, whereas the traditional square root turbulent orifice equation of flow is used for the turbulence regime.

Another problem in the dynamic simulation of fluid power circuits can be associated with the numerical stiffness of ordinary differential equations [9]. The numerical stiffness in fluid power systems can be explained by the fact that such circuits include volumes of different orders of magnitude. This results in difficulties in the numerical integration of ordinary differential equations, and classical explicit integration solvers are not able to generate a stable dynamic response at a high integration time step, slowing down the simulation by implementing significantly small time steps. The numerical stiffness of the system can often be associated with small volumes in a hydraulic circuit. The solution for

The associate editor coordinating the review of this manuscript and approving it for publication was Tingwen Huang.

the systems with small volumes should be derived by using specific numerical solvers to avoid the problem of instability in a dynamic model of a fluid power circuit [10].

The problem of small volumes and the resulting numerical stiffness of fluid power circuits arises in various scientific papers, and as a result, special solvers are developed. This problem was first mentioned in 1990 by Bowns and Wang [11], who proposed an iterative technique to solve the problem of numerical stiffness due to the small volumes in hydraulic pipes. However, the technique was still computationally costly.

Another iterative technique was first presented by Aman and Handroos [12]–[14]. This implicit solver was named the pseudo-dynamic solver. This solver consists of two loops—an outer (or main) loop and an inner (or pseudo) loop. The main loop contains algebraic and differential equations of the whole fluid power system, except for the pressure and flows that are associated with the small volume. The integration of such pressure occurs in the inner loop of the solver with an artificially enlarged volume instead of the real small volume. The idea of the inner loop is to receive the steady-state response of the pressure by iterating such pressure with artificial volume until the convergence criterion is reached.

The advanced version of the pseudo-dynamic solver (AdvPDS) was proposed by Malysheva *et al.* in 2020 [15]. The main difference of this approach from the original pseudo-dynamic method is the implementation of adaptive criterion of convergence. The criterion depend on the pressure levels in the system, and it was experimentally proven that with small levels of pressure, the smaller criterion have more accurate results; and at the same time, the bigger criterion can accelerate the computational speed of the fluid power system. Ultimately, the method is a trade-off between accuracy and speed suitable for real-time or faster than real-time applications. The method has also been improved by Malysheva and Handroos [16], where it was investigated that different integrators can also affect the computational speed of AdvPDS.

One of the most reliable methods proven to be excellent in simulating fluid power systems in theory and practice is the method proposed by Kiani-Oshtorjani *et al.* [17]. This method is based on the singular perturbation theory. The main idea of this approach is to substitute stiff ordinary differential equations with small volumes for algebraic equations modified for fluid power systems simulation in accordance with this theory. The method was tested in simulating multibody systems [18], and an accurate and fast response of the system was achieved. However, the method has its own drawbacks related to the accumulative error in certain cases of use. To overcome the error, a special corrector factor for the model should be used. To solve this problem and allow the simulation without a corrector factor definition, a novel method based on the combined singular perturbation theory and Method of multiple scales (MMS) was proposed by Kiani-Oshtorjani *et al.* [19]. This robust method allows the elimination of the accumulative error and makes the simulation faster and more accurate than the original method based on the singular perturbation theory.

In several works [20]–[22], the components of fluid power systems were introduced as neural networks with basic inputs and outputs. This type of system modeling showed that the use of neural networks in fluid power circuits modeling provides a fast response in the system that allows a simulation of the system in real-time or faster than real-time applications. In addition, predictive neural network models of various dynamic systems with ordinary differential equations (ODE) were studied in [23] and [24]. Both papers are based on the studies of new methods for improving the performance of neural networks based on simple ODEs and complex nonlinear dynamic systems. Nevertheless, the most significant results were shown by using recurrent neural networks (RNN) [25]–[27] in the modeling and simulation of different systems.

However, the systems based on neural networks are simulated as a black box, and the dynamics of the system are totally neglected. Substituting a stiff differential equation with small volumes with a computationally efficient and accurate neural network can solve the problem of singularity arising in the simulation of such stiff fluid power systems. It means that only the stiff equation will be replaced with the neural network and the system dynamics of the entire system will be saved in the mathematical model. And at the same time, the simulation is supposed to be faster due to the absence of stiff differential equations in the areas with small volumes.

The main purpose of this research paper is to introduce a novel hybrid model for a fast simulation of fluid power systems with small volumes using the RNN only for the pressure continuity equation with small volume in calculations. Section II describes the fluid power systems under consideration in the research. Section III provides information about the RNN used in the development. Section IV describes the development in detail, from the collected data and the RNN training to the implementation of the neural network in the fluid power circuits from Section II. Finally, sections V and VI provide the results of the simulations, and a conclusion is made about the model developed.

II. FLUID POWER CIRCUIT DESCRIPTION

This section describes the systems studied in the current research. Overall, two fluid power circuits were investigated. Both systems have one thing in common—the content of one small volume inside. The first circuit is a simple fluid power system with multiple orifices located in series. The second fluid power circuit is a simple pressure-compensated system with a 2-chamber hydraulic cylinder controlled by a directional control valve.

The systems were modeled in accordance with the lumped fluid theory, which assumes that a fluid power system can be divided into sections with separate volumes where the pressure can be distributed. A differential equation is formed for each pressure in such a fluid power system where the

derivative of pressure can be expressed with the general formula:

$$\dot{p}_i = \frac{B_e}{V_i}(Q_i - Q_{i+1} - \frac{dV_i}{dt}) \quad (1)$$

where p_i is the pressure in at ith section, B_e is the effective bulk modulus, V_i is the volume in the same section, Q_i and Q_{i+1} are the inlet and outlet volumetric flows, and $\frac{dV_i}{dt}$ is the time rate changes of volume V_i. The detailed description of the fluid power circuits studied will be in the following subsections.

A. CIRCUIT 1: MULTIPLE ORIFICES

The first fluid power circuit is related to the system of three identical orifices in series. The system contains the constant pressure pump, which is assumed as an ideal pressure source and tank for recovery of the fluid. Fig. 1 shows the schematic representation of the circuit. The position of a small volume in such a system is between the orifice number 2 and 3. The total simplicity of this circuit allows the use of a large integrator time step for the dynamic simulation of the circuit even with a small volume inside, and it requires less computational time than more complex fluid power systems.

Each pressure in the circuit can be represented by the lumped fluid theory and a general formulation (1). Therefore, pressures in this circuit are integrated from the following formulations:

$$\begin{aligned} \dot{p}_1 &= \frac{B_{e1}}{V_1}(Q_1 - Q_2) \\ \dot{p}_2 &= \frac{B_{e2}}{V_2}(Q_2 - Q_3) \end{aligned} \quad (2)$$

where V_1 and V_2 are pipe volumes in two pressure sections; Q_1, Q_2, and Q_3 are volume flows through orifices 1, 2, and 3, respectively, and B_{e1} and B_{e2} are pressure-dependent effective bulk modulus for pressures p_1 and p_2, respectively. The effective bulk modulus in such a system can be derived as follows:

$$B_{ei} = a_1 E_{max} \log\left(a_2 \frac{p_i}{p_{max}} + a_3\right) \quad (3)$$

where E_{max} is the maximum bulk modulus of the oil, p_{max} is the maximum pressure in the system, p_i denotes pressure corresponding to the bulk modulus, and a_1, a_2, and a_3 are the empirical constants [28]. Volume flows in the circuit can be calculated with the orifice equation as follows:

$$Q_i = C_d A_i \sqrt{\frac{2(p_{i-1} - p_i)}{\rho}} \quad (4)$$

where C_d denotes the discharge coefficient, A_i is the cross-sectional area of orifice i (where $i = 1, 2$ or 3), ρ is the density of the hydraulic fluid, and p_i and p_{i-1} are the outlet and inlet pressures, respectively. The system has a total of 3 volumetric flow variables corresponding to each orifice. The values of all parameters used in the modeling and simulation of the multiple orifice fluid power circuit are represented in Table 1.

TABLE 1. Circuit 1 parameters.

C_d	0.6	ρ	900 kg/m^3	d_1	1.0×10^{-3} m
V_1	1.0×10^{-3} m^3	p_s	1.0×10^{7} Pa	d_2	1.0×10^{-3} m
V_2	1.0×10^{-5} m^3	p_t	0 Pa	d_3	1.0×10^{-3} m
E_{max}	1.8×10^{9} Pa	p_{max}	2.8×10^{7} Pa	a_3	3
a_1	0.5	a_2	90		

B. CIRCUIT 2: HYDRAULIC CYLINDER CONTROLLED BY A DIRECTIONAL CONTROL VALVE

The second circuit under consideration is the system with a more complex architecture and which is more practical and applicable for real-time simulation. The circuit consists of a two-chamber double-acting hydraulic cylinder with a mass attached to the end of the horizontal cylinder's rod. The mass is not totally fixed, having 1 degree of freedom to slide in a piston movement direction. The cylinder is controlled by the 4/3-proportional directional control valve. The pressure in the system is supported by the constant pressure pump, which is assumed to be an ideal pressure source. A pressure compensator is also used in the circuit between the pump and the directional control valve. All the components in the system are connected with the hydraulic pipes of different volumes.

The circuit contains one extremely small pipe volume, located between the pressure compensator and the directional control valve. Fig. 2 depicts the whole circuit; the small volume is denoted as V_v. All the parameters of this system are presented in Table 2. The mathematical model of the circuit is represented with differential and algebraic equations. The system is controlled and activated by the voltage signal U, obtained from the following equation:

$$\ddot{U}_s = K_v \omega_n^2 U - 2\zeta\omega_n \dot{U}_s - \omega_n^2 U_s \quad (5)$$

where K_v is the valve gain, U_s is the signal proportional to the valve spool displacement, ζ is the valve damping ratio and ω_n is the natural angular frequency. The flow Q_v through the throttle of the pressure compensator is calculated according to a semi-empirical approach, as in [27]:

$$\begin{aligned} Q_v &= K\sqrt{p_s - p_v}, \\ \dot{K} &= \frac{1}{C_3}(C_5 - p_v + p_{shuttle} - (C_1 + C_2(p_s - p_v))K) \end{aligned} \quad (6)$$

where K denotes the semi-empirical flow coefficient, C_1, C_2, C_3, and C_5 denote empirical constants [29], p_s and p_v are the constant pump pressure and the pressure in small volume, respectively. The output pressure of the shuttle valve between way A and B (Fig. 2) $p_{shuttle}$ is dependent on the maximum value of pressures p_1 and p_2 and can be expressed as $p_{shuttle} = max(p_1, p_2)$.

The volume flow rates Q_1 and Q_2 of the 4/3-proportional directional control valve are calculated with the use of the turbulent orifice model with a triangular groove

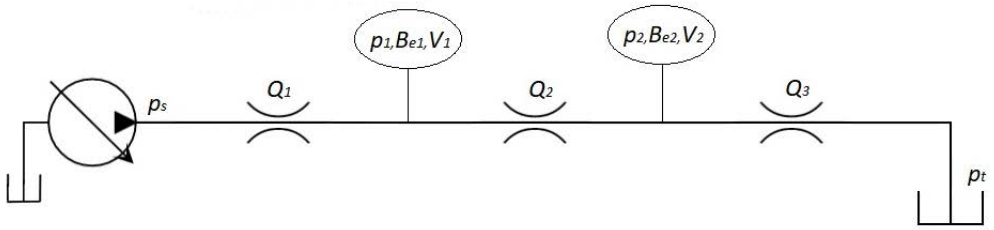

FIGURE 1. Three-orifice fluid power circuit.

cross-section, as follows:

$$Q_1 = \begin{cases} C_v(U_s - U_d)\sqrt{|p_v - p_1|}sign(p_v - p_1), \\ \qquad U_s \geq U_d \\ C_v(U_s - U_d)\sqrt{|p_1 - p_t|}sign(p_1 - p_t), \\ \qquad U_s \leq -U_d \\ 0, \\ \qquad \text{otherwise} \end{cases}$$

$$Q_2 = \begin{cases} -C_v(U_s - U_d)\sqrt{|p_2 - p_t|}sign(p_2 - p_t), \\ \qquad U_s \geq U_d \\ -C_v(U_s - U_d)\sqrt{|p_v - p_2|}sign(p_v - p_2), \\ \qquad U_s \leq -U_d \\ 0, \\ \qquad \text{otherwise} \end{cases} \tag{7}$$

where C_v is the flow constant that accounts for cross-sectional areas and the geometry of the valve orifices, U_d is the insensitivity area for the applied signal, and p_1, p_2, p_v, and p_t are the pressures in two cylinder chambers, the pressure in small volume V_v, and the pressure in the tank, respectively.

Pressures in the system are integrated from the pressure continuity equations in accordance with the lumped fluid theory, as follows:

$$\begin{aligned} \dot{p}_1 &= \frac{B_{e1}}{V_1}(Q_1 - A_1\dot{x}) \\ \dot{p}_2 &= \frac{B_{e2}}{V_2}(-Q_2 + A_2\dot{x}) \\ \dot{p}_v &= \frac{B_{e3}}{V_v}(Q_v - Q_3) \end{aligned} \tag{8}$$

where V_v is the small volume between the pressure compensator and directional control valve, Q_v is the volume flow through the throttle of pressure compensator, $\dot{x}$ is sliding speed of the piston, A_1 and A_2 are cross-sectional areas of chambers of the cylinder, V_1 and V_2 are volumes of the pipelines and chamber in way A and way B, respectively. B_{e1}, B_{e2}, and B_{e3} are effective bulk moduli for each pressure in the system and are represented by (3). Volumes V_1 and V_2 are calculated as follows:

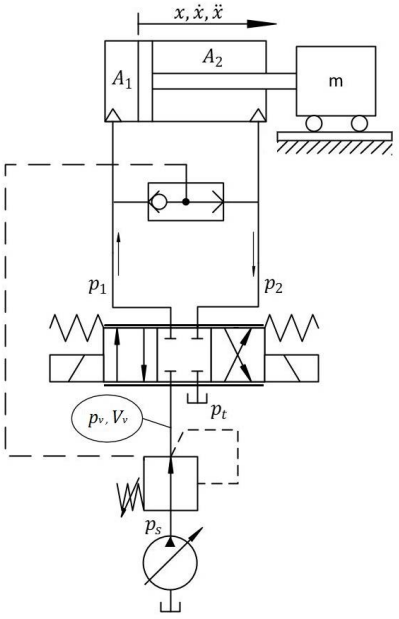

FIGURE 2. Hydraulic cylinder controlled by a directional control valve.

$$\begin{aligned} V_1 &= A_1 x + V_{dead} \\ V_2 &= A_2(S_c - x) + V_{dead} \end{aligned} \tag{9}$$

where S_c is the full stroke of the cylinder, x is the position of the piston, and V_{dead} is the dead volume, which represents the volume of pipelines. The outlet flow Q_3 from (8) depends on the valve position, which can be

determined as follows:

$$Q_3 = \begin{cases} Q_1, & U_s \geq U_d \\ -Q_2, & U_s \leq -U_d \\ 0, & \text{otherwise} \end{cases} \tag{10}$$

The equation of motion for the system with a total force acting on it can be represented by the following relation:

$$F_{tot} = p_1 A_1 - p_2 A_2 - F_\mu = m\ddot{x} \tag{11}$$

where F_μ denotes friction between the walls of the cylinder and piston, m is the mass of the load attached to the end of the rod, and $\ddot{x}$ is the acceleration of the piston. The friction model used for the simulation is based on the LuGre friction model [30]–[32]. This model can be introduced with the following set of equations:

$$\begin{aligned} \dot{z} &= \dot{x} - \frac{|\dot{x}|}{g(\dot{x})} z \\ g(\dot{x}) &= \frac{1}{\sigma_0}\left(F_c + (F_s - F_c)e^{(-|\frac{\dot{x}}{v_s}|)^2}\right) \end{aligned} \tag{12}$$

where F_μ is the total friction force; z is the non-measurable internal state, F_c is the Coulomb friction force, $\dot{x}$ is the sliding velocity of the piston, v_s is the sliding speed coefficient, F_s is the static friction force, k_v is the viscous friction coefficient, and σ_0 and σ_1 are the flexibility and damping coefficients, respectively.

III. RECURRENT NEURAL NETWORK ARCHITECTURE DESCRIPTION

In this section, the features of the RNN selection are presented. In addition, the description of the selected RNN is provided in detail. The most common RNN architectures used in modeling dynamic systems are the nonlinear finite impulse response (NFIR), the nonlinear autoregressive network with exogenous inputs (NARX), and the nonlinear autoregressive moving average network with exogenous inputs (NARMAX). There are also more complex and advanced architectures used in dynamic systems modeling, which are Long Short-Term Memory (LSTM) and Gated Recurrent Unit (GRU) neural networks.

The NFIR architecture, described in [33], is the simplest RNN architecture of all the architectures mentioned above. The operating process of this network occurs through feeding all values of past inputs to achieve the current output value. The defining equation for the network is formulated as follows:

$$y(t) = \Psi_H(x(t-1), \ldots, x(t-d)) \tag{13}$$

where $y(t)$ is the RNN output vector at time t, Ψ_H is mapping performed by a multilayer feedforward network, d is the past values of series $x(t)$, and $x(t)$ is the RNN input vector at time t. The main advantage of the NFIR architecture is its stability while all past inputs are fed to the network.

The NARX neural networks principle is related to the utilization of the outputs of the network for feeding the input with past states of the outputs and inputs while remembering the state of the system at every step of the network operation. The ordinary NARX RNN can be defined by the following equation [34]:

$$y(t) = \Psi_H(x(t-1), \ldots, x(t-d), y(t-1), \ldots, y(t-d)) \tag{14}$$

where $y(t)$ is the RNN output vector at time t. The main feature of the NARX RNN is an accurate approximation of output values. However, in certain cases, it can be inherently less stable due to operation in a closed loop using the past values of the output.

Another architecture that can be presented as an advanced NARX structure is NARMAX RNN. The main difference with this RNN architecture is the ability to use error of previous values in the loop. Thus, the defining equation for NARMAX networks is the following [35]:

$$\begin{aligned} y(t) = \Psi_H(&y(t-1), \ldots, y(t-d), \\ &x(t-1), \ldots, x(t-d), \\ &e(t-1), \ldots, e(t-d)) \end{aligned} \tag{15}$$

where $e(t-1)$ is an RNN error vector at time $t-1$. In the NARMAX architecture, all elements defined by x and e are sometimes called "controlled" and "uncontrolled" inputs [25]. This means that NARMAX is the most prevalent architecture in cases with real-world data, including the system error generated by noise. The structure also uses the error as an input dataset, which makes the method more complex than the above-mentioned NFIR and NARX.

In addition to the mentioned RNN architectures, more complex architectures are used in dynamic systems modeling. These architectures are more suitable for training and may easily store long-term dependencies. Such architectures, which are LSTM and GRU neural networks, were studied and compared [36]. Both architectures show significantly good performance in case of complex dynamics persisting in the system. In the case of LSTM networks, the accuracy of predictions is at a high level, but selecting numerous hyperparameters can affect the performance of the network. GRU networks are similar to LSTM due to their functionality, however, in several cases, it can be applied less time to train the network.

The features of the selected RNN architecture for fluid power system simulation were also described in [25]. According to the author, the data obtained from the simulation model of a similar fluid power system does not contain real system noise, and the use of a large number of RNN parameters can affect the simulation time and speed. At the same time, the maximal accuracy of the system with the embedded RNN is required. In such a case, the NARX RNN is the most suitable architecture of neural network for fluid power system simulation even in the case of the simulation of one stiff differential equation since it is more accurate than NFIR due

TABLE 2. Circuit 2 parameters.

p_s	140×10^5 Pa	C_1	4.65×10^7	A_1	8.04×10^{-4} m^2	C_v	2.315×10^{-9}
p_1	9×10^5 Pa	C_2	-1.79×10^4	A_2	4.24×10^{-4} m^2	U_d	2 V
p_2	9×10^5 Pa	C_3	4.0×10^{11}	m	200 kg	K_v	0.99
p_v	9×10^5 Pa	C_5	10^6	V_{dead}	1.0×10^{-3} m^3	ω_n	331 rad/s
p_t	9×10^5 Pa	K	0.05×10^{-9}	V_v	1.0×10^{-5} m^3	ζ	0.62
S_c	1 m	σ_0	320 N/m	k_v	1.28×10^3 Ns/m	F_c	2.15×10^6 N
x_0	1 m	σ_1	6.368 Ns/m	v_s	347 m/s	F_s	1.1376×10^{10} N

to the use of output data as feedback. Ultimately, the NARX architecture provides a trade-off between speed and accuracy in simulating the final system, which is the main objective of the research.

Fig. 3 illustrates the basic structure of the NARX network used in the modeling of the system. The RNN consists of one input layer with four input values, and one feedback value that can be used only during the training of the network, two hidden layers with 40 neurons, and one output layer with one output activated with a linear function. Because the system has to be modeled as a mathematical model of one differential equation of pressure, the number of layers and neurons were manually selected by trial and error during the training process to ensure the accuracy of the network. The sigmoid function $\sigma(x)$ was selected as the activation function for hidden layers of the network; the function is defined as follows:

$$\sigma(x) = \frac{1}{1 + e^{-x}} \tag{16}$$

where x is the argument of the function $\sigma(x)$ and e is the Euler's number.

IV. HYBRID MODEL DEVELOPMENT

The whole development of the hybrid model was divided into two stages. The first stage of development included the collection of the training data and training of the NARX RNN. The second stage of the development is related to the implementation of the neural network to the fluid power systems from Section II. The modeling and simulation of the systems were performed in MATLAB R2020a software in a form of MATLAB code, and the formulation of the RNN was performed through the embedded MATLAB Deep Learning Toolbox.

A. DATA COLLECTING AND TRAINING OF THE RNN

The data collected for the training was based on the simulation results of the practical fluid power circuit 2 described in Section II. The original system was simulated for 3,000 seconds with an integrator time step of 1.0×10^{-5} s and an input voltage that was supplied randomly in a range between -10 and 10 Volts. The integrator time step was selected empirically to ensure the correct response of the system in the presence of small volume. The data set of 300 million samples was created from several parameters of the system, where each sample displayed the data of parameters obtained at every time step of the simulation. The number of samples was reduced to 3 million by saving each 100th sample to reduce the computational load of the computer and provide relatively fast training of the neural network. The input data chosen for the training were data arrays of volumetric flows Q_3 and Q_v, effective bulk modulus B_{e3} and the fixed small volume V_v obtained from the simulation of the original system mentioned above. Pressure in small volume p_v was also saved and utilized as the output data for the training of the neural network. This data was chosen for training, validation, and testing of the neural network. Since all the input data, except the small volume, is variable, the neural network based on such data will work with any system with similar variable parameters. In case of changes of the small volume, new training of the network might be required.

At the beginning of the training, the training data was distributed for training, validation, and testing sets in the proportion of 70/15/15 percent. The input and output data were normalized in a range between -1 and 1 to achieve effective training results. The NARX RNN was trained multiple times in order to find the appropriate number of neurons in hidden layers for the most accurate and effective simulation. The Levenberg-Marquardt algorithm was utilized in the training process as a main backpropagation-based training algorithm due to its relatively fast training of the network and accurate results [37]. The Early-Stopping technique was also utilized in cases when the generalization stopped improving. The network was trained a total of ten times, for a maximum of 1,000 epochs with a different number of neurons in each hidden layer. The results of the training are displayed in Table 3. The results show that the number of neurons affects the training time of the neural network, and at the same time, the most accurate validation performance was obtained at training 8 and 9 with 40 and 45 neurons in a hidden layer, respectively. Based on the obtained data, the number of neurons in the RNN was selected to achieve the most accurate result, and the most accurate network in terms of Mean-Square error (MSE) was selected for the Hybrid model simulation.

The most accurate network (see Fig. 4a and 4b) contains 40 neurons in hidden layers. The validation performance of the network was expressed in the form of MSE, equal to 0.000216 (normalized data). The training time of the selected network was 3 hours and 33 minutes.

B. IMPLEMENTATION OF THE RNN IN THE HYBRID MODEL

After the training, the most accurate and fastest network was implemented in the MATLAB code of the traditional or

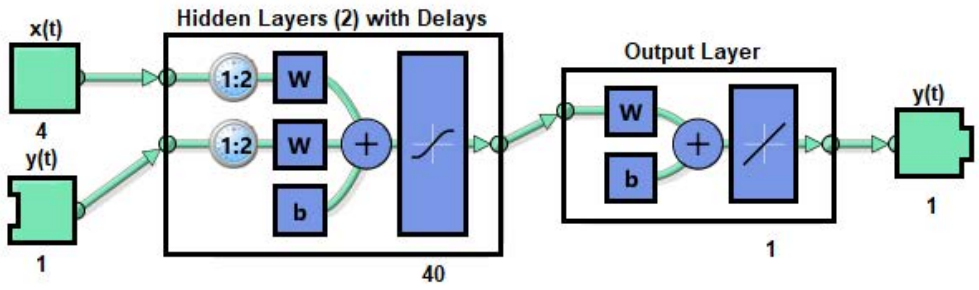

FIGURE 3. Structure of the NARX RNN.

TABLE 3. Results of the training of the NARX RNN with normalized data.

Training	Number of neurons in hidden layers	Validation stop	Mean-Square Error (MSE)	Training time
1	5	472	0.000313	17 min
2	10	474	0.000290	28 min
3	15	1000	0.000241	1 h 19 min
4	20	1000	0.000266	1 h 50 min
5	25	1000	0.000237	2 h 18 min
6	30	1000	0.000248	1 h 58 min
7	35	1000	0.000241	2 h 33 min
8	40	1000	0.000216	3 h 33 min
9	45	1000	0.000229	3 h 39 min
10	50	1000	0.000243	4 h 30 min

reference mathematical model of both circuits described in Section II. The network was added to the code in the form of a MATLAB function as a substitute for the numerically stiff equation with small volume. First, the traditional mathematical model was simulated to obtain the input dataset for the hybrid system simulation. Such inputs are effective bulk modulus B_{e3}, volumetric flows Q_3 and Q_v, and volume V_v.

Note that the simulation of each hybrid system should be performed after obtaining the inputs for the network, and this means that the simulation of the traditional mathematical model should be completed and input values should be saved. After that, the hybrid system can be simulated an unlimited number of times.

The simulation of the hybrid system includes the stage of preprocessing the RNN before the main model simulation with the use of the data obtained from the previous simulation. The whole system is automatically simulated using the pressure data obtained from the RNN preprocessing stage at the corresponding simulation time step.

V. RESULTS AND DISCUSSION

This section presents the results of the simulation of the fluid power circuits described in Section II. In the case of Circuit 1, the simulation was performed with two variations of the integrator time step to show the responses of the pressure of the reference and hybrid systems at different simulation speeds. Circuit 2 was simulated with a different input signal to ensure the ability of the hybrid system with the RNN was accurate and fast with any set of input signals. The results are presented in the form of a comparison of plots related to the responses of the traditional system modeling and the hybrid approach of system modeling. The results obtained in the simulation also provide an understanding of the advantages and features of the hybrid method compared to the classical mathematical modeling and simulation of fluid power circuits.

A. CIRCUIT 1: RESULTS

Circuit 1 was simulated for 50 seconds using the reference and hybrid model. The first simulation of the circuit was performed using the reference model at integrator time steps of 1.0×10^{-4} s, and 1.0×10^{-3} s. Fig. 5 illustrates the response of the pressure in small volume p_2 for above-mentioned time steps in the reference model. It is seen from the figure that the responses of the reference model at different integrator time steps are different, which is the effect of the small volume described in [10], [11]. In this case, the response of the pressure at the time step of 1.0×10^{-4} is correct. In other words, it is impossible to use the model at large time steps due to its numerical instability.

The Table 4 represents the results of the simulation in the form of the simulation time and Relative Root-Mean-Square

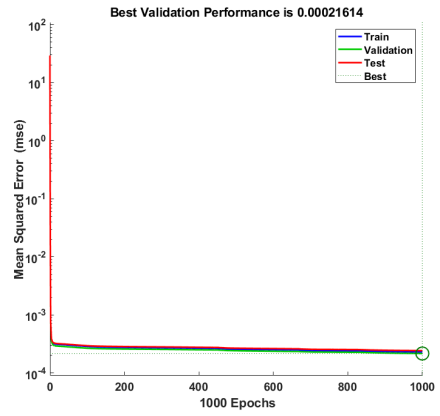

(a)

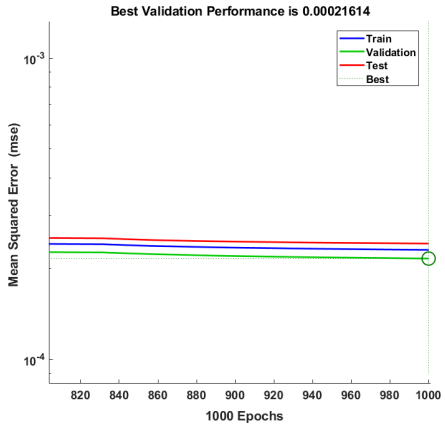

(b)

FIGURE 4. Validation, train and test performance of the selected NARX RNN. (a) Full performance between 1 and 1000 epochs. (b) A close look at the performance plot between 800 and 1000 epochs.

Error (RRMSE), defined as follows:

$$RRMSE = \frac{\sqrt{\frac{1}{N}\sum_{i=1}^{N}(x_i - x_i^m)^2}}{\sum_{i=1}^{N}(|\ x_i\ |)} \times 100 \qquad (17)$$

where N is the number of points, x_i is the value of the reference model at operating point and x_i^m is the value of any comparable model (reference at different time steps or hybrid model) at the same point. The RRMSE of the reference model at the time step of 1.0×10^{-3} in comparison with the reference model at the time step of 1.0×10^{-4} is 802.06%. A high error

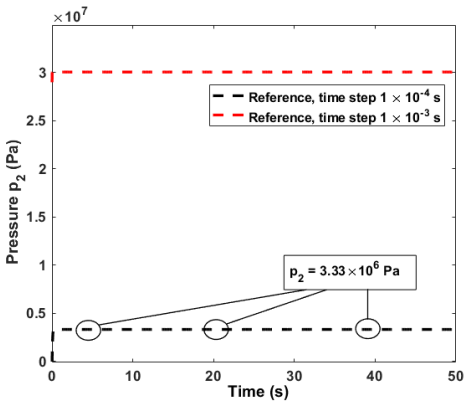

FIGURE 5. Comparison of responses of the reference model at 1.0×10^{-4} and 1.0×10^{-3} integrator time steps.

percentage proves the numerical instability of the reference system at time steps larger than 1.0×10^{-4}.

The hybrid model was simulated at a time step of 1.0×10^{-4}. The simulation shows an accurate pressure response with an RRMSE of 0.895% with respect to the reference system (time step of 1.0×10^{-4}), which is observed from the plot in Fig. 6a. The simulation time of the hybrid system is 23.56 s, which is shorter than the reference system (24.63 s) even at the same simulation time step.

The plot for the next simulation of the hybrid model performed at a time step of 1.0×10^{-3} s is depicted in Fig. 6b. The plot shows the stable response of the hybrid model in relation to the reference model at the integrator time step of 1.0×10^{-4}. The simulation time of the hybrid system is only 2.32 s which is 10 times shorter than the numerically stable response of the reference system, which was obtained at the 1.0×10^{-4} s integrator time step (24.63 s). The RRMSE for the pressure response of the hybrid system at the time step of 1.0×10^{-3} s is 7.333%.

According to the plots in Figures 6a and 6b, the only difference between the responses of the hybrid system at different time steps is the longer pressure rise time, which indicates the stability of the hybrid model. In other words, the difference between the responses of the hybrid model at time steps of 1.0×10^{-4} and 1.0×10^{-3} is neglectable compared to the reference model at the same time steps. At the same time, responses of the hybrid model are close to the reference at the time step of 1.0×10^{-4}. It means that the hybrid model can be used without significant accuracy losses at larger simulation time steps, which makes this model a trade-off between accuracy and simulation speed.

B. CIRCUIT 2: RESULTS

Circuit 2 was simulated with a constant pressure supply of 1.4×10^7 Pa and two different sets of input signals

TABLE 4. Circuit 1 simulation results.

Time step Δt, s	System	Real time, s	Simulation time, s	RRMSE w.r.t Reference, % (at Δt=1.0×10^{-4})
1.0×10^{-4}	Reference	50	24.63	-
	Hybrid		23.56	$RRMSE_{p_2} = 0.895\%$
1.0×10^{-3}	Reference	50	2.47	$RRMSE_{p_2} = 802.06\%$
	Hybrid		2.32	$RRMSE_{p_2}$=7.333%

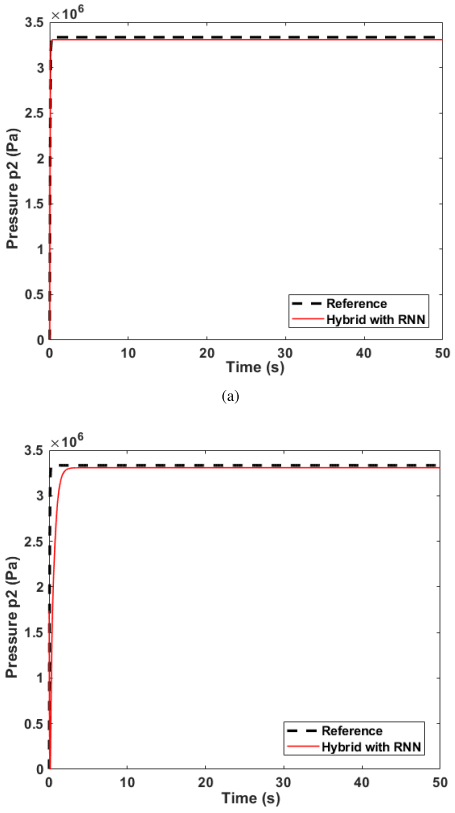

FIGURE 6. Circuit 1 pressure in small volume p_2 response of the reference model and hybrid model at time step: (a) both reference and hybrid models: 1.0×10^{-4} seconds and (b) reference model: 1.0×10^{-4} seconds; hybrid model: 1.0×10^{-3} seconds.

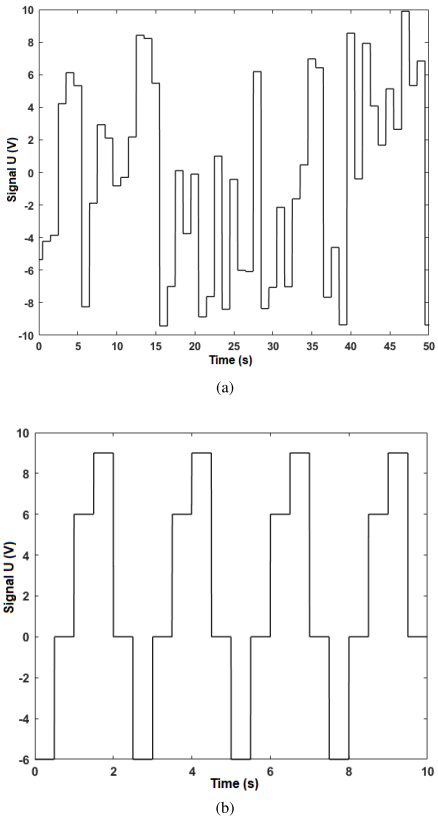

FIGURE 7. Signal U for Circuit 2 simulations: (a) random input signal and (b) repeatable input signal.

(Fig. 7a and 7b) using both traditional (reference) and hybrid models. First, the circuit was simulated for 50 seconds with a randomly distributed input signal in a range between -10 and $+10$ volts (Fig. 7a). The numerical stiffness of the reference system with a small volume between the pressure compensator and the directional control valve allowed the maximal simulation time step of 1.0×10^{-5} s to obtain a numerically stable response. The stiffness of the hybrid model was generally reduced by using the RNN instead of the stiff differential equation related to the pressure in small volume, which allowed an increase in the time step of the simulation to 1.0×10^{-4} s.

As the result, the simulation time for the real 50 seconds was 501.47 seconds for the reference model. Compared to the simulation time of the hybrid model (53.27 s), the reference was almost ten times slower. However, the simulation time difference between the two models is associated with the time step difference at the same level of accuracy, which can be observed among the simulation results in Table 5 (see Fig. 8).

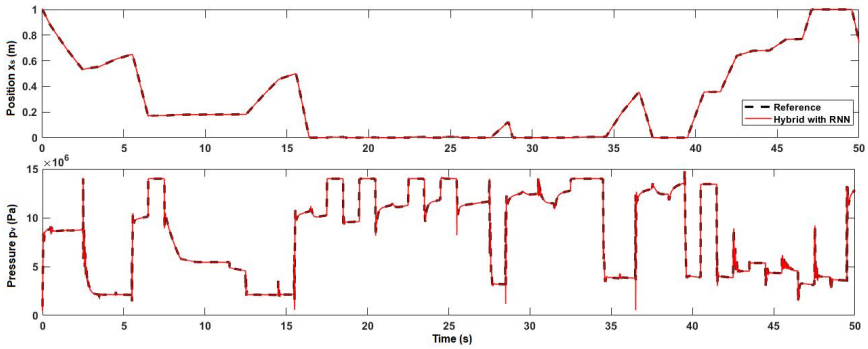

FIGURE 8. Circuit 2 responses of cylinder piston position x_s and pressure p_v at random input voltage comparing the reference model and hybrid model with utilized RNN.

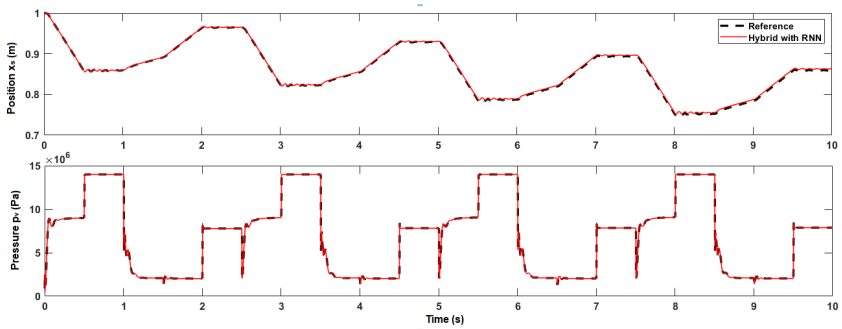

FIGURE 9. Circuit 2 responses of cylinder piston position x_s and pressure p_v at repeating input voltage comparing the reference system and hybrid system with utilized RNN.

TABLE 5. Circuit 2 simulation results.

Input	System	Real time, s	Time step, s	Simulation time, s	RRMSE, %
Random	Reference	50	1.0×10^{-5}	501.47	-
	Hybrid		1.0×10^{-4}	53.27	$RRMSE_{x_s} = 0.089\%$ $RRMSE_{p_v} = 1.479\%$
Repeatable	Reference	10	1.0×10^{-5}	102.96	-
	Hybrid		1.0×10^{-4}	9.89	$RRMSE_{x_s} = 0.260\%$ $RRMSE_{p_v} = 2.441\%$

The responses of pressure p_v related to small volume as well as the cylinder piston position x_s for the reference and hybrid models with a random input signal are illustrated by plots in Fig. 8. The accuracy of the model is well-observed in the plot. The RRMSE for the reference model defined in (17) and represented in the simulation results (Table 5) was calculated for the hybrid system and equals 0.089% for the cylinder piston position x_s and 1.479% for pressure in small volume p_v.

The second simulation of Circuit 2 was performed within 10 seconds utilizing the reference and hybrid models. The repeatable input signal in a range between -6 and $+9$ Volts with a time period of 2.5 seconds was set for both systems. The simulation time steps remained the same for the reference and hybrid models, which were 1.0×10^{-5} s and 1.0×10^{-4} s, respectively. The responses of cylinder piston position x_s and pressure in small volume p_v are plotted in Fig. 9. The plots clearly represent the accurate responses of the hybrid model with respect to the reference with a resultant RRMSE of 0.260% and 2.441% for cylinder piston position x_s and pressure p_v, respectively.

The simulation times of the second simulation for the reference and hybrid models are presented in Table 5. Hybrid model simulation was performed for only 9.89 seconds, while the simulation of the reference model required almost ten times as much time (102.96 seconds).

At the end of the simulation, it can be concluded that at both the random and repeatable sets of input signals, the performance of the hybrid model is stable and accurate despite the RNN utilized instead of the stiff differential pressure equation was trained on the random data obtained from the 3,000-second simulation. Moreover, the simulation time of the hybrid system is significantly shorter than with the traditional mathematical model. And the conversion of the model, for instance to C++ code, may allow simulating it in real-time, or even faster than real-time applications.

VI. CONCLUSION

This paper proposes a novel hybrid method to solve a fundamental problem in the dynamic simulation of fluid power circuits. The problem is associated with the existence of stiff differential equations in the mathematical model of the system in the presence of small volumes that restrict the simulation speed for real-time applications. The method is based on the use of the NARX recurrent neural network in the model, which substitutes the stiff pressure continuity equation. The dynamics of the remaining parts of the system are preserved and modeled with conventional differential and algebraic equations. The network was trained using data from the practical fluid power circuit simulation in order to receive an accurate response.

To demonstrate the features and advantages of the method, the classical mathematical model and the hybrid method were compared. The simple circuit of three orifices in series and the practical circuit with a two-chamber cylinder controlled by a directional control valve were modeled and simulated using the two above-mentioned approaches. A simple circuit was tested at different simulation time steps, whereas the practical circuit was tested at random and repeating inputs. In both case studies, the response of the hybrid method was several times faster than the conventional reference model due to the elimination of the numerical stiffness problem. At the same time, the accuracy of the hybrid method is relatively high, which allows a trade-off between accuracy and simulation speed. Finally, the hybrid method performance allows us to use it in real-time applications, and future research can be associated with the testing and comparison of different time series RNN architectures (e.g. LSTM, GRU architectures in comparison with the NARX architecture) to find the most efficient method for real-time simulation of fluid power circuits.

REFERENCES

[1] V. Zhidchenko, I. Malysheva, H. Handroos, and A. Kovartsev, "Faster than real-time simulation of mobile crane dynamics using digital twin concept," *J. Phys., Conf. Ser.*, vol. 1096, Sep. 2018, Art. no. 012071.
[2] A. Mikkola, "Using the simulation model for identification of the fatigue parameters of hydraulically driven log crane," *J. Mech. Des.*, vol. 123, no. 1, pp. 125–131, Mar. 2001.
[3] C.-G. Park, S. Yoo, H. Ahn, J. Kim, and D. Shin, "A coupled hydraulic and mechanical system simulation for hydraulic excavators," *Proc. Inst. Mech. Eng., I, J. Syst. Control Eng.*, vol. 234, no. 4, pp. 527–549, Apr. 2020.
[4] I. Malysheva, H. Handroos, V. Zhidchenko, and A. Kovartsev, "Faster than real-time simulation of a hydraulically actuated log crane," in *Proc. Global Fluid Power Soc. PhD Symp. (GFPS)*, Jul. 2018, pp. 1–6.
[5] M. Liermann, C. Feller, and F. Lindinger, "Real-time simulation of fluid power systems," in *Proc. ASME/BATH Symp. Fluid Power Motion Control*, Oct. 2021, pp. 1–10.
[6] A. Ellman and R. Piché, "A modified orifice flow formula for numerical simulation of fluid power systems," in *Proc. ASME Int. Mech. Eng. Congr. Expo., Atlanta, Fluid Power Syst. Technol.*, vol. 3, Nov. 1996, pp. 59–63.
[7] A. Ellman and R. Piché, "A two regime orifice flow formula for numerical simulation," *J. Dyn. Syst., Meas., Control*, vol. 121, no. 4, pp. 721–724, Dec. 1999.
[8] R. Åman, H. Handroos, and T. Eskola, "Computationally efficient two-regime flow orifice model for real-time simulation," *Simul. Model. Pract. Theory*, vol. 16, no. 8, pp. 945–961, Sep. 2008.
[9] C. F. Curtis and J. D. Hirschfelder, "Integration of stiff equations," *Proc. Nat. Acad. Sci. USA*, vol. 38, no. 3, pp. 235–243, 1952.
[10] R. Piché and A. Ellman, "Numerical integration of fluid power circuit models using two-stage semi-implicit Runge–Kutta methods," *Proc. Inst. Mech. Eng., C, J. Mech. Eng. Sci.*, vol. 208, no. 3, pp. 167–175, May 1994.
[11] D. E. Bowns and L. M. Wang, "The digital computation of pressures in hydraulic pipes with small volume using an iterative technique," *Proc. Inst. Mech. Eng., C, Mech. Eng. Sci.*, vol. 204, no. 1, pp. 29–36, Jan. 1990.
[12] R. Åman and H. Handroos, "Pseudo-dynamic solution of pressures in small volumes in fluid power circuit simulation," in *Proc. 5th FPNI PhD Symp. Cracow*, Jul. 2008, pp. 406–416.
[13] R. Åman and H. Handroos, "Comparison of numerical effectiveness of three methods for modelling 2-way flow control valves," in *Proc. 7th Int. Conf. Fluid Power Transmiss. Control (ICFP)*, Hangzhou, China, Apr. 2009, pp. 711–715.
[14] R. Åman and H. Handroos, "Optimization of parameters of pseudo-dynamic solver for real-time simulation of fluid power circuits," in *Proc. 7th Int. Fluid Power Conf. Aachen Workshop*, vol. 1, Mar. 2010, pp. 495–507.
[15] J. Malysheva, S. Ustinov, and H. Handroos, "Computationally efficient practical method for solving the dynamics of fluid power circuits in the presence of singularities," *IEEE/ASME Trans. Mechatronics*, vol. 26, no. 5, pp. 2385–2395, Oct. 2021.
[16] J. Malysheva and H. Handroos, "Fast calculation of stiff hydraulic models using the modified pseudo-dynamic solver," in *Proc. BATH/ASME Symp. Fluid Power Motion Control., Fluid Power Syst. Technol.*, Sep. 2020, pp. 1–10.
[17] M. K. Oshtorjani, A. Mikkola, and P. Jalali, "Numerical treatment of singularity in hydraulic circuits using singular perturbation theory," *IEEE/ASME Trans. Mechatronics*, vol. 24, no. 1, pp. 144–153, Feb. 2019.
[18] J. Rahikainen, M. Kiani, J. Sopanen, P. Jalali, and A. Mikkola, "Computationally efficient approach for simulation of multibody and hydraulic dynamics," *Mechanism Mach. Theory*, vol. 130, pp. 435–446, Dec. 2018.
[19] M. Kiani-Oshtorjani, S. Ustinov, H. Handroos, P. Jalali, and A. Mikkola, "Real-time simulation of fluid power systems containing small oil volumes, using the method of multiple scales," *IEEE Access*, vol. 8, pp. 196940–196950, 2020.
[20] M. Krishna and J. E. Bares, "Hydraulic system modeling through memory-based learning," in *Proc. IEEE/RSJ Int. Conf. Intell. Robots Syst.*, vol. 3, Oct. 1998, pp. 1733–1738.
[21] M. Krishna and J. Bares, "Constructing fast hydraulic robot models for optimal motion planning," *J. Aerosp. Eng.*, vol. 12, pp. 34–42, Jan. 1999.
[22] G. Bidini and F. Mariani, "Simulation of hydraulic power plant transients using neural networks," *Proc. Inst. Mech. Eng., A, J. Power Energy*, vol. 211, no. 5, pp. 393–398, Aug. 1997.
[23] S. Pan and K. Duraisamy, "Long-time predictive modeling of nonlinear dynamical systems using neural networks," *Complexity*, vol. 2018, pp. 1–26, Dec. 2018.
[24] R. T. Q. Chen, Y. Rubanova, J. Bettencourt, and D. Duvenaud, "Neural ordinary differential equations," 2018, *arXiv:1806.07366*.
[25] J. Malysheva, M. Li, and H. Handroos, "Hydraulic system modeling with recurrent neural network for the faster than real-time simulation," *Int. Rev. Model. Simulations (IREMOS)*, vol. 13, no. 1, p. 16, Feb. 2020.
[26] J. Vermaak and E. C. Botha, "Recurrent neural networks for short-term load forecasting," *IEEE Trans. Power Syst.*, vol. 13, no. 1, pp. 126–132, Feb. 1998.
[27] A. Patel and J. F. Dunne, "NARX neural network modelling of hydraulic suspension dampers for steady-state and variable temperature operation," *Vehicle Syst. Dyn.*, vol. 40, no. 5, pp. 285–328, Nov. 2003.
[28] M. Jelali and A. Kroll, *Hydraulic Servo-Systems: Modelling, Identification and Control* (Advances in Industrial Control). London, U.K.: Springer-Verlag, 2003.

[29] H. M. Handroos and M. J. Vilenius, "Flexible semi-empirical models for hydraulic flow control valves," *J. Mech. Des.*, vol. 113, no. 3, pp. 232–238, 1991.
[30] C. C. De Wit, H. Olsson, K. J. Astrom, and P. Lischinsky, "Dynamic friction models and control design," in *Proc. Amer. Control Conf.*, Jun. 1993, pp. 1920–1926.
[31] C. C. De Wit, H. Olsson, K. J. Åström, and P. Lischinsky, "A new model for control of systems with friction," *IEEE Trans. Autom. Control*, vol. 40, no. 3, pp. 419–425, Mar. 1995.
[32] H. Olsson, "Control Systems with Friction," Ph.D. dissertation, Dept. Auto-Matic Control, Lund Inst. Technol., Lund, Sweden, 1996.
[33] G. Schram, M. H. G. Verhaegen, and A. J. Krijgsman, "System identification with orthogonal basis functions and neural networks," *IFAC Proc. Volumes*, vol. 29, no. 1, pp. 4150–4155, Jun./Jul. 1996.
[34] H. T. Siegelmann, B. G. Horne, and C. L. Giles, "Computational capabilities of recurrent NARX neural networks," *IEEE Trans. Syst., Man, Cybern. B, Cybern.*, vol. 27, no. 2, pp. 208–215, Apr. 1997.
[35] L. Lacny, "Modelling of the dynamics of a gyroscope using artificial neural networks," *J. Theor. Appl. Mech.*, vol. 50, no. 1, pp. 85–97, 2012.
[36] J. F. Tuttle, L. D. Blackburn, K. Andersson, and K. M. Powell, "A systematic comparison of machine learning methods for modeling of dynamic processes applied to combustion emission rate modeling," *Appl. Energy*, vol. 292, Jun. 2021, Art. no. 116886.
[37] B. Wilamowski and J. Irwin, *Intelligent Systems: The Industrial Electronics Handbook*, 2nd ed. Boca Raton, FL, USA: CRC Press, 2011.

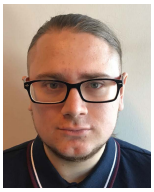

STANISLAV USTINOV received the B.Sc. degree from the Saimaa University of Applied Sciences, Lappeenranta, Finland, in 2016, within the mechanical engineering and production technology program, and the M.Sc. degree in mechatronic systems design from the Lappeenranta-Lahti University of Technology (LUT University), in 2018, where he is currently pursuing the Ph.D. degree. His research interests include fluid power systems, real-time simulation of multibody systems, and artificial intelligence.

HUAPENG WU received the M.Sc. (Eng.) degree from the Huazhong University of Science and Technology, China, in 1993, and the Doctor of Science (Tech.) degree from the Lappeenranta-Lahti University of Technology (LUT University), Finland, in 2001. Since 2004, he has been an Associate Professor with LUT University, where he was a Professor, from 2008 to 2011. His research interests include robotics, AI control, mechatronics, and machine manufacturing and automation. He has published four books and more than 150 publications in his research areas.

HEIKKI HANDROOS (Member, IEEE) received the M.Sc. (Eng.) and D.Sc. (Tech.) degrees from Tampere University, Finland, in 1985 and 1991, respectively. He has been a Full Professor in machine automation with the Lappeenranta-Lahti University of Technology (LUT University), since 1992. He has been the supervisor of about 30 doctoral students and has served as a principal investigator for the international and domestic projects, whose total funding exceeds €30M. He has published more than 300 journal and conference articles in the field of mechatronics, robotics, and control. He is a member of ASME. He has served as an Associate Editor for *Journal of Dynamic Systems, Measurement and Control* (ASME), from 2013 to 2020.

ACTA UNIVERSITATIS LAPPEENRANTAENSIS

1040. AFKHAMI, SHAHRIAR. Laser powder-bed fusion of steels: case studies on microstructures, mechanical properties, and notch-load interactions. 2022. Diss.

1041. SHEVELEVA, NADEZHDA. NMR studies of functionalized peptide dendrimers. 2022. Diss.

1042. SOUSA DE SENA, ARTHUR. Intelligent reflecting surfaces and advanced multiple access techniques for multi-antenna wireless communication systems. 2022. Diss.

1043. MOLINARI, ANDREA. Integration between eLearning platforms and information systems: a new generation of tools for virtual communities. 2022. Diss.

1044. AGHAJANIAN, SOHEIL. Reactive crystallisation studies of CaCO3 processing via a CO2 capture process: real-time crystallisation monitoring, fault detection, and hydrodynamic modelling. 2022. Diss.

1045. RYYNÄNEN, MARKO. A forecasting model of packaging costs: case plain packaging. 2022. Diss.

1046. MAILAGAHA KUMBURE, MAHINDA. Novel fuzzy k-nearest neighbor methods for effective classification and regression. 2022. Diss.

1047. RUMKY, JANNATUL. Valorization of sludge materials after chemical and electrochemical treatment. 2022. Diss.

1048. KARJUNEN, HANNU. Analysis and design of carbon dioxide utilization systems and infrastructures. 2022. Diss.

1049. VEHMAANPERÄ, PAULA. Dissolution of magnetite and hematite in acid mixtures. 2022. Diss.

1050. GOLOVLEVA, MARIA. Numerical simulations of defect modeling in semiconductor radiation detectors. 2022. Diss.

1051. TREVES, LUKE. A connected future: The influence of the Internet of Things on business models and their innovation. 2022. Diss.

1052. TSERING, TENZIN. Research advancements and future needs of microplastic analytics: microplastics in the shore sediment of the freshwater sources of the Indian Himalaya. 2022. Diss.

1053. HOSEINPUR, FARHOOD. Towards security and resource efficiency in fog computing networks. 2022. Diss.

1054. MAKSIMOV, PAVEL. Methanol synthesis via CO2 hydrogenation in a periodically operated multifunctional reactor. 2022. Diss.

1055. LIPIÄINEN, KALLE. Fatigue performance and the effect of manufacturing quality on uncoated and hot-dip galvanized ultra-high-strength steel laser cut edges. 2022. Diss.

1056. MONTONEN, JAN-HENRI. Modeling and system analysis of electrically driven mechatronic systems. 2022. Diss.

1057. HAVUKAINEN, MINNA. Global climate as a commons — from decision making to climate actions in least developed countries. 2022. Diss.

1058. KHAN, MUSHAROF. Environmental impacts of the utilisation of challenging plastic-containing waste. 2022. Diss.

1059. RINTALA, VILLE. Coupling Monte Carlo neutronics with thermal hydraulics and fuel thermo-mechanics. 2022. Diss.

1060. LÄHDEAHO, OSKARI. Competitiveness through sustainability: Drivers for logistics industry transformation. 2022. Diss.

1061. ESKOLA, ROOPE. Value creation in manufacturing industry based on the simulation. 2022. Diss.

1062. MAKARAVA, IRYNA. Electrochemical recovery of rare-earth elements from NdFeB magnets. 2022. Diss.

1063. LUHAS, JUKKA. The interconnections of lock-in mechanisms in the forest-based bioeconomy transition towards sustainability. 2022. Diss.

1064. QIN, GUODONG. Research on key technologies of snake arm maintainers in extreme environments. 2022. Diss.

1065. TAMMINEN, JUSSI. Fast contact copper extraction. 2022. Diss.

1066. JANTUNEN, NIKLAS. Development of liquid–liquid extraction processes for concentrated hydrometallurgical solutions. 2023. Diss.

1067. GULAGI, ASHISH. South Asia's Energy [R]evolution – Transition towards defossilised power systems by 2050 with special focus on India. 2023. Diss.

1068. OBREZKOV LEONID. Development of continuum beam elements for the Achilles tendon modeling. 2023. Diss.

1069. KASEVA, JANNE. Assessing the climate resilience of plant-soil systems through response diversity. 2023. Diss.

1070. HYNNINEN, TIMO. Development directions in software testing and quality assurance. 2023. Diss.

1071. AGHAHOSSEINI, ARMAN. Analyses and comparison of energy systems and scenarios for carbon neutrality - Focus on the Americas, the MENA region, and the role of geo-technologies. 2023. Diss.

1072. LAKANEN, LAURA. Developing handprints to enhance the environmental performance of other actors. 2023. Diss.

1073. ABRAMENKO, VALERII. Synchronous reluctance motor with an axially laminated anisotropic rotor in high-speed applications. 2023. Diss.

1074. GUTIERREZ ROJAS, DANIEL. Anomaly detection in cyber-physical applications. 2023. Diss.

1075. ESANOV, BAKHTIYOR. Adaptive user-controlled personalization for virtual journey applications. 2023. Diss.

1076. SILTANEN, JUKKA. Laser and hybrid welding of high-strength structural steels. 2023. Diss.

1077. NOUSIAINEN, JALO. Model-based reinforcement learning and inverse problems in extreme adaptive optics control. 2023. Diss.

ISBN 978-952-335-941-3
ISBN 978-952-335-942-0 (PDF)
ISSN 1456-4491 (Print)
ISSN 2814-5518 (Online)
Lappeenranta 2023